



Università degli Studi di Cagliari

Facoltà di Ingegneria e Architettura

IMT Atlantique Bretagne-Pays de la Loire

École Mines-Télécom

*Corso di Laurea Magistrale in Ingegneria per l'Ambiente e il Territorio*

TESI DI LAUREA MAGISTRALE

# Study on the use of biochars derived from textile waste as adsorbents for ibuprofen removal from wastewater

Relatore Estero:

Prof. Yves Andres

Relatrice:

Prof.ssa Giovanna Cappai

Candidato:

Andrea Pinna

A.A. 2021/2022

# Table of contents

# Table of Figures

# Table of tables

# Introduction

This study explored the valorization of a textile waste applying a pyrolysis treatment. The product created was a biochar that had a high specific surface area and porosity, consequently it was considered interesting to evaluate its properties as an adsorbent material. As such, the disposal of the material as it is could be avoided since a new life could be found for this product. The raw material used was recycled textile insulation panels, which are fibrous materials characterized by a heterogeneous nature and consequently tricky to recycle. First, research on what biochar is and what its properties are were conducted. This to explore which characteristics were more important for the different possible applications. Also, the activation and other modifications were explored.

Wastewater treatment was the field in which this potential adsorbent could be applied, thus selecting the target pollutant to remove was crucial. The presence of pharmaceuticals in urban and industrial wastewater is well known and their possible harmful effects on the environment and human health are leading to their inclusion in the list of emerging pollutants. Legislative organizations, like the European Union, are taking action to stop this emerging problem, putting in place regulations on the discharge of pharmaceuticals in water bodies. Ibuprofen was chosen as the molecule targeted for the adsorption, being an extensively used drug and a difficult molecule to biodegrade.

The adsorbents produced were two biochars: one made via a pyrolysis process and the second, steam activated, synthesized via a steam gasification process. The physico-chemical characteristics, such as specific surface area, porosity, and elemental composition, have been studied. The adsorption capacity of the biochar has been investigated initially with batch tests and subsequently with a dynamic experiment, both using synthetic wastewater. The influence of particle size was also investigated. With the first laboratory test the kinetics of adsorption and the isotherms were found, so the adsorption capacity of the biochar and the steam-activated one were determined. The dynamic experiment carried out was a fixed bed adsorption column where the packing material used was only the steam-activated biochar. Furthermore, the data from the experiments were used to fit models and obtain information about the adsorption mechanism and properties of the adsorbents.

# CHAPTER 1

# Production and Engineering of Biochar

## 1.1 Biochar

Biochar is a carbon-rich solid produced by heating biomass or synthetic organic materials in an oxygen-depleted atmosphere. With the advancement of biochar research, people are progressively discovering the numerous environmental and economic benefits it provides, so scientific studies on biochar are done to adapt it to engineering applications (Bian et al., 2018). In Figure 1.1, a schematic of biochar is shown. Biochar has a large specific surface area, a porous structure, rich surface functional groups, and mineral components, which allow it to be utilized as a suitable adsorbent to remove contaminants from aqueous media (Zhu et al., 2018). Biochar, with a porous structure comparable to activated carbon, is the most widely used and efficient adsorbent in the world for removing different contaminants from water (Wu and Liu, 2018). Biochar, on the other hand, is a novel type of adsorbent with cheap cost and great efficiency, as opposed to activated carbon (Tan et al., 2015). Activated carbon synthesis needs a higher temperature and activation procedure. Biochar, instead, is less expensive to create and consumes less energy. Biochar is a renewable resource that, due to its economic and environmental advantages, is an attractive resource for environmental technology for water pollution remediation ("International Biochar Initiative," 2022).

## 1.2 Biomass used as feedstocks

Biochar can be produced from a material with high carbonaceous content, such as lignocellulose, animal manure, agricultural and forest residues, industrial bio-waste, plastic waste, microalgae, waste tires, dewatered sludges, marine and aquatic organisms (Krasucka et al., 2021; Oba et al., 2021). Lignocellulosic biomass, which corresponds to forest and agricultural wastes, is the most often utilized raw material for biochar synthesis (Li et al., 2020). In general, the physicochemical characteristics of biochar are connected to and influenced by the biomass used in its production. Lignocellulosic biomass generated from woodlands, agriculture, and forest leftovers, in particular, has demonstrated significant potential as a feedstock for achieving sustainable industrial biochar production. This biomass

is mostly composed of cellulose (25–50 %), hemicellulose (15–40 %), and lignin (10–15 %), with a minor quantity of extractives (0–15 %) and minerals (Monga et al., 2022). Depending on the method adopted, each biomass ingredient reacts differently throughout the carbonization process, resulting in a wide range of products. For example, cellulose and hemicellulose are vital in the production of bio-oil by pyrolysis, whereas lignin assists in the production of biochar (Kan et al., 2016). The carbon content of biochar is related to the lignin content of raw biomass (Zhou et al., 2014). Forests and agricultural wastes include a wide range of biomaterials such as grass, nutshell, straw, bagasse, and husk, that serve as a significant supply of raw carbonaceous precursors (Kumar et al., 2021; Wang et al., 2021). Because of their plentiful availability, renewable nature, and low cost, the use of these resources in biochar synthesis gives various benefits (Wang et al., 2020). Rather than cellulosic materials, poultry and animal wastes, insect shells, sewage sludge, and algae contain a high concentration of lipids and proteins. The biochar produced from these feedstocks has a high concentration of minerals and heteroatoms, as well as a variety of surface functional groups (Li and Jiang, 2017). Chitin is the second most abundant nitrogen-rich biopolymer in nature, and it may also be used to produce nitrogen-doped biochars by pyrolysis (Carpenter et al., 2014; Liu et al., 2017). Heavy metal-rich sewage sludge produces biochar with a high ash concentration and a low carbon content, as well as an alkaline pH (Ho et al., 2017; Y. Yang et al., 2018).

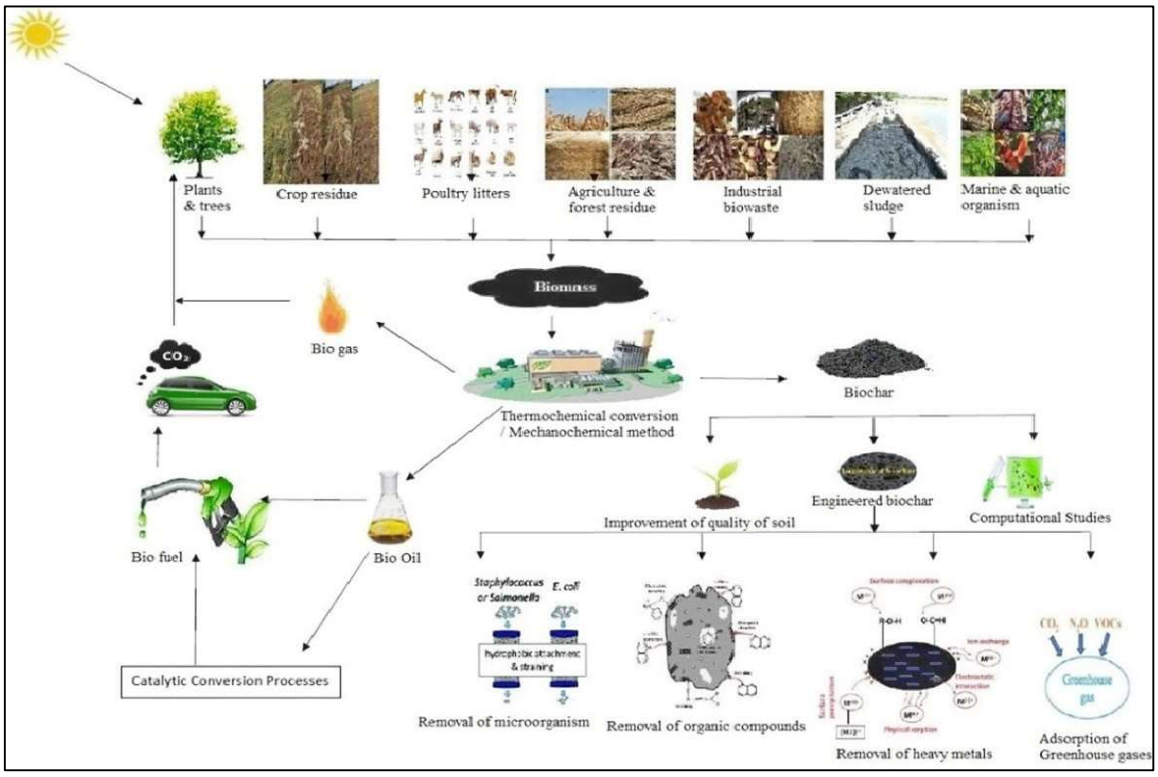


**Figure 1.1** Overall look of biochar production chain and applications **(Jeyasubramanian et al., 2021)**.

## 1.3 Methods of biochar production

Thermochemical conversion is a typical method for producing biochar. Many researchers, to produce biochar for a variety of purposes, apply pyrolysis, gasification, hydrothermal carbonization, flash carbonation, which are all thermochemical conversion methods, and other carbonization techniques like mechanochemical technology.

### 1.3.1 Pre-treatment

The first step in the biochar synthesis process is the pre-treatment of the biomass used as feedstock. There are three types of pre-treatments: physical, chemical, and biological. Before carbonization, biomass can be dried (unless hydrothermal carbonization is considered), crushed, sieved, and washed to remove pollutants and condition the precursor form. The process for removing the precursor impurities will be determined by the source and properties of the raw biomass. For example, paper mill sludge may be washed with acid and deionized water to produce mineral-free sludge (Cho et al., 2017), whereas alkaline algae can be washed with water, dried, and flaked before pyrolysis (Roberts and de Nys, 2016; Son et al., 2018). Chemical pre-treatment procedures affect the characteristics and surface chemistry of feedstocks by using inorganic and organic chemical compounds, as well as various precursors and nanoparticles (Zhu et al., 2020). Engineered biochar can be made by pre-treating biomass with oxidants, acids, and alkalis to change the biochar's ultimate surface characteristics, such as functional groups, pore size distribution, and specific area (Zhao et al., 2018; Zhou et al., 2017). The biological pre-treatment technique is a relatively recent way of producing engineered biochar, which uses microorganisms and their biological-related activities to modify and enhance biomass characteristics and composition before carbonization to produce biochar (B. Wang et al., 2017; Zhang et al., 2020).

### 1.3.2 Production via Pyrolysis

Pyrolysis is the thermal degradation of organic materials in an oxygen-free atmosphere at temperatures ranging from 250 to 900 °C (Osayi et al., 2014). This process is an alternative method for turning organic wastes into value-added products such as biochar, syngas, and bio-oil. At various temperatures, lignocellulosic components such as cellulose, hemicellulose, and lignin undergo reactions such as depolymerization, fragmentation, and cross-linking, resulting in products in a different state such as solid, liquid, and gas. Char and bio-oil are respectively solid and liquid products, whereas carbon dioxide, carbon monoxide, hydrogen, and syngas are gaseous products ($C_1$-$C_2$ hydrocarbons). Biochar is

produced using a variety of reactors, including paddle kilns, bubbling fluidized beds, wagon reactors, and agitated sand rotating kilns. The amount of biochar produced during the pyrolysis process is determined by the type and nature of biomass utilized. The key operational process condition that determines product efficiency is the temperature (Wei et al., 2019). When the temperature of the pyrolysis process is raised, the biochar yield drops while the generation of syngas increases. Pyrolysis can be characterized as rapid or slow based on the heating rate, temperature, residence time, and pressure. Fast pyrolysis is considered a direct thermochemical technique capable of liquefying solid biomass into liquid bio-oil with great potential for energy use. Fast pyrolysis conditions are defined as follows: fast warming rates of biomass particles (>100 °C/min), along with short times of biomass particles and pyrolysis fumes (0.5–2 s) at high and moderate pyrolysis treatment temperatures (400-600 °C). To achieve high bio-oil quality, a fundamental distinguishing innovation feature of rapid pyrolysis is the requirement to keep the fume residence time in the hot zone to a minimum. This can be achieved by ensuring that the vapors are quickly extinguished or cooled (Wang et al., 2014). For slow pyrolysis, the heating rate is relatively low, about 5-7 °C/min, and it has a prolonged residence duration of more than 1 hour (W.-J. Liu et al., 2015). Slow pyrolysis gives a higher char production when compared to other pyrolysis and carbonization processes.

#### *1.3.2.1 Microwave pyrolysis*

Microwave pyrolysis is a kind of pyrolysis in which the biomass is heated by intense radiation generated by a microwave source. It has several advantages, such as non-contact heating, rapid start-up and shutdown of the heating process, greater heating rate, increased safety, and volumetric heating. As a result, it's commonly utilized to make biochar for a variety of purposes, including pasteurization, drying, vulcanization, and food processing (Wan Mahari et al., 2020; Y. Wang et al., 2018).

#### *1.3.2.2 Flash carbonation*

Flash carbonation is a technique in which biomass is heated by passing it through a flash fire at high pressures (>1 MPa) regularly. The pyrolysis chamber is packed with biomass, and a flash fire is introduced from the bottom in an upward direction while airflow is maintained in a downward direction. Biomass is transformed into gaseous fuel and leaves the carbon content as biochar, under these conditions (Hirst et al., 2018; Horne and Williams, 1996).

### 1.3.3 Production via Gasification

Gasification is a thermochemical technique of decomposing carbonaceous material into gaseous products, namely syngas, which contains CO, $CO_2$, $CH_4$, $H_2$, and traces of hydrocarbons in the presence of a gasifying agent such as oxygen, air or steam, at very high temperatures. It should be emphasized that the reaction temperature is the most important element in determining syngas generation. Carbon monoxide and hydrogen production increase as temperature rises, whereas other components such as methane, carbon dioxide, and hydrocarbons decline (Prabakar et al., 2018). The main outcome of this method is syngas, while char is a by-product with a lower yield.

### 1.3.4 Production via Hydrothermal carbonization

Hydrothermal carbonization is another thermochemical conversion method for producing biochar from cellulose, lignocellulosic biomass, animal manures, food waste, municipal sludge, pulp and paper industry sludge, agricultural and algae residues, and other feedstocks heated in closed environments at low pressure and temperature between 200 and 300 °C. (T. Wang et al., 2018). Wet pyrolysis is another term for it, and the biochar produced is known as hydrochar, to differentiate the products produced from dry processes such as pyrolysis and gasification (Fang et al., 2018; He et al., 2013; Zhou et al., 2019). The biomass is combined with water and placed in a closed reactor during the process. To ensure stability, the temperature is gradually raised. At different operating temperatures, different processes occur and consequently different products are obtained, for instance; below 250 °C biochar is produced and the process is known as hydrothermal carbonization; between 250 and 400 °C bio-oil is obtained by hydrothermal liquefaction; and above 400 °C gaseous products such as CO, $CO_2$, $H_2$ and $CH_4$ are produced by hydrothermal gasification (Khorram et al., 2016; Zhang et al., 2017).

### 1.3.5 Production via Torrefaction

Torrefaction is a thermochemical process that involves heating organic materials in a specific temperature range of 200 to 300 °C in an inert or nitrogen environment for 15 to 60 minutes. Under these conditions, the biomass or waste materials slowly degrade and emit $CO_2$ and $H_2O$. As a result, the carbon content of the biomass increases, and it has high energy density, hydrophobic behavior, homogeneity, and other properties comparable to coal (Chen et al., 2012). The depolymerization of the feedstock is driven by this process, and its quality is determined by the torrefaction temperature and heating duration (Simonic et al., 2020).

## 1.4 Biochar characterization parameters

The physicochemical properties of biochar are very important to be assessed because they will allow understanding in which applications it can be better used. Characterization techniques are based on the structure, surface functional groups, and elemental analysis of the biochar.

### 1.4.1 Chemical properties

The chemical characteristics of biochar are generally affected by the percentages of carbon (C), hydrogen (H), nitrogen (N), sulfur (S), and oxygen (O) in the feedstock, as well as the type of the biomass and carbonation method. C, H, O, S, and N are found in biomass as complex biomolecules such as hemicellulose, lignin, and cellulose. These molecules break down and leave as condensable and non-condensable gaseous components such as $CH_4$, CO, $H_2$ and $CO_2$, resulting in carbon-rich biochar. The type of biochar remaining after pyrolysis is also determined by qualities such as aromaticity, hydrophobicity, and hydrophilicity, which are determined by the atomic ratios of O/C, H/C, (O + N)/C, and (O + N + S)/C present in the biomass (Al-Wabel et al., 2013). Because of the degradation of lignocellulose structure and dehydration of oxygen-containing functional groups, high-temperature carbonation processes increase the hydrophobic character and decrease the polar functional groups (Usevičiūtė and Baltrėnaitė-Gedienė, 2021). According to study of (Zornoza et al., 2016), pyrolysis at a temperature between 300 and 500 °C increases the hydrophobic properties of biochar, whereas pyrolysis above 500 °C produces hydrophilic biochar because the removal of labile aliphatic functional groups on the surface of biochar results in the formation of high porosity, which facilitates the wettability. Carboxylic (COOH), hydroxyl (OH), amine, amide, and lactonic groups are key functional groups present on the surface of biochar that boost its sorption capabilities. Biochar surface functional groups are mostly influenced by the biomass and temperature used during the production (Li et al., 2017). The pH of raw biomass is usually slightly acidic, whereas the produced char is alkaline. This is because, during the carbonation process, the acidic COOH and OH groups are decomposed and removed mainly as $CO_2$ and $H_2$ (Weber and Quicker, 2018); thus, the pH range is expected to increase with increasing carbonation temperature.

### 1.4.2 Physical properties

The physical qualities of biochar are mostly determined by its size and porosity. The surface area is the most important factor in determining biochar adsorption capacities. Biochar with

a large surface area and a high porosity will typically have a strong adsorption capacity. The elimination of volatile materials, dehydration, and other processes cause the creation of pore volume in the biochar (Zhu et al., 2020). The pores in biochar might be micro (2 nm), meso (2 50 nm), or macro (>50 nm), according to the International Union of Pure and Applied Chemistry (IUPAC). The surface area of treated and untreated biochar may differ. Commercially, activated carbon has a larger surface area. Without the activation step, biochar has a low surface area and is less porous (Kim et al., 2012). Increasing surface area and pore volume are appropriate for catalytic activity, hydrogen gas storage, adsorption investigations, and other applications. Furthermore, various relevant post-treatment techniques, including physical and chemical treatments, have been discovered to improve the physical and chemical characteristics of biochar. Prior to calcination, the raw biomass is often combined with magnetic precursors, alkalis, functional agents, and other additives that increase the quality of the biochar in terms of porosity, surface area, and catalytic activity. The surface modified biochar formed following functionalization have a wide range of applications (Wan et al., 2020; Xiang et al., 2020).

## 1.5 Biochar Activation

Activation is a method of improving the physical properties and absorption capacity of biochar thanks to the increase of specific surface area, pore density, and functionalization. Many studies are now focusing on the synthesis of functionalized biochar since it has significant advantages over raw biochar. It was established that biochar produced by pyrolysis has a low specific surface area, limited porosity, and a low surface functional group (N. Liu et al., 2015; W.-J. Liu et al., 2015). Because of the relatively low surface area and porosity, several applications are restricted. Functionalized biochar is often produced using a variety of synthetic procedures such as physical methods, chemical methods, surface functionalization, heteroatom doping, metal/metal oxide impregnation methods etc. (Figure 1.2). After carbonation of the feedstock derived from raw biomass, the biochar contains only conventional metal oxides such as $SiO_2$, CaO, $Fe_2O_3$, $Al_2O_3$, and so on, and has limited applicability. Several researchers have recently created biochar by impregnating the appropriate metal oxides on the biochar matrix. The biomass is combined with the precursor solution of the various chemicals in this procedure. The warmed biomass is carbonated after the medium has been dried. The needed catalyst is added to the biochar by mixing the precursor metal ion with the feedstock. When metal salt-loaded biomass is pyrolyzed, it yields catalyst-loaded biochar, which has a wide range of uses (Saifullah et al., 2018).

However, the functionalization and activation of raw biochar need corrosive chemicals, several synthesis processes, and significant energy inputs, all of which result in time-consuming, costly, and complex procedures in large-scale manufacturing (Zhou et al., 2019). The type of biomass, feedstock, physicochemical properties of the biomass, operational methods used in synthesis, and so on should all be carefully studied in order to provide designed biochar with the appropriate features. There are two main kinds of activation procedures in general: thermal physical and chemical.

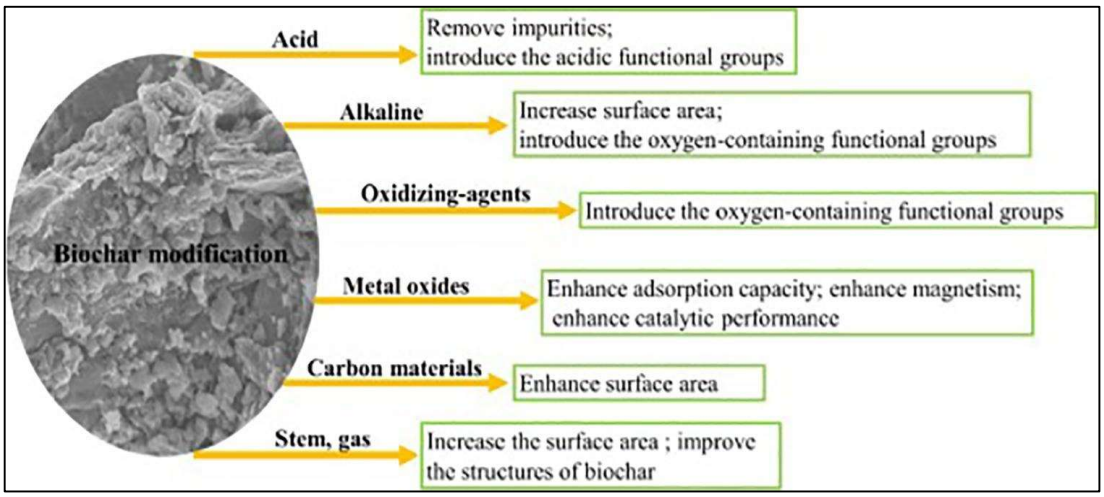


**Figure 1.2** Biochar activation and its effect on the final product **(Monga et al., 2022)**.

### 1.5.1 Thermal/Physical activation

Physical activation or thermal activation is the process by which an increase in porosity is induced due to a high temperature of about 700 and 900 °C in an oxidative environment (Prauchner and Rodríguez-Reinoso, 2012). Physical activation may eliminate the majority of the volatile carbon components of carbonized precursors, and closed holes in the biochar matrix can be opened and connected with other pores (N. Liu et al., 2015; W.-J. Liu et al., 2015). As a result, the specific surface area of physically activated biochar may be significantly increased, and a strong microporous structure with low mesopore intensity can be seen in the physically activated biochar matrix. Temperature, degree of activation, kind of precursor and activation agent (if any) are all important factors in physical activation (Sakhiya et al., 2020). The activation process is divided into two stages: the first stage involves the burning of scattered carbon, followed by the second step, which involves the burning of carbon contained in the aromatic rings (Murillo et al., 2004; Wigmans, 1989). Steam or $CO_2$ are the most often utilized gases for thermal activation. According to the general tendency stated in the literature, the greater the activation temperature and duration, the better the porosity increase. It does, however, result in an expanded pore size range. It is

difficult to control the activation process when air is employed as an activation agent because the interaction with air and char (rich in carbon) tends to move toward combustion if not controlled, resulting in increased ash production and lower activated carbon production. Nevertheless, it could be a preferred method for biochar activation since oxygen in the air takes less activation energy than $CO_2$ and steam, making the total activation process more cost-effective (Prauchner and Rodríguez-Reinoso, 2012).

#### *1.5.1.1 Steam activation*

The most typical reaction that occurs during steam activation is depicted in the following Equation (1) (Cunliffe and Williams, 1999).

$$C + H_2O \rightarrow CO + H_2 \quad (1)$$

In the study of Lima et al., 2010., biochar was created from broiler litter using rapid pyrolysis and then activated with steam. Later, the effect on the specific surface area, porosity, and adsorption of heavy metal ions ($Cu^{2+}$, $Cd^{2+}$, $Zn^{2+}$, and $Ni^{2+}$) were investigated. The specific surface area and pore volume rose from 136 to 789 $m^2/g$ and 0.052 to 0.344 $cm^3/g$, respectively, after steam activation (800 °C for 45 minutes). Also, it was discovered that the increased surface area and porosity improved metal ion adsorption ability. Furthermore, the projected activation energy, according to Random Pore Model, to activate the biochar by steam (175.9 kJ/mol) was lower than that of $CO_2$ (197.7 kJ/mol), due to the ease of carbon removal during chemical reactions (Aranda et al., 2007; Murillo et al., 2004).

#### *1.5.1.2 $CO_2$ activation*

Another frequent agent for activating char is $CO_2$. At temperatures above 800 °C, the most prominent reaction during $CO_2$ activation was the one in Equation (2) (Doja et al., 2022).

$$CO_2 + C \rightarrow 2CO \quad (2)$$

Referring to the study of Hofman and Pietrzak, 2011, an activation without any chemical pre-treatments at a temperature of 800 °C was not acknowledged to be successful in activating tire char with $CO_2$ (55 $m^2/g$), due to residual ash in the material that interfere with the process. According to different available researches, $CO_2$ is better suitable for producing micropores in tire char than steam (Molina-Sabio et al., 1996; Rodríguez-Reinoso et al., 1995; Ryu et al., 1993). This was because $CO_2$ was thought to begin the activation process with the production of micropores and then their subsequent expansion, as opposed to steam, which induced pore widening from the start of the activation process (Molina-Sabio et al., 1996).

### 1.5.2 Chemical activation

Chemical activation is a heat treatment technique that occurs when raw biochar combines with a chemical activating agent at temperatures ranging from 450 to 900 °C. In comparison to physical activation, the chemical activation mechanism is still uncertain. Inside the biochar, two types of processes occur that result in the production of micropores: dehydration and oxidation. Chemical activation has the following benefits over physical activation (Sakhiya et al., 2020):

- lower temperature;
- higher carbon yield;
- high surface area;
- qualitative and quantitative high micro-porosity;
- higher efficiency.

While producing an active carbon for adsorbent applications, these compounds were found to integrate carbonyl and hydroxyl functional groups in the final product surface (Gupta et al., 2011). Chemical activation, on the other hand, causes equipment deterioration. At high temperatures, the corrosiveness of this chemical agent can be strong. These substances, on the other hand, prevent tar formation by eliminating partial carbon molecules from biochar structures and volatile compounds (Azargohar and Dalai, 2008). Biochar is also produced via acid, alkali, and oxidation treatments to improve its physicochemical qualities. In chemical activation of biochar acids such as HCl, $ZnCl_2$, $MgCl_3$, $HNO_3$, $H_2SO_4$, and $H_3PO_4$ are frequently utilized, as well as alkalis such as KOH, NaOH, and $K_2CO_3$; and oxidants such as $H_2O_2$ and $KMnO_4$ (Sakhiya et al., 2020). Other chemicals that have been used are $K_2Fe_4$ (Adhikari et al., 2000), NaCl (Putra et al., 2019), and $BaCl_2$ (Benjamin and Sajjid, 2017). $ZnCl_2$, $H_3PO_4$, and KOH are widely used in industrial-scale processes (Gogotsi et al., 2009; Ströbel et al., 2006). The material-to-agent ratios are typically in the 1:0.5 to 1:3 range based on dry content. The effect of chemical activation is determined by the type of chemical utilized, the degree of mixing, the temperature, and the time interval between subsequent activations (Sakhiya et al., 2020). It was also discovered that pore volume shrank at high chemical concentrations, due to the physical collapse of the carbon structure. The activated biochar must be rinsed after chemical activation to remove the activation agent from the surface before it can be recycled. Thus, chemical activation on an industrial scale necessitates significant effort in the washing process to prevent environmental effects, which raises production costs (Smisek and Cerny, 1970).

### *1.5.2.1 Alkaline activation*

KOH was found to be the most efficient chemical, allowing char to be activated in three phases (Shilpa et al., 2018):

- the reaction of C and KOH:
  1. if the temperature is between 700 and 800 °C, $K_2O$ is produced;

$$K_2CO_3 \rightarrow K_2O + CO_2 \quad (3)$$

  2. if it is in the range from 400 to 600 °C $K_2CO_3$ is formed;

$$6KOH + 2C \rightarrow 2K + 3H_2 + 2K_2CO_3 \quad (4)$$

- removal of carbon in the form of CO or $CO_2$ at a temperature above 700 °C;

$$K_2CO_3 + 2C \rightarrow 2K + 3CO \quad (5)$$

$$C + K_2O \rightarrow 2K + CO \quad (6)$$

- C matrix expands due to the intercalation of K.

The processing temperature and KOH: char ratio were the most important parameters influencing the specific surface area during KOH activation (Acosta et al., 2016). There was a clear association between surface area and impregnation ratio, as the ratio rose the area increased, and this can be attributable to the micropore expansion (Acosta et al., 2016; Shilpa et al., 2018). By compacting the KOH-char mixture into a pellet before activation, it has been achieved a high surface area (955 $m^2/g$) with KOH activation (Rambau et al., 2018). NaOH, by raising the $O_2$ concentration of the char, obtain activation in the same way as KOH did (Alexandre-Franco et al., 2011; González-González et al., 2020; Saleh and Danmaliki, 2016). Although NaCl was the least harmful chemical employed for activation, it did not achieve a high surface area (28 $m^2/g$) but did achieve a large pore volume (6.64 $cm^3/g$) (Putra et al., 2019). Unfortunately, one significant disadvantage of this type of activation was the high cost of the chemicals utilized, as well as the requirement for char neutralization once the activation process was completed (Antoniou et al., 2014).

### *1.5.2.2 Acid activation*

Acids such as $HNO_3$, $H_2SO_4$, HCl, or $H_3PO_4$ are used to pre-activate the char, resulting in enhanced macro-porosity in the finished char (Alexandre-Franco et al., 2011; González-González et al., 2020; Manchón-Vizuete et al., 2005; Saleh and Danmaliki, 2016; Sirimuangjinda et al., 2012a, 2012b). For the chemical activation of char, researchers varied the activation temperature from 100 to 900 °C and the activation duration from 0 to 3 h. At 500 °C, $H_2SO_4$ had the largest specific surface area of 1066 $m^2/g$ (Sirimuangjinda et al., 2012a) and the lowest of 2.3 $m^2/g$ (Manchón-Vizuete et al., 2005) at 400 °C. It has been

proposed that increasing the temperature enhances cross-linking of char, resulting in increased surface area values (Sirimuangjinda et al., 2012a). This was made feasible by a more successful dehydrogenation at higher temperatures, resulting in a stronger char with more cross-linking. Furthermore, the variation of $H_2SO_4$ may have affected the outcomes, with enhanced ash removal for higher dosing, presumably because of the greater quantity of acid available for the removal of impurities, ash, from the char (Doja et al., 2022).

## 1.6 Applications of Biochar

Biochar is a hot topic among researchers due to its eco-friendliness, low cost, and simplicity of manufacture from diverse biomass employing thermochemical processes for addressing a wide range of environmental applications. Biochar is useful in removing contaminants and pollutants from soil and aquatic environments, which may be determined by the kind of biomass and pyrolysis temperature. Other applications for biochar include catalysts, wastewater treatment, composting, energy storage, carbon sequestration, and soil amendment. Many researchers are now working on the utilization in numerous areas and a multitude of the applications are discussed in the following sections. Table 1.1 shows a summary of applications in which biochar can be used.

**Table 1.1** Applications of biochar **(Yaashikaa et al., 2020)**.

| Applications | Aim | Benefits | Limitations |
|---|---|---|---|
| **Catalyst** | Act as supporting materials for direct catalysis | Low cost, more functional groups, large surface area | Efficiency may be less |
| **Energy storage** | Utilized as electrode materials | Low cost, highly porous, large surface area | Performance is low |
| **Soil amendment** | Enhancing soil fertility and quality and carbon sequestration | Low cost, minimize the emission of greenhouse gases, helps to retain nutrients and water, controls nutrient loss | Contamination of heavy metals and polyaromatic hydrocarbons may persist |
| **Adsorbents** | Removal of organic and inorganic pollutants in soil and aqueous system | Low cost and more oxygen groups present in biochar enhance adsorption of pollutants | Removal efficiency of pollutants is undetermined and heavy metals retain in the soil |
| **Composting** | Improving the structure of microbial population and carbon mineralization | Porous, reducing the emission of greenhouse gases, large surface area and retains nutrients | There may be a chance of heavy metals and other contaminants invading the soil |

## 1.6.1 Remediation of pollutants

The presence of pollutants in water and soil requires the research for low-cost methodology to remove them and biochar, due to is physical-chemical characteristics cloud be a possible option to face pollution. The contaminants can be divided in two groups, organic and inorganic pollutant, and the adsorption of them in the biochar surfaces can occur due to different mechanisms (Figure 1.3).

### *1.6.1.1 Organic pollutants*

Recent biochar applications emphasize the use of biochar to remove organic contaminants from soil and water. When added to soil, biochar adsorbs organic contaminants contained in the soil. Some of the organic contaminants include (Mondal et al., 2016):

- agricultural chemicals such as insecticides, herbicides, pesticides, and fungicides like atrazine, simazine, carbofuran, etc.;
- industrial chemicals such as polycyclic aromatic hydrocarbons (PAHs) including phenanthrene, catechol, pyrene, naphthalene, anthracene, etc.;
- antibiotics and drugs like acetaminophen, tetracycline, ibuprofen, sulfamethazine, tylosin, etc.;
- cationic dyes such as methylene blue, rhodamine, methylene violet, etc.;
- volatile organic compounds such as butanol, benzene, furan, trichloroethylene, etc.

When the concentration of biochar in soil is raised, the pesticide content, such as carbofuran, is reduced owing to adsorption or degradation. Because of the quality of -COOH and phenolic functional groups, pesticides may be adsorbed on the surface of biochar. The removal process is closely connected to the interaction of biochar with contaminants. In the presence of different functional groups such as -OH, -COOH, and others, the mechanism occurs via physisorption (electrostatic attraction/repulsion, pore diffusion, H-bonding, and hydrophobic) and chemisorption (electrophilic contact). Chemical transformation, partitioning, and biodegradation are some of the other removal pathways (Xiong et al., 2019).

Polluted water frequently contains volatile organic compounds, pesticides, phenolic compounds, nitrogen-containing compounds, dioxins, polynuclear aromatic compounds, raw materials for plastics, and other contaminants (Barco-Bonilla et al., 2013). Traditionally, these compounds are eliminated by adding oxidizing agents such as Fenton's reagent, $H_2O_2$, chlorine dioxide, ozone, and others, which react with the contaminants and generate oxygen-

containing functional groups known as disinfection by-products. These by-products cause cytotoxic, genotoxic, and mutagenic actions in living components (Shin et al., 2018). Recently, these drawbacks were solved by employing biochar as an adsorbent, which removed the organic molecules via an adsorption process (Zhou et al., 2020). The hydrophobic interaction, pore filling, electrostatic interaction, hydrogen bonding formation, and π-π interaction between organic compounds and biochar all contribute to the effectiveness of organic compound adsorption by biochar (Abbas et al., 2018). In the study of Maya et al., 2020, biochar has been developed to remove fluoride and chromium from industrial effluents. Magnetic biochar made from rice straw has been used to remove tetracycline from water (Dai et al., 2020). Paper sludge and wheat husk biochar were employed to remove 2,4-dichlorophenol from water (Kalderis and Akay, 2017).

#### *1.6.1.2 Inorganic pollutants*

Inorganic pollutants such as metals are toxic, non-biodegradable, and when present at higher concentrations pose a serious threat to all living creatures in the polluted environment. These inorganic contaminants enter the environment via industrial effluents or municipal wastewater (Zhang et al., 2013). The more carcinogenic and toxic are heavy metals (HMs) like chromium (Cr), lead (Pb), cadmium (Cd), mercury (Hg), arsenic (As), copper (Cu), selenium (Se), and others. Currently, the release of these HMs from industries such as metals finishing, electroplating, textiles, batteries, glass, mining, refining ores, pesticides, papers, fertilizers, tanneries, and several others has had a significant impact on the environment. (Alalwan et al., 2020). The prolonged buildup of such HMs can harm all living organisms by a well-known process known as biomagnification. To avoid such a dangerous situation, it is critical to remove HMs from discharged effluents using proper technology. In general, HMs in industrial effluents are removed via ion exchange, reverse osmosis, chemical precipitation, chelation/complexation, floatation, phytoremediation, chemical oxidation/reduction, ultrafiltration, membrane technologies, adsorption, electrochemical approaches, and other ways (Godwin et al., 2019). Removal of HMs from industrial effluents by adsorption process is very simple, versatile and less expensive, been not affected by secondary problems like the formation of sludges, disposal, and others which resulted in further complications (Jeyasubramanian et al., 2021).

Interestingly, HMs in industrial effluents have been removed by employing biochar as an adsorbent, however, the process is dependent on the type of the HMS. The HMs are divided into two types:

- cationic such as Hg(II), Cd(II) and Pb(II);
- anionic such as Cr(VI) and As(V);

Surface treatment using oxidizing agents such as $KMnO_4$, $K_2Cr_2O_7$, and others provides oxygen-containing functional groups to the biochar and promotes the removal of cationic HMs. The surface modification allows for the interchange of $H^+$ ions with cations present in effluents due to the production of oxygen-containing functional groups such as -COOH, -OH (Jeyasubramanian et al., 2021).

Magnetic particle or metal oxide-loaded biochar improves anionic HM elimination. Three techniques are used to remove anionic HMs from effluents: anion exchange, adsorption with reduction, and electrostatic attraction. Soaking the biomass feedstock in $FeCl_3$ solution produces magnetic particle-impregnate biochar. After drying, it is pyrolyzed to make biochar impregnated with the selected metal ion, which improves the exchange of anionic HMs from the effluent (Khitous et al., 2016). The adsorption and reduction of Cr(VI) are then assisted by the oxidation of organic contaminants, resulting in the production of Cr (III). The anionic form of Cr(VI) was transformed by researchers into the cationic form of Cr(III), which was subsequently removed by biochar derived from rice husk (T. U. Han et al., 2020). Another aspect that influences removal efficiency is pH, however, the process is dependent on the metal. For example, Cr removal was shown to be greatest at pH 2.0, but Pb removal was highest between pH 2.0 and 5.0 (Yaashikaa et al., 2020).

Furthermore, inorganic anions such as phosphate and nitrate found in water and responsible for eutrophication were removed using magnetic biochar made from corn straw activated with $FeCl_3$ (Tan et al., 2020). They concluded that the one-step technique reduces As(V) and $NO_3^-$ levels by 5.94 and 7.69 times, respectively, as compared to pristine biochar. Also, iron-modified biochar has been produced from pyrolyzed activated sludge waste and found that the maximal phosphate adsorption capacity of $FeCl_3$-modified biochar was 111.0 mg/g (Q. Yang et al., 2018).

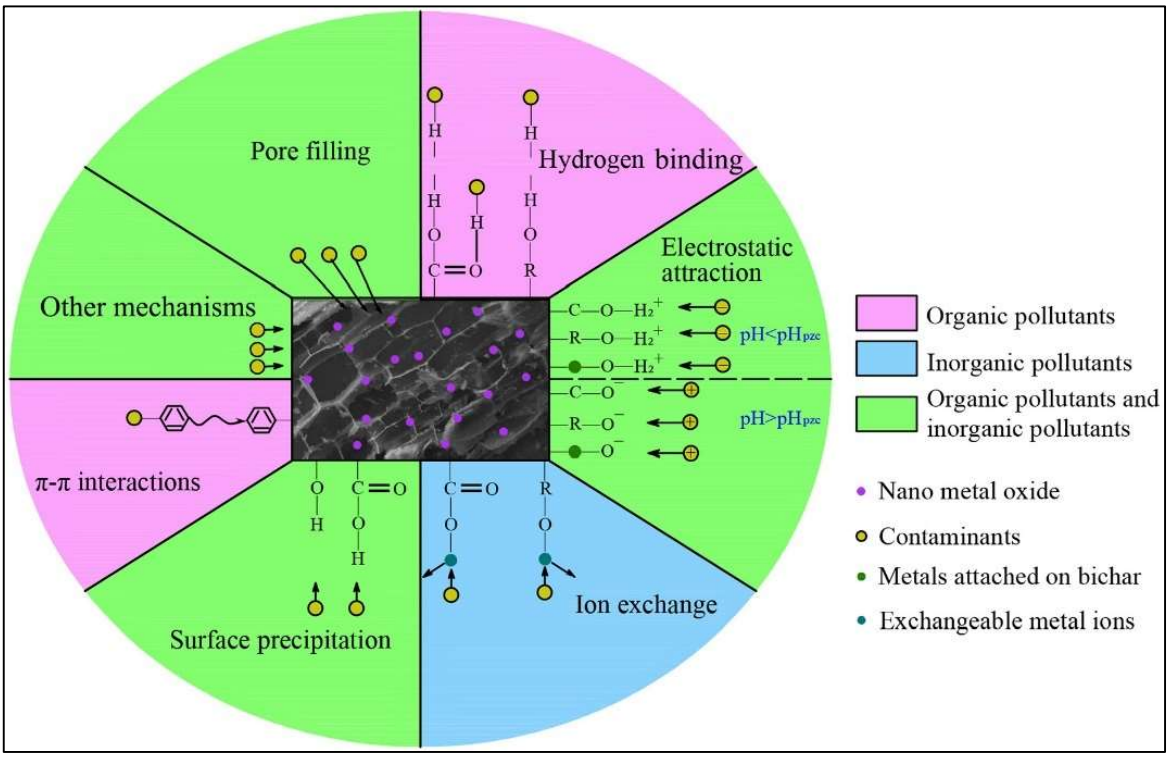


**Figure 1.3** Adsorption mechanism for the different types of pollutant **(Zhao et al., 2021)**.

## 1.6.2 Catalyst

Biochar can operate as a catalyst in a variety of industries, including agriculture, environment, and energy. Due to the general characteristics of biochar, it is regarded as a potential catalyst. Because of the functional groups presence, a high surface area is critical for biochar catalytic performance. Biochar has a wide range of applications as a catalyst, including biodiesel synthesis, energy generation, tar removal, waste management, syngas production, electrodes in microbial fuel cells, chemical industries, and contaminants removal.

### *1.6.2.1 Energy production*

The formation of tar during biomass gasification process is unpleasant because it causes pollution and clogging of downstream operations, as well as a loss in energy efficiency. Tar catalytic transformation has the capacity to convert tar to hydrogen ($H_2$) and carbon monoxide (CO). These two elements, $H_2$ and CO, are regarded as critical components of syngas. The char formed from various biomass, such as corn straw char and rice straw char, affects tar removal. Thus, char varieties impact tar removal efficiency. With increasing char particle size, the tar removal effectiveness drops. This is because the surface area and the

active sites impact the removal efficiency. Biochar boosts hydrogen generation during the gasification/pyrolysis process (Yaashikaa et al., 2020).

#### *1.6.2.2 Biofuel production*

Biofuel is an excellent replacement for petroleum products since it is biodegradable, non-toxic, renewable, and has equivalent fuel properties to fossil fuels. Transesterification of vegetable oils or esterification of free unsaturated fats (FFAs) with alcohols can be used to produce biofuel. Biochar catalysts are employed during the transesterification and esterification processes (Yaashikaa et al., 2020). Biofuel manufacturing is a new technology that is seen as a viable alternative to petroleum fuels. Because of its renewability and simplicity of storage, biodiesel is considered a sustainable alternative to petroleum diesel. Biodiesel is made up of fatty acid alkyl esters that are formed by the transesterification or esterification of animal fat, vegetable oil, and microalgal oil (Chai et al., 2012). Poor quality or waste oils contain a lot of FFAs, which will most likely reduce the reaction rate and biodiesel production. As a result, the development of catalysts capable of accelerating both esterification and transesterification at the same time is intriguing. The acid-functionalized biochar catalysts were made from biomass via two major processes: sulfonation with vaporous $SO_3$ or liquid $H_2SO_4$ and carbonization (Yaashikaa et al., 2020). CaO biochar, $K_2CO_3$ biochar, and KOH functionalized biochar were also used as catalysts for biofuel production. These catalysts have demonstrated a high biofuel output and good reusability, therefore, they can be considered a viable alternative to conventional transesterification catalytic systems (Chen et al., 2011).

#### *1.6.2.3 Control of air pollutants*

In the literature, biochar has been used as a low-temperature catalyst for selective catalytic reduction. Studies on biomass like sewage sludge and rice straw for synthesizing biochar and using it as low-temperature catalysts with ammonia as a reducing agent have been published. The removal efficacy of the char was evaluated after being physically or chemically activated. Chemical activation outperformed physical activation in terms of removal efficiency. Chemical characteristics, such as functional groups and adsorption sites, were shown to be critical elements for better removal. Under the catalysis effect of biochar, sulfate and free radicals were released. The combination increased the catalytic activity of the catalyst due to the biochar (Yu et al., 2009; Zheng et al., 2010).

#### *1.6.2.4 Energy storage and supercapacitors*

The storage of energy in electrical items is critical for consumer use of electrical and electronic equipment. Supercapacitors are energy storage devices that attract interest owing to their quick charge and discharge capacity, high power density, and extended cycle stability, whereas rechargeable batteries have a high energy density and a lower charge/discharge rate (Nag et al., 2011). The performance of an energy storage device is predicted by the electrode materials. These electrode materials have a large surface area and a porous structure, which offer the necessary active sites for the oxidation process. Carbon nanotubes, activated carbon, graphene, and other materials are commonly utilized as electrode materials. Because these carbon materials are costly, their use is limited. Because of this disadvantage, the use of biochar as an electrode is gaining popularity. Biochar, like carbon material, has a high surface area, is porous, and is less expensive. Biochar has the potential to be used as an electrode in microbial fuel cells and supercapacitors (Rhodes et al., 2008).

### 1.6.3 Soil amendment

Biochar can be used in agriculture for a variety of purposes, such as improving soil fertility and structure (Sopeña et al., 2012), increasing soil cation exchange capacity, supporting carbon sequestration and reducing the effect of greenhouse gases (Venegas et al., 2016), improving productivity by maintaining water retention and enhancing microbial activity by reducing nutrient leaching (Bian et al., 2013). Furthermore, the use of biochar has been regarded as a feasible strategy for remediating polluted soil with harmful contaminants such as heavy metals, pesticides, hydrocarbons, and others. Biochar from Moso bamboo chips was synthesized and utilized to study the leaching loss of fixed organic carbon and soluble nitrate nutrients, revealing the mitigating impact of biochar during spring, fall, and winter (Lei et al., 2018).

### 1.6.4 Carbon sequestration

Climate change is raising concerns about reducing $CO_2$ emissions into the atmosphere. Soil plays an important part in the carbon cycle, which has a direct impact on climate change. Carbon sequestration in soil is a sustainable approach for lowering $CO_2$ emissions (Méndez et al., 2012). Because biochar is barely resistant to destruction by bacteria due to the presence of aromatic structures, it has a favorable effect on carbon sequestration in soil. Many studies have been published on biochar's ability to sequester carbon. However, because both good

and negative impacts were found, no optimal outcomes were reached. Carbon emissions were shown to be increasing as well as decreasing (Jiang et al., 2012; Moon et al., 2017). The carbon content of biochar is divided into two types: liable carbon and recalcitrant carbon. Liable carbon is easily used by microorganisms during biochar application, resulting in higher carbon mineralization in the early stage. As a result, the use of biochar restored carbon mineralization. Recalcitrant carbon, on the other hand, remains in the soil for a longer period (Puga et al., 2015). As a result, the carbon fixed by biochar application (amendment) exceeds the carbon released via relevant liable carbon mineralization. Recently, $CO_2$ adsorption was achieved by employing biochar because of its outstanding features such as high porosity and greater surface area. Researchers have examined the absorption of $CO_2$ by magnesium-loaded biochar produced from pyrolyzed walnut shell (Lahijani et al., 2018). The selective absorption of $CO_2$ was studied in the presence of competing gases such as $CH_4$, CO, and $N_2$. They also said that the metal-impregnated biochar absorbed 82.0 mg/g and the pure biochar 72.6 mg/g. Similarly, another study documented that, the use of magnesium oxide impregnated biochar made from sugarcane bagasse to remove $CO_2$, with thermogravimetric measurement proving its effectiveness (Creamer et al., 2018). However, the impact of biochar on carbon sequestration is yet unclear. The impact varies depending on the type of biomass and the pyrolytic conditions. Because pyrolysis conditions have a significant impact on the physico-chemical features of biochar, it is critical to establish a link between reaction conditions and the effects of biochar on carbon sequestration (Yaashikaa et al., 2020).

### 1.6.5 Wastewater treatment

Biochar is a solid substance with a large surface area and porosity, making it an intriguing choice in wastewater treatment. Biochar has been demonstrated to be a good medium for capturing nutrients from wastewater and can later be used in soil as an amendment. Because of its high porosity and strong adsorption qualities, which allow pollutants to be collected on its surface, biochar is successfully created for contaminants removal from wastewater. Carbonized materials and crude biowaste are increasingly being used in wastewater treatment. The production of activated carbon has a strong natural effect, as seen by biochar's decreased greenhouse gas emissions. Similarly, the production of activated carbon (97 MJ/kg) necessitates a significantly larger energy demand than biochar (6.1 MJ/kg). As a result, biochar may outperform activated carbon in the removal of hazardous pollutants from wastewater while considering greenhouse gases emissions, energy demand, and therefore

production costs (Yaashikaa et al., 2020). Of all the possible application this is the one chosen for the biochar produced in this study. Due to its characteristics, it was decided to assess the possible use of the biochar as an adsorbent for the treatment of wastewater, targeting pharmaceutical compound, one of the emergent problems in the wastewater treatments field, aspect that will be discussed in the next chapter.

# CHAPTER 2

# Pharmaceuticals presence in the environment

## 2.1 Presence and effects of pharmaceuticals in the environment

The detection of a vast number of so-called emerging micro-pollutants in surface waters around the world has become a source of concern for the global community. Emerging pollutants exhibit ubiquity, persistence, and non-biodegradability. Furthermore, pharmaceutical compounds such as analgesics and anti-inflammatory drugs, contraceptive hormones, antibiotics, beta-blockers, lipid regulators, psychiatric drugs, and many others are particularly prone to bioaccumulation in animal and human organisms and are typically eliminated from the body in the form of metabolites, which can sometimes be much more harmful than the original compounds (Fent et al., 2006; Oaks et al., 2004). These compounds, due also to the exponential increase in the human population, are more frequently detected as environmental pollutants (Evgenidou et al., 2015; Lapworth et al., 2012). After human and veterinary use, a large number of pharmaceutical chemicals, about 4000 in Europe, are released into the environment (Mompelat et al., 2009). The main sources of medicines in waters are hospitals, pharmaceutical industries, wastewater treatment plant (WWTP) effluents, and landfill leachates (Holm et al., 1995). Antimicrobial resistance (AMR), a decrease in plankton variety, and restriction of human embryonic cell growth are some of the rising potential toxic effects on life forms residing in the aquatic and terrestrial environment (Nawab et al., 2015; Zhang et al., 2014). Also, the AMR of pathogenic bacteria and antagonizing hormones inside the human body are both the result of the constant action of pharmaceutical substances present in the environment, even at low concentrations, so undermining the usefulness of pharmaceuticals (Ternes et al., 2002). It should also be acknowledged that pharmaceuticals are frequently detected in the environment as mixtures. Despite low environmental concentrations, typically at trace levels (ng/L to g/L), pharmaceuticals can still cause harm due to cumulative effects and continuous exposure, which is common in aquatic ecosystems (Dordio et al., 2009). As a result, multiple investigations have found that their toxicity to non-target organisms can appear at environmentally relevant concentrations due to synergic effects (Pomati et al., 2008) and due to their long persistence in the environment (Saravanan et al., 2014). Non-steroidal anti-

inflammatory drugs have analgesic, antipyretic, and anti-inflammatory properties. Ibuprofen, a member of this family of drugs, is one of the most widely used chemicals in the world (e.g., 345 t in Germany in 2001) and is commonly found in WWTP effluents, surface waters, and seawater (Ternes et al., 1998; Wiegel et al., 2004). Antibiotics, anti-inflammatory drugs, lipid-lowering agents, and anticonvulsants are the most commonly detected pharmaceuticals in the aquatic environment (Boudrahem et al., 2017), and their toxicity has been summarized in Figure 2.1. Antibiotics enter the environment through a variety of human activities. Animals and humans are the principal users of antibiotics, and as such, they are the leading causes of antibiotic contamination in the environment. An antibiotic is metabolized in the body and its residue is expelled, mostly in feces (up to 75%) and/or urine (up to 90%) (Gelband et al., 2015). These contaminants are then transferred with sewage to wastewater treatment plants, where they can build up in sewage sludge that after treatment can be utilized as a soil amendment. In the last decades, fruit (Ben et al., 2019), vegetables (Ahmed et al., 2015; Li et al., 2014), meat (Tao et al., 2012; H. Wang et al., 2017), fish and shellfish (Chiesa et al., 2018; He et al., 2016), milk (Zheng et al., 2013), eggs (Yamaguchi et al., 2017), and even drinking water (Boleda et al., 2014; Collier, 2012) have been shown to contain traces of antibiotics. As a result of consuming contaminated foods, people have become "secondary consumers" of antibiotics (Krasucka et al., 2021).

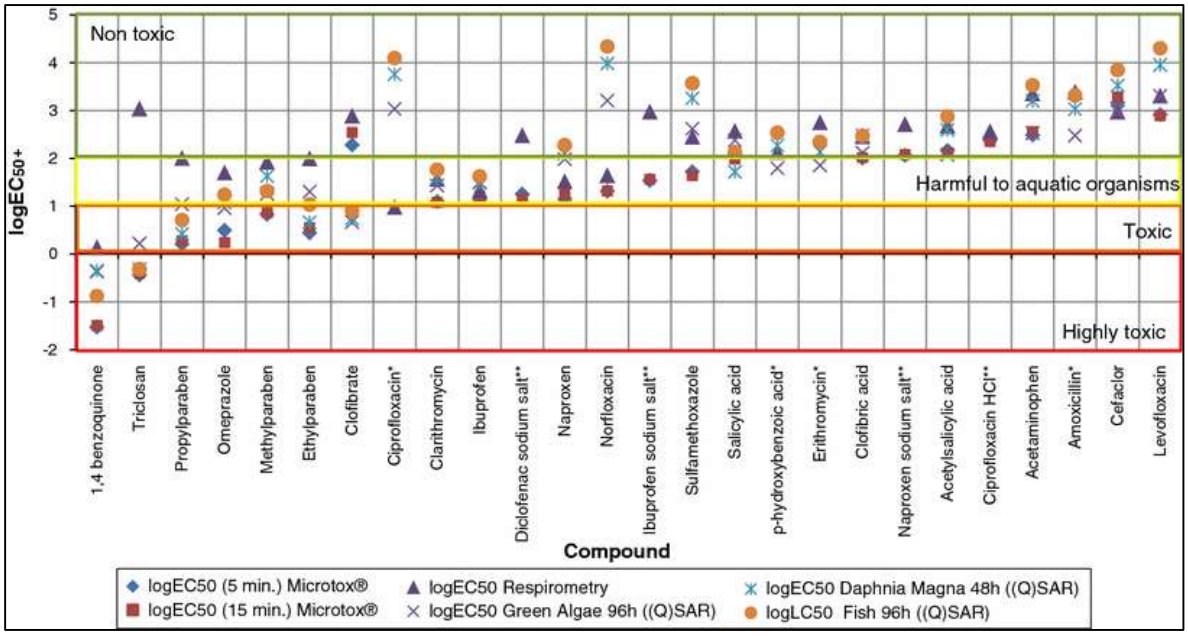


**Figure 2.1** Toxicity of pharmaceuticals for the aquatic life **(De García et al., 2014)**.

## 2.2 Ibuprofen

Ibuprofen (IBP) is a colorless and crystalline solid, and it has a characteristic odor (de Oliveira et al., 2019). Its general chemical structure is shown in Figure 2.2 and its main properties are detailed in Table 2.1.

The compound is one of the so-called non-steroidal anti-inflammatory drugs (NSAID). IBP is obtained from propionic acid, and it is considered the first of the propionics (2-(4-Isobutylphenyl) propanoic acid). It was developed by Stewart Adams in 1960 while researching a safer alternative for aspirin. IBP was patented the following year of its discovery and first launched for the treatment of rheumatoid arthritis in the UK and USA in 1969 and 1974, respectively. IBP is available by prescription and also it was the first NSAID available over the counter. It is considered to be one the safest NSAIDs, generally causing no harm after administration but, rarely, undesired clinically apparent effects, such as serious acute liver injury, can occur (PubChem, 2021). So it is not unexpected that it is one of the most marketed drugs, and its traces are present both in industrial and municipal wastewater discharges (Chakraborty et al., 2018; Mompelat et al., 2009).

The pKa of this drug (Table 2.1) shows a weakly acid character so having a low tendency to be adsorbed into sludges of WWTPs (Álvarez-Torrellas et al., 2016). Therefore, the removal from aqueous media has to take place to reduce the content of this compound. However, IBP removal via traditional wastewater treatment plants has been proved difficult, because of its moderate water solubility (21 mg/L) and high polarity (Jiang et al., 2015).

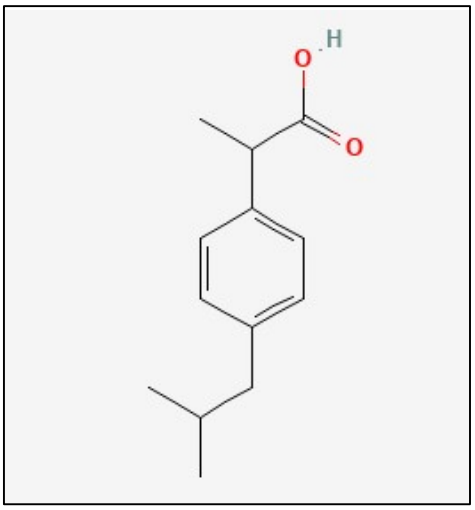


**Figure 2.2** Chemical Structure Depiction of Ibuprofen **(PubChem, 2021)**.

**Table 2.1** Ibuprofen properties **(PubChem, 2021)**

| | |
|---|---|
| **CAS ID** | 15,687-27-1 |
| **IUPAC Name** | 2-(4-Isobutylphenyl) propanoic acid |
| **Chemical Formula** | $C_{13}H_{18}O_2$ |
| **Molar mass** | 206.28 g/mol |
| **Specific gravity** | 1.03 |
| **Solubility in water (at 25 °C)** | 21 mg/L |
| **Boiling point** | 157 °C |
| **pKa** | 4.91 |
| **Log Kow** | 3.97 |
| **Melting point** | 75–77 °C |

### 2.2.1 Source and presence of IBP pollution

Researchers can now identify the causes of contamination of particular contaminant species based on rigorous monitoring and assessment of water (Ighalo et al., 2021b, 2021a). NSAIDs are often found in the environment in quantities of ng/L and g/L, and even at these amounts, they can have severe ecotoxicological consequences (Davarnejad et al., 2018). IBP, like other pharmaceutically active chemicals, enters the environment via hospital and medical effluents (Caicedo et al., 2020), pharmaceutical wastewaters (Davarnejad et al., 2018), and veterinary usage (Y. Han et al., 2020). IBP was found in WWTP effluents at greater concentrations than other medications (Balakrishna et al., 2017). Moreover, IBP has one of the highest concentrations in estuaries across the world, ranging from 18 to 6297 ng/L (Letsinger et al., 2019).

### 2.2.2 Ecotoxicity Source and presence of IBP pollution

The ecotoxicology of IBP is examined in order to comprehend the harmful consequences of its presence in the aquatic environment. IBP is routinely discovered in surface waters at ng/L, and pharmaceutical effluent is the primary cause of pollution (Aguilar-Romero et al., 2020) It has been discovered that while acute effects of IBP in the aquatic environment are minimal, they may be severe when combined with diclofenac, another NSAID (Cleuvers, 2003). IBP caused nonpolar narcosis in algae and "*Daphnia"* and conforms to the concentration addition notion (Cleuvers, 2003). It has been demonstrated that IBP influences the metabolism and substrate attachment ability of Baltic Sea blue mussels "*Mytilus edulis trossulus*" (Ericson

et al., 2010). Biomagnification was detected, so the concentration of IBP in the animal cells was found to be greater than in the contaminated aqueous environment around them. Even if not toxic, it has been discovered that IBP and its sodium salt are hazardous to aquatic species in studies on "*Vibrio fischeri"*, algae, crustaceans, and wastewater treatment plant biomass, Figure 2.3 (De García et al., 2014). IBP has an endocrine-disrupting impact on Japanese medaka "*Oryzias latipes"* and freshwater *"cladocerans Daphnia magna"* and *"Moina macrocopa"* (Han et al., 2010). In vitro biomarker studies on the haemocytes of the freshwater bivalve zebra mussel "*Dreissena polymorpha"*, it was revealed that IBP has a higher genotoxic potential than other NSAIDs such as paracetamol and diclofenac (Parolini et al., 2009). Also, a chronic cyto-genotoxic impact was detected in mussel haemocytes (Parolini et al., 2011). IBP has been found to promote the growth of the cyanobacterium "*Synechocystis sp*." but reduced the growth of the duckweed "*Lemna minor*" (Pomati et al., 2004). Keeled Ramshorn snails "*Planorbis carinatus*" have shown acute and chronic effects (Pounds et al., 2008). The chloroplast energy transduction and electron transport chain of the diatom "*Phaeodactylum tricornutum"* has been demonstrated to be inhibited by IBP (Silva et al., 2020). In addition, the pharmaceutical has been demonstrated to be somewhat harmful to *"Aliivibrio fischeri"* (Zuriaga et al., 2019). Based on these findings, it is reasonable to conclude that IBP should be reduced in hospital and medical effluents, as well as pharmaceutical wastes, before they are released into the environment.

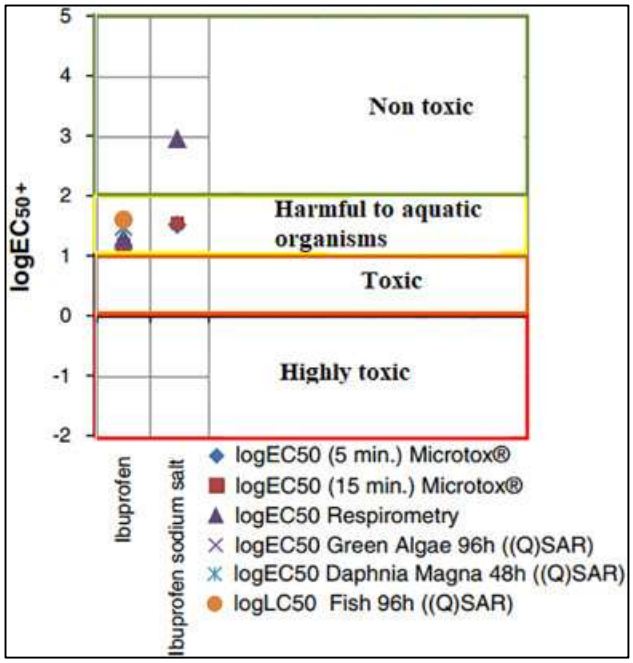


**Figure 2.3** IBP and its sodium salt toxicity **(De García et al., 2014).**

## 2.3 European Union strategy against pharmaceutical pollution

To address the problem of pharmaceutical presence in the environment, the European Union (EU) has studied some strategies to reduce the knowledge gap about the presence and effects, to define the necessity of reducing and removing pharmaceutical products from the environment, especially from the aqueous ecosystems.

The document created by the European Commission in March,2019 is entitled "*European Union Strategic Approach to Pharmaceuticals in the Environment*" (PiE) in which the problem is exposed, the objectives are well defined along with the required actions to achieve the targeted goals ("Strategic Approach to Pharmaceuticals in the Environment - Environment - European Commission," 2019).

Here follow some of the objectives taken from PiE at point 3 "*The objectives of the strategic approach*" which are more related to this study:

- identify actions to be taken or further investigated to address the potential risks pharmaceutical residues in the environment, not least to contribute to the EU's action on combatting antimicrobial resistance;
- encourage innovation where it can help to address the risks and promote the circular economy by facilitating the recycling of resources such as water, sewage sludge and manure;
- ensure that actions to address the risk do not jeopardize access to safe and effective pharmaceutical treatments for human patients and animals.

The PiE at point 5 "*Actions*" explains that measures have to be taken at EU and/or Member State level to address the possible environmental impacts of pharmaceutical substances. Besides, strategies have to be installed to control the sources (consumption of pharmaceuticals) and the end-of-pipe controls (improved wastewater treatment).

Here are the Actions taken from point 5.4 that are more related to this study:

- Concerning urban wastewater treatment:
    1. Use EU programs to invest in technologies to improve the efficiency of removal of pharmaceuticals (and antimicrobial resistance genes);
    2. As part of the study supporting the evaluation of the existing urban wastewater treatment legislation, assess whether it sufficiently controls pharmaceutical emissions and investigate the feasibility of upgrading selected urban wastewater treatment plants to more advanced treatment technologies.

In 2020, the PiE has been followed by an Update on Progress and Implementation of the PiE, and on the 17th of September, the European Parliament adopted a resolution of the European Union Strategic Approach to Pharmaceuticals in the Environment (2019/2816(RSP)). This renovated attention to the argument has been the result of the European Green Deal and the COVID-19 pandemic.

As the problem is becoming more serious and government institutions are taking aware of it, it is highly probable that in the coming years new regulation will be released about wastewater treatment and pharmaceuticals removal, hence the necessity of investigating efficient and cost-effective methods for eliminating these pollutants.

# CHAPTER 3

# Materials and Methods

## 3.1 Biochar Production

### 3.1.1 Feedstock

Thermal-insulation panels, produced with recycled textiles, were used as the raw material for biochar production, supposing to treat them at the end of their lifecycle. Their physico-chemical characterization has been carried out in a previous phase of this study. The raw material is shown in Figure 3.1 and its characteristics are reported in Table 3.1. The material presented a big heterogeneity to the eye, in terms of both composition and size of the components, this is probably due to the recycled nature of the product. The unprocessed source is mainly shredded jeans and other cotton fibers, but also synthetic ones are presents.

**Table 3.1** Summary of the raw material characterization obtained in the previous study.

| **Bio-based building material** | | **Recycled textile** |
|---|---|---|
| **Ultimate analysis (wt% on dry basis)** | **C** | 45.14 ± 0.40 |
| | **H** | 5.34 ± 0.10 |
| | **N** | 1.50 ± 0.02 |
| | **S** | < LQ |
| | **O*** | 48.55 ± 0.40 |
| **Proximate analysis (wt% on dry basis)** | **Moisture (%)** | 4.99 ± 0.10 |
| | **Ash (%)** | 0.97 ± 0.05 |
| | **Volatile matter (%)** | 75.05 ± 0.60 |
| | **Fixed carbon (%) **** | 18.99 ± 0.50 |
| **Biomass composition (wt% on dry basis)** | **Hemicellulose (%)** | 31.28 |
| | **Cellulose (%)** | 30.98 |
| | **Lignin (%)** | 6.41 |
| **Heating value** | **HHV (MJ/kg)** | 18.05 ± 0.40 |
| | **LHV (MJ/kg)** | 16.97 ± 0.40 |

*: Oxygen calculated from the difference of C, H, N, S and Ash

**: Fixed carbon calculated from the difference from moisture, ash and volatile matter

< LQ: Lower than the quantification limit (LQ < 0.2 % on CHNS-O analyzer)

**Figure 3.1** Thermal insulation panels

### 3.1.2 Feedstock pre-treatment

The pre-treatment applied to the raw material has been a mechanical treatment. The panels, after being cut, have been pelletized manually by applying a pressure of 1 ton/cm$^2$ to ensure enough structural cohesion of the fibers as illustrated in Figure 3.2.

**Figure 3.2** Pellets of recycled textiles

### 3.1.3 Biochar

The pellets were pyrolyzed in a semi-rotating Inconel reactor (Figure 3.3) under the following conditions:

- temperature of 550 °C;
- heating rate of 10 °C/min;
- dwelling time of 2 hours at the fixed temperature;

- intake of nitrogen gas ($N_2$) with a flow rate of 750 mL/min during pyrolysis to keep an oxygen-depleted environment.

At the end of this process, biochar (BC) was recovered for further analysis (Figure3.4)
The yield of the BC production was obtained using the following Equation (7).

$$Y = \frac{W}{W_0} \cdot 100 \quad (7)$$

Where Y (%) is the yield, W (g) the dry weight of the products and $W_0$ (g) the dry weight of the raw material before the thermal treatment.

**Figure 3.3** Furnace with Inconel reactor.

**Figure 3.4** BC obtained after the pyrolysis of the recycled textiles pellets

### 3.1.4 Steam Activated Biochar

Steam activated biochar (SABC) was produced by steam gasification of the pelletized biomass in the same semi-rotating Inconel reactor. The gasification process has been preceded by pyrolysis to reach the temperature at which the water becomes active. The operating conditions of steam pyro-gasification are the following:

- temperature of 850 °C;
- heating rate of 10 °C/min;
- dwelling time of 1 hour at the fixed temperature;
- intake of $N_2$ with a flow rate of 750 mL/min during the ramp and 570 mL/min during the dwelling time.
- intake of water ($H_2O$) during the dwelling time of 0.7 mL/min.

During the process, the non-condensable gases at the outlet of the ice-cooled condenser were monitored using gas chromatography (Micro GC Fusion gas analyzer) at a regular time interval of 3 minutes; while condensable compounds (bio-oil and tars) were recovered at the

end of the experiment for the mass balance. The complete apparatus used is shown in the Figure 3.5. The SABC obtained is shown in Figure 3.6. The yield was estimated with the Equation (7).

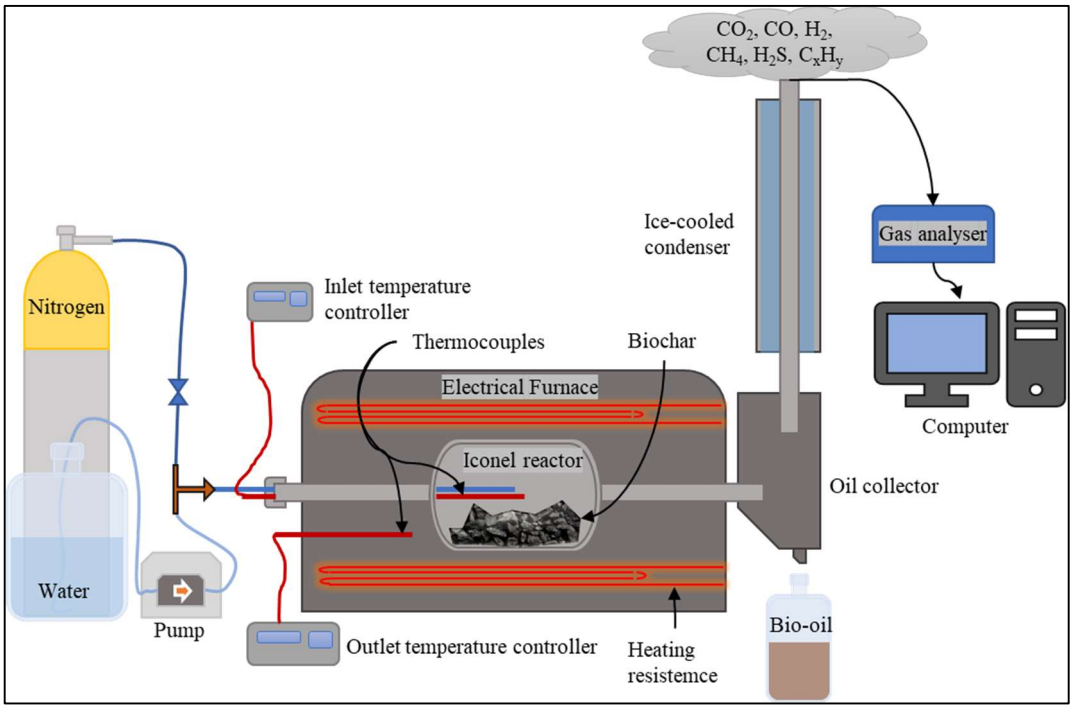


**Figure 3.5** Schematic representation of the apparatus used for the production of the SABC.

**Figure 3.6** SABC produced by steam activation of the pellets.

### 3.1.5 Post-treatment

To obtain a representative fraction of the product in each of the experiences carried out, the obtained biochars have been crushed and sieved. The size fraction selected for running the kinetics and isotherms has been $0.5<\Phi<0.8$ mm and $0.5<\Phi<1.6$ mm for the column, that needed a large fraction and could accommodate bigger particles. The sieved pellets used in the adsorption column are shown in Figure 3.7.

**Figure 3.7** SABC after sieving.

## 3.2 Characterization

To assess the chemical and physical properties of the biochars, a variety of analyses have been carried out, which are described in the following.

### 3.2.1 BET

To obtain the surface area and pore size of the adsorbents produced, the Brunauer-Emmett-Teller (BET) analysis has been done. The investigation has been preceded, as follows, by a drying phase at 105°C for 24 h and a degassing phase at a heating rate of 10 °C/min until 350°C maintained for 48 h under vacuum conditions of about 30 mmHg in the Micrometrics Smart VacPrep apparatus. BET analysis was realized in *Micromeritic 3Flex unit-1* using nitrogen as adsorbent, at 77 K (-195,618 °C), the boiling temperature of liquid nitrogen (Figure 3.8).


**Figure 3.8** BET quartz glass tube (on the left), vacuum degassing unit (in the middle) and *Micromeritics 3Flex* unit for surface area determination (on the right)

### 3.2.2 Ash content

To obtain the ash content, the products have been dried at 105 °C for 24 h and then burned in a muffle furnace (Figure 3.9) at 815 °C for 4 hours. The samples have been weighed before and after burning, the difference between the two weights divided by the initial one is the ash content.


**Figure 3.9** Muffle furnace.

### 3.2.3 pH point of zero charge

To find the pH point of zero charge ($pH_{pzc}$), BC and SABC have been crushed. To carry out the experience, 50 mL of $10^{-2}$ M NaCl solution was placed in different flasks along with 0.15 g of adsorbent. Then, the pH was adjusted to a value between 2 and 12 by adding HCl or NaOH 0.1 M solutions. After 5 days under agitation at room temperature (20 °C), the final pH has been measured (Figure 3.10). The $pH_{pzc}$ value is found at the point where the curve $pH_{final}$ vs $pH_{initial}$ crosses the line $pH_{final} = pH_{initial}$.

**Figure 3.10** pH meter used for the measurement of the pH point of zero charge.

### 3.2.4 Chemical Characterization

To determine the chemical composition of the product an elemental analysis has been carried out. The BC and SABC have been dried at 105 °C and then powdered using a ball milling apparatus. Samples between 0.5 and 1 mg have been used for the measurements. The *FLASH-EA 1112-SERIES CHNS-O Analyzer* has been used (Figure 3.11). The percentage of C, H, N, and S have been obtained directly from the analysis, meanwhile, the fraction of Oxygen (O) has been obtained by difference.

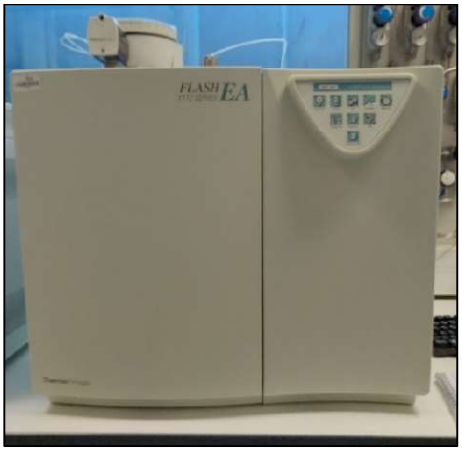


**Figure 3.11** CHNS-O Analyzer.

## 3.3 Absorption Kinetics

During this work, numerous kinetic experiments have been performed with the aim to find the optimum conditions. The IBP molecule used has been the IBP sodium salt. This choice has been made to avoid the problem of the low solubility of the molecule without using an organic solvent, that could compete for the active site in the adsorption process. Different solutions of IBU have been prepared with deionized water (DW) and tap water (TapW) at concentrations of 50 and 100 mg/L. Bottles were first filled with 400 mL of DW or TapW. Next, the adsorbent has been inserted in various quantities, starting from 100 mg to 700 mg (crushed) and 1g (full pellets). The bottles were left stirring for at least 24 h to stabilize the pH. Subsequently, 400 mL of IBU sodium salt solution (100 and 200 mg/L) was transferred into the bottles. The mixing speed was fixed at 200 rpm and the flasks were kept in a room with temperature controlled at 20 °C during the kinetics (Figure 3.12).

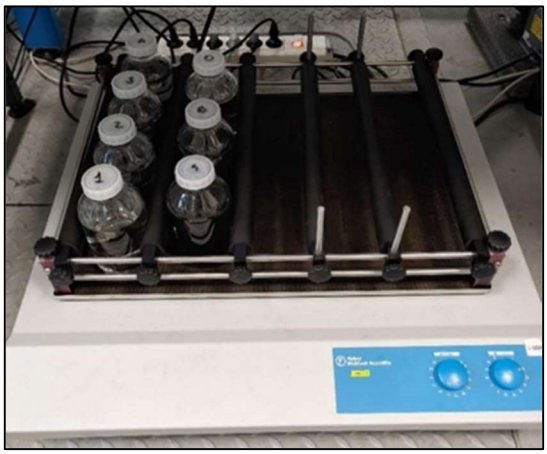

**Figure 3.12** Shaker use for mixing.

To monitor the absorption kinetics, the IBU concentration was assessed by periodic sampling at different time intervals for a minimum of 5 days and evaluating the samples absorbance using a UV-Visible spectrophotometer, shown in Figure 3.13 (*Shimadzu UV-1800 UV/Visible Scanning Spectrophotometer; 115 VAC*), at the wavelength of 222 nm after filtering the samples with 45 µm filters. The absorbance values have been converted into concentration using Equation (8) obtained with the calibration curves.

$$C_t = k \cdot Abs \tag{8}$$

Where $C_t$ is the concentration at the time t in mg/L, k is the conversion factor and Abs is the absorbance value measured.

Besides, the pH of the flasks has been monitored. Additionally, a blank bottle (without adsorbent) has been prepared and kept under the same conditions to obtain an initial concentration and to control if any degradation of IBU molecules occurs.

The amount of IBU adsorbed has been calculated by using Equation (9).

$$q_t = \frac{(C_o - C_t)}{m} \cdot V \tag{9}$$

Where $q_t$, in mg/g, is the amount of IBP adsorbed at the time t per unit mass of adsorbent, $C_0$ is the initial concentration at $t_0$ in mg/L, Ct is the concentration at t time, m is the amount of adsorbent in g, and V is the volume of the solution in L.

**Figure 3.13** UV/Visible Scanning Spectrophotometer.

### 3.3.1 Kinetics Modeling

To fit the data to the model the software Minitab® has been used. The models used to fit the experimental data have been three:

- the pseudo-first-order kinetic (Eq. 10) (Lagergren, 1898):

$$\frac{dq_t}{dt} = k_1(q_e - q_t) \qquad (10)$$

  where $k_1$ is the rate constant of pseudo-first-order adsorption (1/h), $q_e$ and $q_t$ (mg/g) are the amounts of adsorbed IBP at equilibrium and at time t (h) respectively.
  This equation assumes that the rate of change of solute uptake with time is directly proportional to difference in saturation concentration and the amount of solute uptake with time, which is generally applicable over the initial stage of an adsorption process. It is commonly observed that kinetics follows this Lagergren pseudo–first-order rate equation when adsorption occurs through diffusion through the interface;

- the pseudo-second-order kinetic (Eq. 11) (Ho and McKay, 1999):

$$\frac{dq_t}{dt} = k_2(q_e - q_t)^2 \qquad (11)$$

  where $k_2$ is the rate constant of pseudo-second-order adsorption (g/mg·h), $q_e$ and $q_t$ (mg/g) are the amounts of adsorbed IBP at equilibrium and at time t (h) respectively. The pseudo–second-order kinetic model assumes that the rate-limiting step is chemical sorption or chemisorption and predicts the behavior over the whole range of adsorption. In this condition, the adsorption rate is dependent on the adsorption capacity and not on the concentration of adsorbate. One significant benefit of this model over the Lagergren model is that the equilibrium adsorption capacity can be

determined from the model; hence, there is no need to assess adsorption equilibrium capacity from experiment;

- Elovich model (Eq.12) (Chein and Clayton, 1980):

$$q_t = \frac{1}{\beta}\ln(\alpha\beta) + \frac{1}{\beta}\ln(t + t_0) \quad (12)$$

where a is the adsorption initial rate (mg/g·h, $t_0 = 1/(\alpha \cdot \beta)$) and β is a constant (g/mg) related to the external surface area and activation energy of adsorption (chemisorption).

The Elovich kinetic model is often used to interpret the kinetics of adsorption and successfully describe second-order kinetics assuming that the surface is energetically heterogeneous.

### 3.3.2 Intraparticle diffusion model

The data from the kinetics experiments have been used to fit also the Weber and Morris intraparticle diffusion model shown in Equation (13) (Weber and Morris, 1963).

$$q_t = k_p t^{0.5} + C_i \quad (13)$$

where $k_p$ (mg/g·h$^{0.5}$) is the intraparticle diffusion rate constant, $C_i$ the intercept.

The graphs of $q_t$ as a function of $t^{0.5}$ should be straight lines if intraparticle diffusion is involved in the adsorption process. The slope and intercept of the regression line are used to get the rate constants $k_p$ and $C_i$. The thickness of the boundary layer can be determined by $C_i$. The higher the value of $C_i$, the greater will be the influence of the boundary layer in the sorption.

Nonlinearity is, nevertheless, occasionally encountered. This indicates that the total adsorption rate is limited by various mechanisms. If the data show multilinear plots, it means that more than one process was involved in the adsorption. As a result, these rate-limiting processes may be divided into several linear sections of the data across time, where they exert control over the whole process.

## 3.4 Isotherms

The batch experiments for the isotherm were conducted, similar to the kinetics ones, with a solution of 50 mg/L IBP sodium salt, at 20 °C and 200 rpm, also, different amount of adsorbent have been used for each bottle, obtaining different ration of IBP/adsorbent. The sampling has been performed only when the equilibrium was reached. The $C_e$ measured at t equilibrium were then plotted against the $q_e$ obtained using Equation (9).

### 3.4.1 Modeling

These are the different isotherms models used to fit experimental data from batch test:

- Freundlich (Freundlich, 1907) model applies to the description of heterogeneous and reversible multilayer adsorption, with the occurrence of lateral interaction between adsorbed molecules. For the Freundlich model, there is always a rapid decline in energy distribution as the adsorption process progresses. The nonlinear form of this empirical model is expressed in Equation (14).

$$q_e = K_F \cdot C_e^{\frac{1}{n_F}} \quad (14)$$

  where $K_F$ (L/g) and $n_F$ are Freundlich constants. The value of $1/n_F$ is representative of the adsorption intensity or the adsorbent surface heterogeneity.

  Also, when $0 < 1/n_F < 1$ the adsorption is considered favorable. Unfavorable adsorption occurs when $1/n_F > 1$ and is irreversible at $1/n = 1$;

- Langmuir model (Langmuir, 1916) is one of the most commonly applied empirical models in the sorption of aqueous pollutants. It proposes the following assumptions:
  1. monolayer adsorption on distinct homogeneous adsorbent sites;
  2. constant sorption energy which is independent of the extent of active site saturation;
  3. rapid weakening of the forces of attraction between adsorbate molecule with coverage;
  4. existence of fixed sorption capacity on structurally homogenous adsorbents;
  5. existence of identical and energetically uniform sites with the capacity for lateral interaction with adjacent sites.

  The nonlinear form of the Langmuir model is depicted in Equation (15).

$$q_e = \frac{q_{max} \cdot b \cdot C_e}{1 + b \cdot C_e} \quad (15)$$

  where $q_{max}$ (mg/g) is the maximum adsorbate uptake and b (L/mg) is a constant related to the affinity between adsorbate and adsorbent.

  An important parameter related to the Langmuir model is the separation factor or equilibrium parameter $R_L$ (Eq.16 ), which is used to check if adsorption is favorable or unfavorable.

$$R_L = \frac{1}{1 + b \cdot C_e} \quad (16)$$

The adsorption nature can be linear ($R_L$=1), irreversible ($R_L$=0), unfavorable ($R_L$>1), or favorable (0 < $R_L$<1);

- Sips, or Langmuir–Freundlich, proposed an equation that combines the Freundlich and Langmuir isotherms to solve problem of a continuous rise in the adsorbed amount with an increase in concentration in the Freundlich equation (Sips, 1948). As a result, at high concentrations, the equation specifies a finite limit. For mono-layer surfactant adsorption, the Sips model is the most suited three-parameter isotherm (Al-Ghouti and Da'ana, 2020). It works for heterogeneous systems and localized adsorption without adsorbate-adsorbate interactions. The nonlinear form of this equation is the following (Eq. 17).

$$q_e = \frac{q_{max} \cdot (b \cdot C_e)^{\frac{1}{n}}}{1 + (b \cdot C_e)^{\frac{1}{n}}} \tag{17}$$

where b (L/mg) and 1/n are Sips parameters dependent on the temperature, and $q_{max}$ (mg/g) can be considered or not as a function of temperature;

- Temkin model presumes a multilayer adsorption process, considers interactions between the adsorbent and the adsorbate, but it ignores very small and very large concentration values (Temkin and Pyzhev, 1940). The nonlinear form of the Temkin isotherm is expressed in Equation (18).

$$q_e = \frac{RT}{b} \ln(A \cdot C_e) \tag{18}$$

where R is the universal gas constant in J/(mol K), T is the temperature in K, b is the Temkin constant related to sorption heat in J/mol, and A is the Temkin isotherm constant in L/g.

## 3.5 Fixed Bed absorption column

For the dynamic experiment, a fixed bed adsorption column has been carried out (Figure 3.14). After sieving, the fraction having a diameter in the interval 0.5<Φ<1.6 mm was collected. The column used had a diameter of 1.5 cm and a total length of 45 cm, also three sampling ports were present at 10, 20 and 30 cm, respectively. A peristaltic pump was used for setting the flow rate to 0.22 mL/min. To better manage the flow rate and counteract the dispersion through advection, an up-flow feeding method has been chosen. The fixed bed has been first filled with 6.5 g of SABC reaching the sampling port at 30 cm. Then the penetrability has been tested by running the column with DW, so washing also possible

impurities. The synthetic wastewater, used as influent for the column, was prepared with DW and IBP sodium salt solution with a consecration of 25mg/L. The sampling was performed from the three heights for the all duration of the experiment and absorbance was measured using the same UV-Visible spectrophotometer of the previous experience. A scheme of the apparatus used during this experiment is showed in Figure 3.15.

**Figure 3.14** Picture of the adsorption column experience.

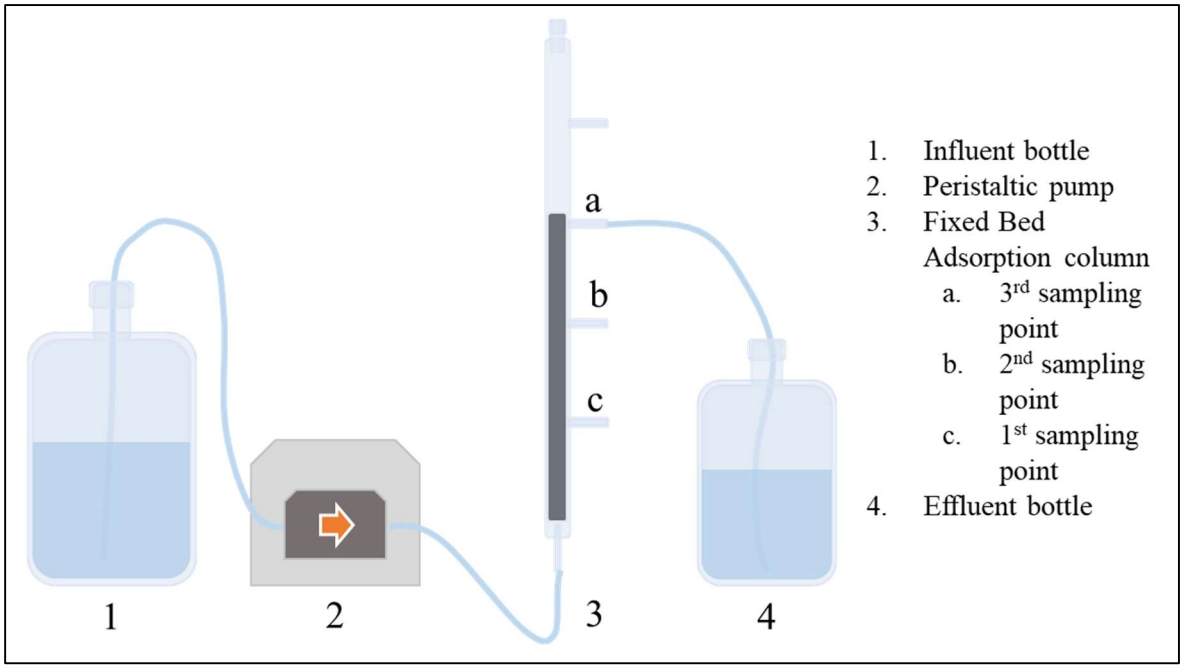


**Figure 3.15** Scheme of the apparatus used to run the adsorption column.

The breakthrough curves from the three sampling ports have been plotted. The breakthrough ($t_b$) and saturation ($t_s$) times have been obtained at $C/C_0$ =0.05 and 0.95, respectively. The adsorption capacity of the bed was obtained at $t_b$ with the following formula (Eq. 19).

$$q_b = \frac{Q \cdot C_0 \cdot t_b}{m} \tag{19}$$

Where Q is the flow rate in L/h, $C_0$ the influent concentration in mg/L and $t_b$ in h.

Also, the adsorption capacity at saturation ($q_s$) was calculated as follow (Eq. 20)

$$q_s = \frac{Q \cdot C_0 \cdot A_s}{m} \tag{20}$$

Where $A_s$ is the area over the breakthrough curve until $t_s$ estimated using the Equation (21).

$$A_s = \int_0^{t_s} 1 - \frac{C_t}{C_0} dt \cong \sum_{i=1}^{s} 1 - \frac{1}{2}\left(\frac{C_i}{C_0} + \frac{C_{i-1}}{C_0}\right) \cdot (t_i - t_{i-1}) \tag{21}$$

The total removal efficiency (Y) of the column at $t_s$ was found using the following formula (Eq. 22).

$$Y = \frac{Q \cdot C_0 \cdot A_s}{Q \cdot C_0 \cdot t_s} \times 100 = \frac{A_s}{t_s} \times 100 \tag{22}$$

An estimation on the degree of utilization of the fixed bed at breakthrough was derived from the calculation of the following parameters:

- percentage of utilized bed (UB) (Eq. 23);

$$UB = \frac{t_b}{A_s} \tag{23}$$

- Length of unused bed also known as the mass transfer zone (MTZ) (Eq. 24);

$$MTZ = L\left(1 - \frac{t_b}{A_s}\right) \tag{24}$$

where L is the length of the fixed bed in cm. In addition, a t* when $C/C_0$=0.5 can be defined, if the breakthrough curve is symmetric, it can be used in place of $A_s$. Furthermore, $A_s/t^*$ can be used to evaluate the symmetry of the curve, so values close to 1 mean a higher symmetry.

### 3.5.1 Modeling

The data from the breakthrough curves were fitted to the following model:

- Yoon and Nelson have proposed a straightforward model (Yoon and Nelson, 1984). This model is not only simpler than others, but it also does not require any comprehensive data on the adsorbate, the kind of adsorbent, or the physical properties of the adsorption bed. Equation (25) shows the Yoon and Nelson model in the nonlinear form used to fit the experimental data.

$$\frac{C}{C_0} = \frac{1}{1 + e^{K_{YN}(t^* - t)}} \tag{25}$$

  where $K_{YN}$ is the rate constant (1/h);

- Clark have developed a model on the assumption of (Clark, 1987):
    1. mass transfer concept in combination with the Freundlich isotherm;
    2. the fix bed column is considered a plug flow reactor;
    3. contributions from the dispersion phenomenon are negligible;

  The nonlinear equation of the Clark breakthrough curve model is the one given in the following formula (Eq. 26).

$$\frac{C}{C_0} = \left(\frac{1}{1 + A \cdot e^{-rt}}\right)^{\frac{1}{n_F - 1}} \tag{26}$$

  where A and r are parameters of the kinetic equation and $n_F$ corresponds to the exponent of the Freundlich isotherm.

# CHAPTER 4

# Results and Discussion

## 4.1 Biochar production

The results of the mass balance are reported in Table 4.1. Due to the higher temperature and steam presence in the activation process, a lower yield of SABC was expected compared to BC owing to the Water gas reaction (Eq. 27), and Water gas-shift reaction (Eq. 28) that occur simultaneously as follows:

$$C + H_2O \rightarrow CO + H_2 \qquad \Delta H\ (850\ ℃) = 19.06\ kJ/mol \qquad (27)$$

$$CO + H_2O \rightarrow CO_2 + H_2 \qquad \Delta H\ (850\ ℃) = 7.61\ kJ/mol \qquad (28)$$

The yield of the BC was 27.46 ± 0.31 % and that of SABC was 17.65 ± 0.53 %, showing a 10 % decrease after activation. Also, an increase in the condensable may be explained by the unreacted water that is found condensed in the oil collector. Also, the yield of the gaseous phase has increased owing to syngas production (mainly composed of $H_2$, CO, and $CO_2$) throughout the gasification process.

**Table 4.1** Mass balance in pyrolysis and steam gasification processes.

| | **Mass fraction (wt.%) of** | **BC** | **SABC** |
|---|---|---|---|
| **Inlet** | **Biomass** | 100.00 | 78.71 |
| | **Water** | 0 | 21.29 |
| **Outlet** | **Biochar** | 27.46 ± 0.31 | 13.89 ± 0.72 |
| | **Water** | 3.46 ± 0.51 | 11.19 |
| | **Oily phase** | 0.71 ± 0.11 | |
| | **Gel phase** | 22.37 ± 0.51 | 28.46 |
| | **Gaseous phase** | 17.69 ± 0.60 | 29.66 ± 0.67 |
| | **Total** | 71.68 | 83.20 |

## 4.2 Characterization

The chemical analysis assessed that the C content, after activation, has increased from 79.56 ± 0.60 % for the BC to 87.15 ± 0.44 % for SABC, as suggested in the literature, hence better

adsorption performance for the SABC could be expected. Also, H, N, and O were all decreased. The ash content of BC and SABC was 2.90 and 4.19 % respectively, showing that after activation part of the volatile matter was lost and ash became more concentrated in the solid phase. The results are summarized in Table 4.2.

**Table 4.2** Chemical composition and Ash content of BC and SABC.

| Adsorbent | wt.% on dry basis of | BC | SABC |
|---|---|---|---|
| Ultimate analysis | C | 79.56 ± 0.60 | 87.15 ± 0.44 |
| | H | 2.65 ± 0.10 | 0.78 ± 0.04 |
| | N | 3.94 ± 0.20 | 1.68 ± 0.01 |
| | S | < LD | 1.06 ± 0.11 |
| | O* | 10.95± 0.20 | 5.14± 0.49 |
| Proximate analysis | Ash | 2.90 ± 0.10 | 4.19 ± 0.17 |

*: Oxygen calculated from the difference of C, H, N, S and ash

< LD: Lower than the detection limit (LD < 0.06 % on CHNS-O analyzer)

### 4.2.1 BET

In Table 4.3, the data from the BET experiments are presented. The BET specific surface areas were found to be 375.5 and 560.4 $m^2/g$ for BC and SABC respectively, so about 50% increase has been obtained after steam activation. The standard deviation of the BET is ± 15 $m^2/g$. The most noticeable variation between the two adsorbents is the increase of the mesopores. The BC has 6.74% and SABC 24.46 % of mesopores. This increase has a positive influence on the adsorption mechanism, because, the presence of mesopores allows more micropores to be available for the sorption (Hsieh and Teng, 2000). The median pore width of SABC can be considered a positive parameter for tetracycline removal as this latter molecule is adsorbed on an adsorbent having a median pore width not smaller than 1.5 nm (Li et al., 2019).

**Table 4.3** Results from BET analysis of BC and SABC

| | BET surface area ($m^2/g$) | Total volume of pores $V_{total}$ ($cm^3/g$) | Mesopores | | Micropores | | Median pore width (nm) |
|---|---|---|---|---|---|---|---|
| | | | Volume $V_{meso}$ ($cm^3/g$) | $V_{meso}/V_{total}$ (%) | Volume $V_{micro}$ ($cm^3/g$) | $V_{micro}/V_{total}$ (%) | |
| **BC** | 375.5 | 0.2093 | 0.0141 | 6.74 | 0.1372 | 65.55 | 0.52 |
| **SABC** | 560.4 | 0.3297 | 0.0806 | 24.46 | 0.2415 | 73.26 | 2.35 |

### 4.2.2 Results pH Point of zero charge results

After physico-chemical characterization, the investigation of the $pH_{pzc}$ of BC and SABC was performed. In Figures 4.1 and 4.2, the curves used to obtain $pH_{pzc}$ are plotted. Where the curves intersect the pH-initial = pH-final and the $pH_{pzc}$ is determined. The $pH_{pzc}$ of BC and SABC were found to be at 9 and 10, respectively. Therefore, negatively charged functional groups are present at the surface of both adsorbents. However, according to the literature, the pKa of IBP is 4.91 (PubChem, 2021). Thus, electrostatic attraction and H-bonding take place between IBP and the adsorbents when the pH of the solution is between the pKa and $pH_{pzc}$ (Table 4.4).

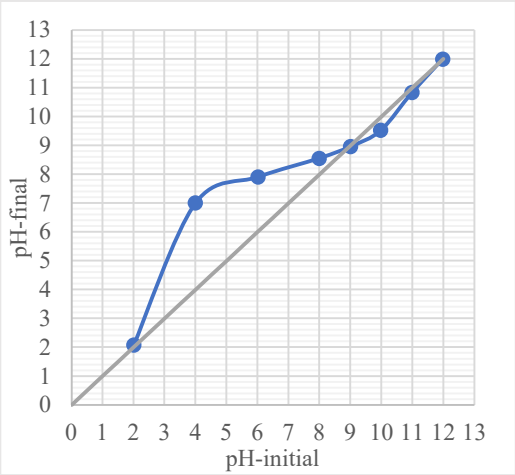


**Figure 4.1** $pH_{pzc}$ of BC.

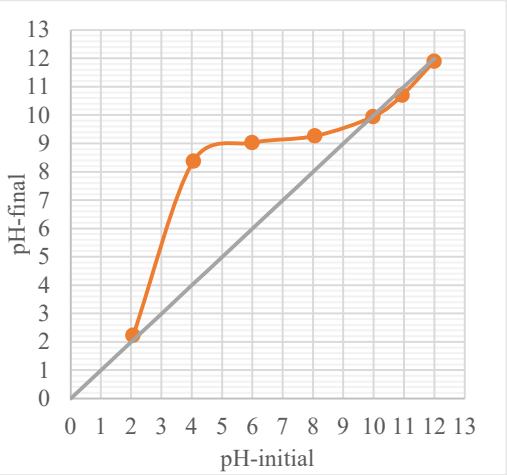


**Figure 4.2** $pH_{pzc}$ of SABC.

**Table 4.4** Charge of IBP and the adsorbents surface and their interaction on different pH.

| | pH<4.91 | 4.91<pH<9 | pH>9 |
|---|---|---|---|
| IBP | + | - | - |
| BC | + | + | - |
| interaction | Electrostatic repulsion | Electrostatic attraction | Electrostatic repulsion |
| | pH<4.91 | 4.91<pH<10 | pH>10 |
| IBP | + | - | - |
| SABC | + | + | - |
| interaction | Electrostatic repulsion | Electrostatic attraction | Electrostatic repulsion |

+: positively charge; -: negatively charge.

## 4.3 Kinetics results

In this section, the kinetics results of the experimental data from the batch tests are first presented followed by the fitting of the experimental data with the appropriate models.

### 4.3.1 Biochar

The batch adsorption test on the BC has been conducted with a concentration of 50 mg IBP/L in 800 mL of DW with 0.5g of BC. The results, shown in Figure 4.3, highlight that the removal capacity of the BC is very limited, having a maximum removal efficiency of about 5 %. Therefore, BC is not an efficient adsorbent for the removal of IBP.

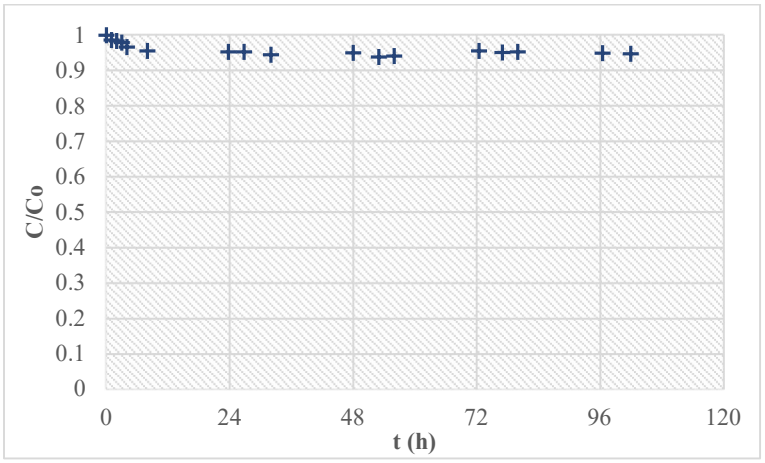


**Figure 4.3** Normalized trend of IBP concentration with 0.5 g of BC.

In Figure 4.4, the experimental adsorption kinetics of BC is plotted. The equilibrium time was set to be at 24 h; with a fast increase in the first 8 h. At equilibrium, the experimental adsorbed IBP for 1 g of adsorbent ($q_t$) has been around 3.9 mg/g.

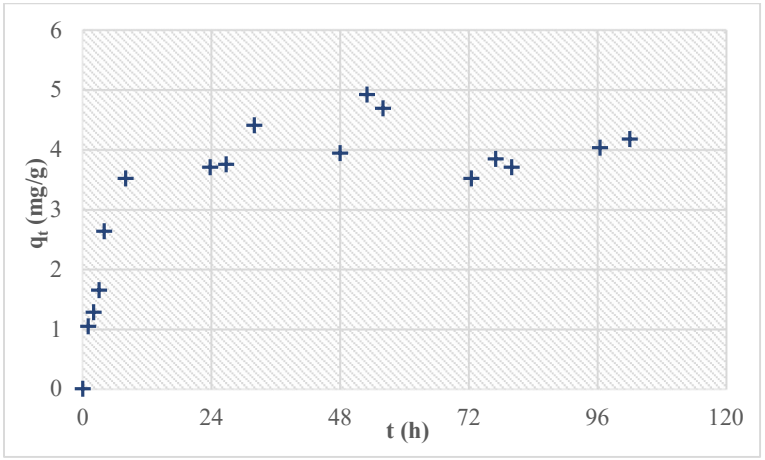


**Figure 4.4** Adsorption kinetic of 0.5 g of BC.

As the removal of BC was very low and the kinetics were very slow, this adsorbent does not exhibit good adsorptive performance towards IBP removal from water, thus it has been neglected in the following steps of this study.

### 4.3.2 SABC Intact pellets

For the full pellets, a quantity of 1 g has been used, to ensure a representative sample of SABC. Due to the low surface area in direct contact with the bulk of the solution, the removal has been slower, whereas C/Co has been higher until the equilibrium is reached at 120 h (Figure 4.5). In this batch, a maximum removal efficiency of about 92 % was obtained.

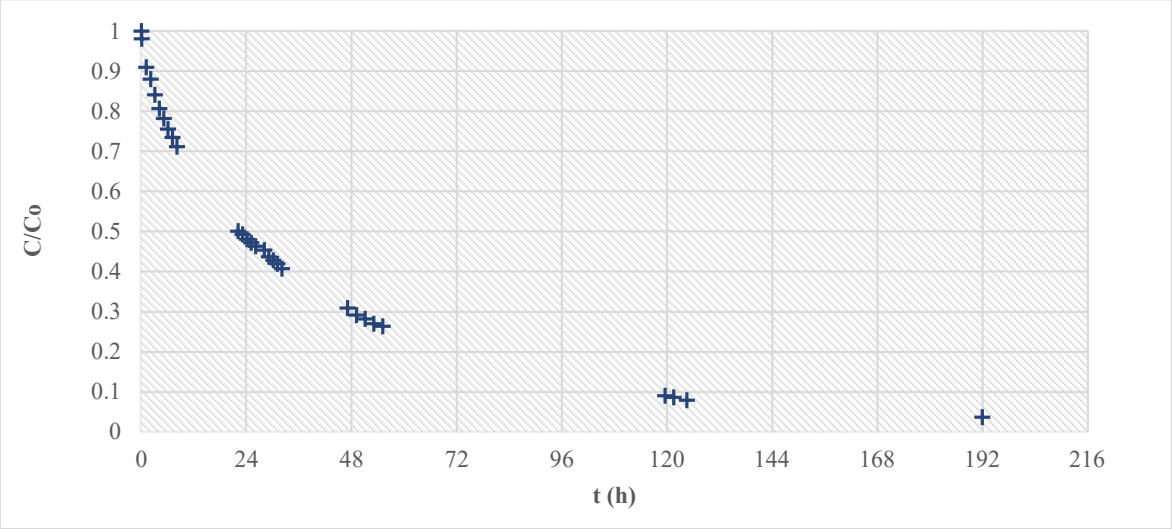


**Figure 4.5** Normalized trend of IBP concentration with 1 g of SABC intact pellets (1 g).

The adsorption kinetic (Figure 4.6) of SABC intact pellets (SABC-P) show an adsorption capacity at equilibrium of 38 mg/g. Due to physical constraints of intact pellets, at 24h only around 50% of the total capacity was obtained.

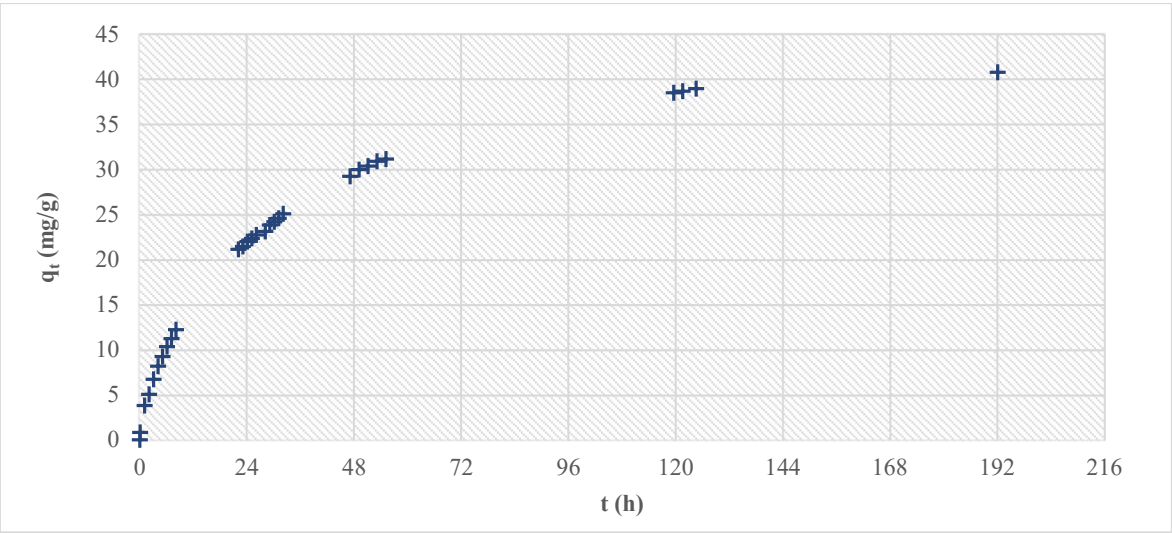


**Figure 4.6** Adsorption kinetic of SABC intact pellets (1 g).

### 4.3.3 Crushed SABC pellets

Different amounts of crushed SABC (SABC-C) were used, to explore more in detail the behavior of the adsorbent (Figure 4.7). Compared to the SABC pellets, the batch with 0.7 g of crushed SABC outperformed the 1 g full pellets at 24 h, having a removal of about 60 and 50 %, respectively. As expected, the removal of IBP was higher with an increasing amount of SABC-C added, and the same equilibrium state (120 h) was obtained.

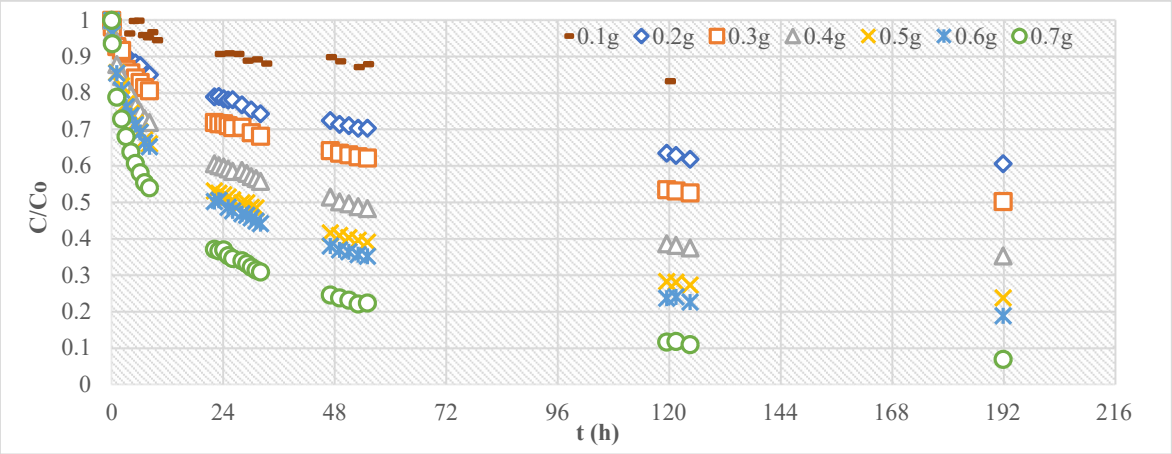


**Figure 4.7** Normalized trend of IBP concentration with different amounts of SABC crushed pellets.

The experimental adsorption kinetics are shown in Figure 4.8. Adsorption can be divided into three macro-phases. In the first one, the majority of the active sites are free, so this induces a more rapid adsorption in the initial 24 h. In the second phase, where the readily available free active sites are decreasing, the adsorption slows until reaching equilibrium at 120 h. The last part is after equilibrium is reached where the adsorption continues but at a very slow rate. Furthermore, two-thirds of the adsorption capacity at equilibrium (120 h) in all the kinetics was reached in the first 24 h.

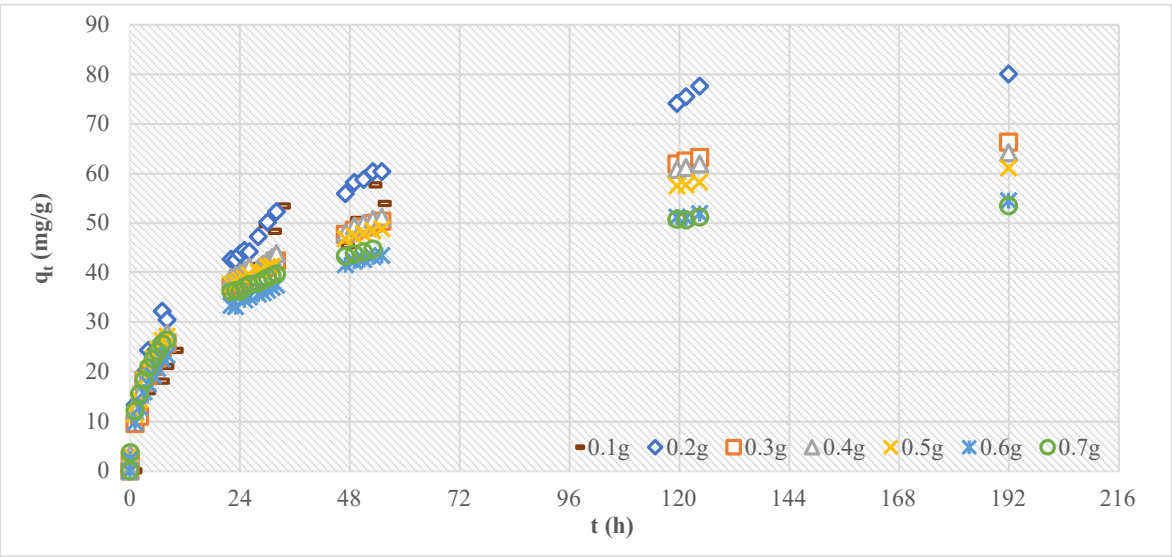


**Figure 4.8** Adsorption kinetic with different amounts of SABC crushed pellets.

### 4.3.4 Sieved SABC

For the sieved SABC (SABC-S), the kinetics data are plotted in Figures 4.9 and 4.10. The same observation of the crushed (not sieved) pellets can be made, such as, that the increase of adsorbent has allowed higher removal of IBP; the presence of a faster phase in the 24 h in which the majority of the removal is expressed and a slowdown of the absorption afterwards. However, it is to be considered that the adsorption capacity is reduced compared to the SABC-C. This can be an effect of inconsistency in the crushing and sieving such as the removal of dusty fraction with the higher surface area. Nevertheless, removal over the 50% and adsorption capacity comparable with the not sieved batch was obtained. At 24 h, the adsorption capacities were in the range of 25 and 45 mg/g and the removal were 45 % at the same time for the highest SABC-S concentration.

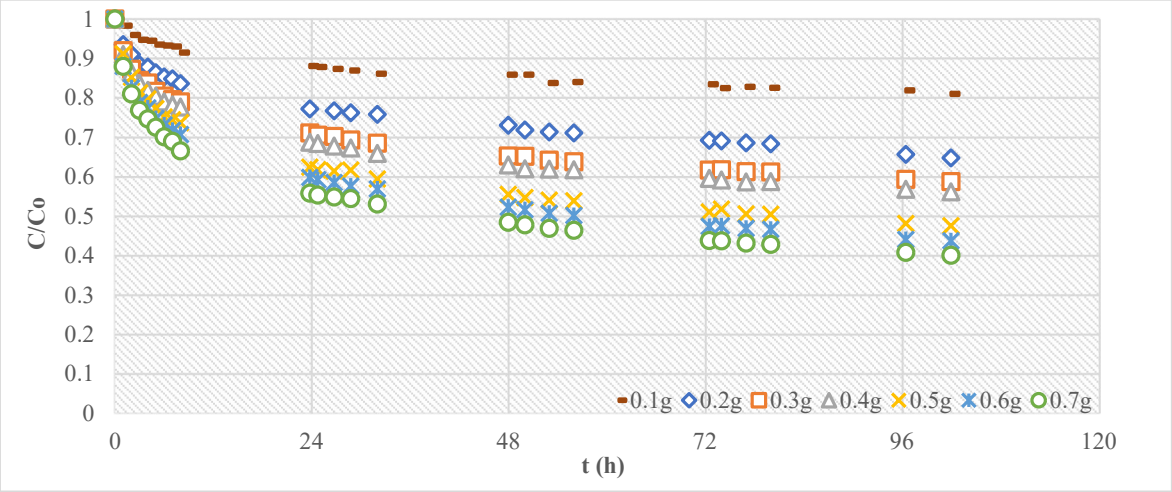


**Figure 4.9** Normalized trend of IBP concentration with different amounts of sieved SABC.

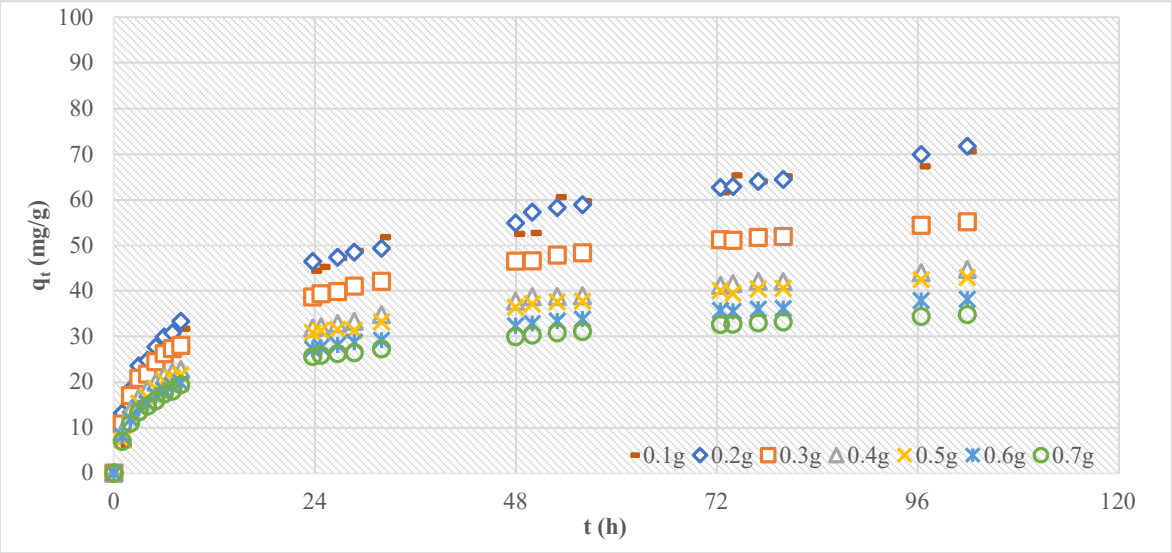


**Figure 4.10** Adsorption kinetic with different amounts of sieved SABC.

### 4.3.5 Tap water

To explore the possibility to apply this kind of adsorbate in a real scenario, an experiment with Tap water (TapW) in place of distilled water was performed. It was found that the adsorption capacity was not negatively affected by the presence of ions in the TapW, so competition for the active site between them and the IBP sodium salt was negligible. In Figure 4.11, the removal of SABC-C in TapW is seen greater than the removal in DW. Besides, Figure 4.12 shows that the removal capacity was increased from 61 mg IBP/g of SABC in DW to 73 mg/g in TapW. However, this result cannot be considered completely relevant, because later in the research, during the isotherms study with TapW, a shift in the baseline of the UV-Visible spectrophotometer was discovered.

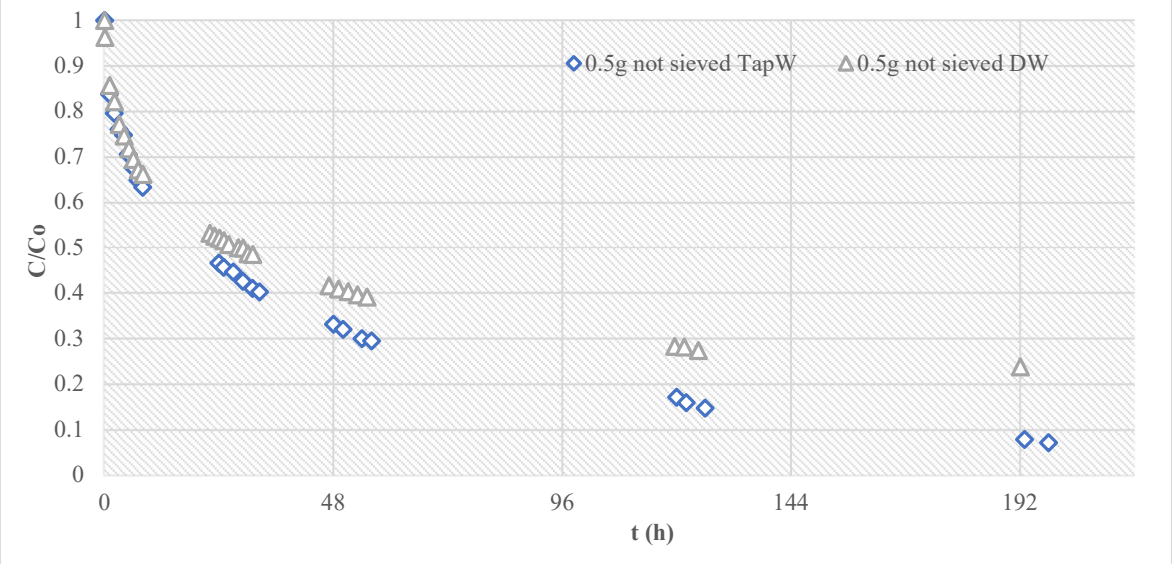


**Figure 4.11** Normalized trend of IBP in TapW.

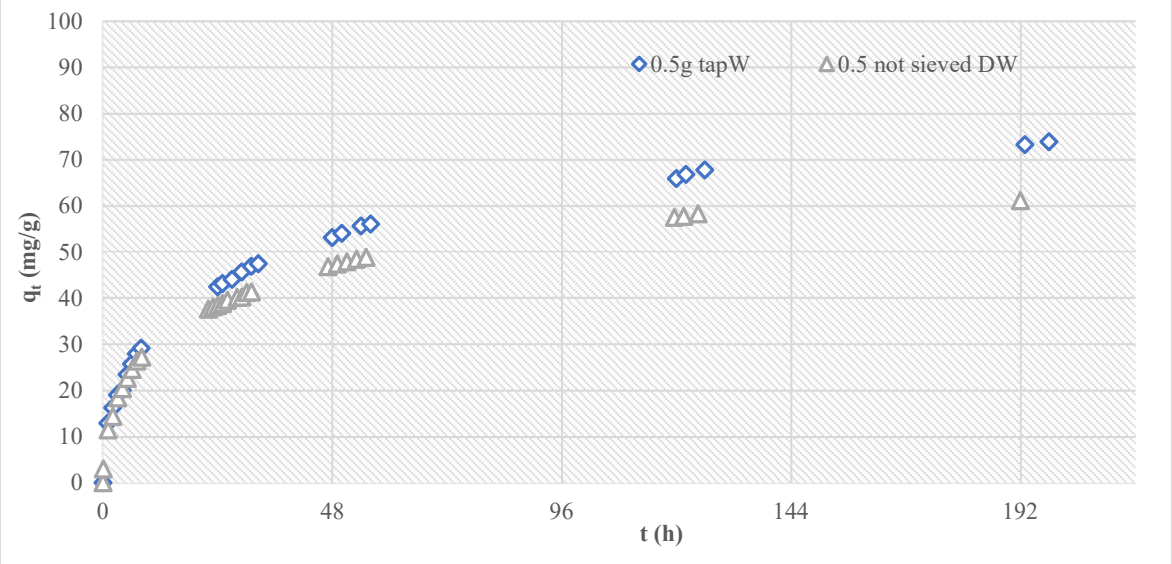


**Figure 4.12** Adsorption capacity of SABC in TapW.

### 4.3.6 Modeling of Kinetics

In this section the results of the kinetic models are presented. Every figure was plotted with the experimental data and the three models, a continuous line was used to highlight the model with the higher $R^2$. In Figure 4.13 the kinetics resulting from 0.5 g of BC are showed, the model of best fit was found to be the PFO kinetic closely followed by the PSO, with an $R^2$ of 0.9793 and 0.9673 respectively. The $q_e$ for BC was established to be 3.9 and 4.1 mg/g according to the PFO and PSO model respectively. The PFO kinetic expressed its adsorption capacity very fast (highest $k_1$ and $k_2$), in the first 24h, and then a stable equilibrium is found.

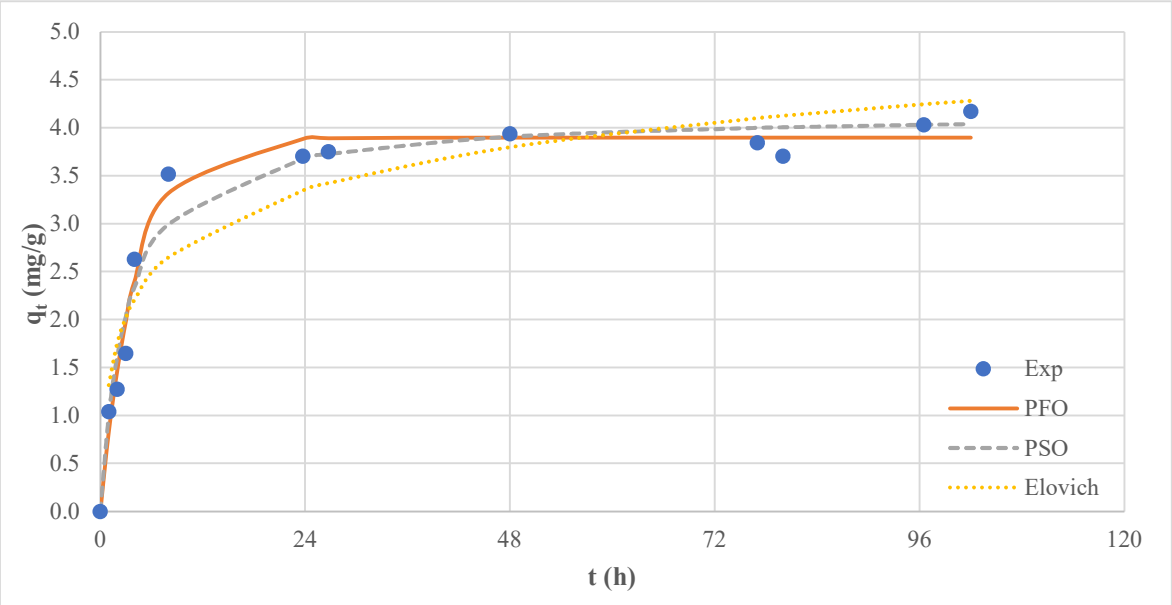


**Figure 4.13** Kinetics of 0.5 g BC.

In Figure 4.14 the kinetics of 1 g SABC-P are given. The model that better matches the experimental data has been the PSO kinetic, with an $R^2$ of 0.9954. The respective $q_e$ was 45.7 mg/g. Comparing the $k_2$ with the others PSO, the one from SABC-P was the lowest of them all, highlighting that this was the slowest of the kinetics. This, as previously said, could have been the result of the less surface directly exposed to the bulk of the solution, so intraparticle diffusion could have been a key mitigation factor in the adsorption.

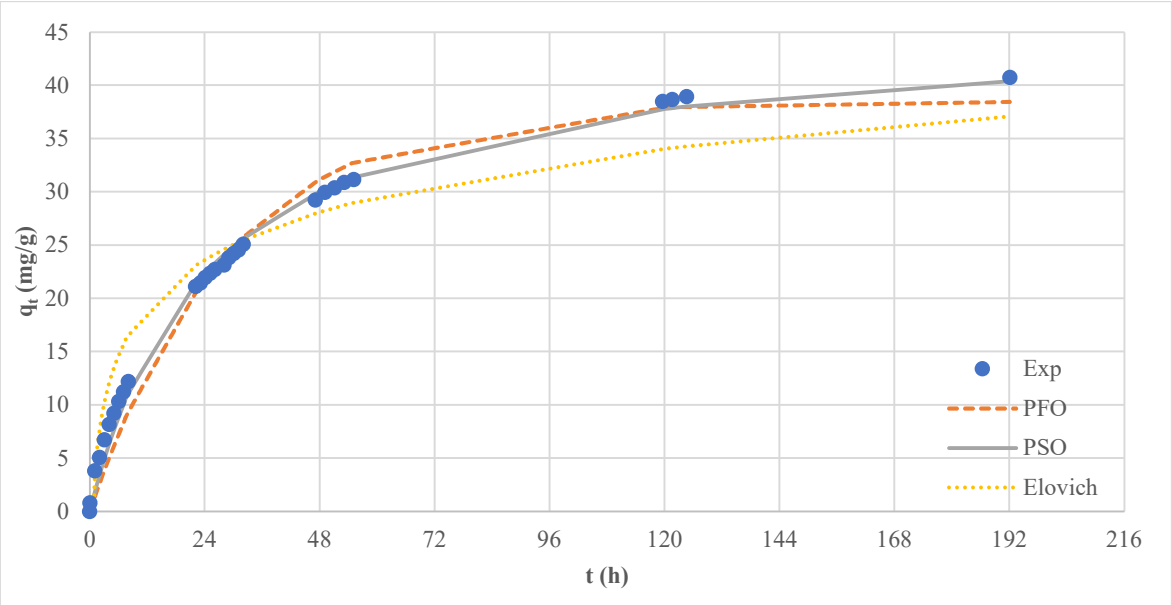


**Figure 4.14** Kinetics of 1 g SABC-P.

In Figure 4.15 the plot of 0.5 g SABC-C are presented. The PSO modeling was the one with the higher $R^2$ with a value of 0.9704. In this batch the highest $q_e$ was obtained, with a value of 58.4 mg/g.

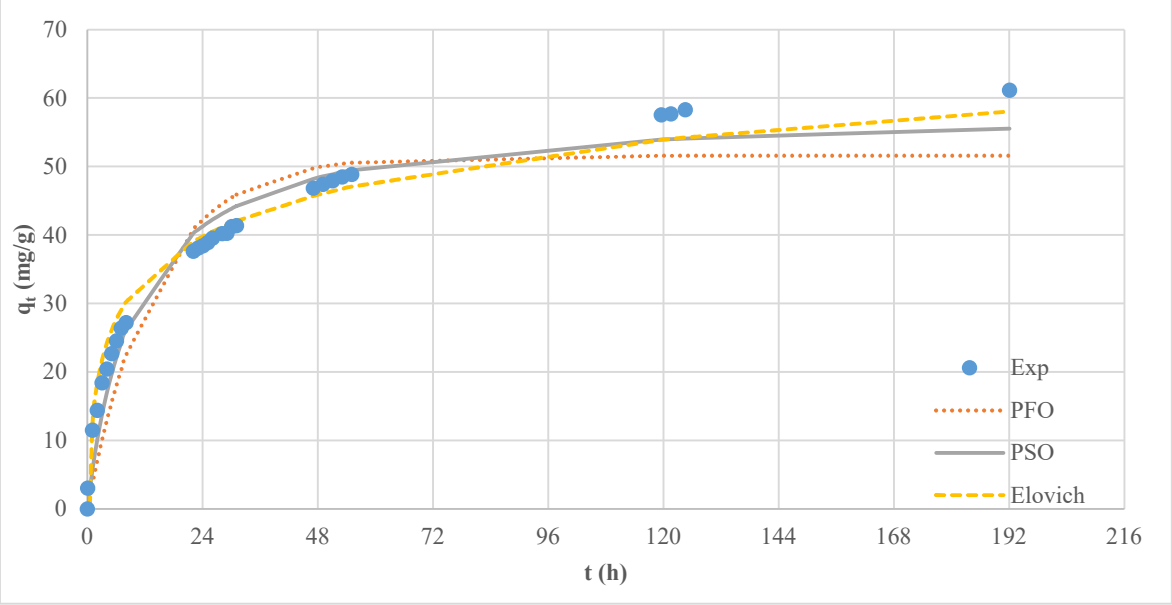


**Figure 4.15** Kinetics of 0.5 g SABC-C.

In Figure 4.16 the kinetics resulting from the modeling of the 0.5 g SABC-S experimental data are shown. From the graph a matching with the Elovich kinetic is clearly visible and its $R^2$ is 0.9984. From the 1/b the number of adsorption site can be obtained; however, this modeling does not give a $q_e$ that could be useful for comparison with the other result. In

order to overcome this problem, the $q_e$ found with the PSO ($R^2$ of 0.9835) can be used, so this adsorption capacity was estimated to be around 42.9 mg/g, lower than the SABC-C but comparable to the SABC-P. This can be explained by the crushing treatment, which has released dusts, and the heterogeneity of the material. However, the $k_2$ was the highest of the SABC batches.

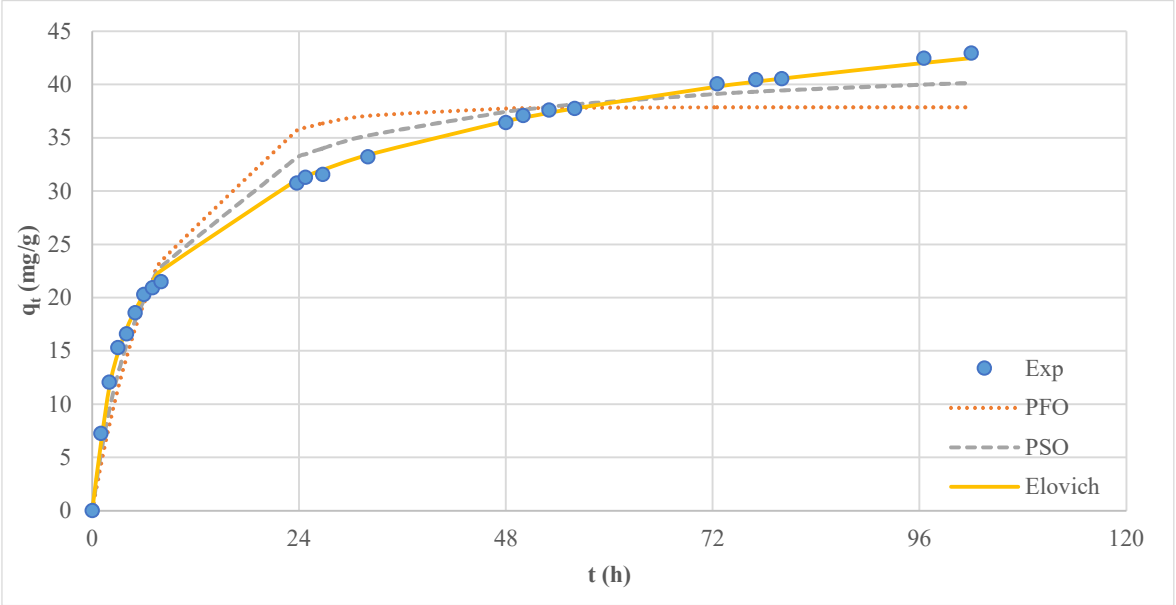


**Figure 4.16** Kinetics of 0.5 g SABC-S.

All the parameters resulting from the modeling with Minitab® of each adsorbent kinetics and the related $R^2$ are summarized in Table 4.5.

**Table 4.5** Parameters of kinetic modelling.

| **Model** | **PFO** | | | **PSO** | | | **Elovich** | | |
|---|---|---|---|---|---|---|---|---|---|
| Parameter | $q_e$ | $k_1$ | $R^2$ | $q_e$ | $k_2$ | $R^2$ | a | b | $R^2$ |
| **BC** | 3.899 | 0.238 | 0.9793 | 4.163 | 0.0769 | 0.9673 | 5.003 | 1.5598 | 0.8662 |
| **SABC-P** | 38.487 | 0.0345 | 0.9883 | 45.657 | 0.0009 | 0.9958 | 10.288 | 0.1543 | 0.8825 |
| **SABC-C** | 51.591 | 0.071 | 0.9260 | 58.434 | 0.0017 | 0.9704 | 34.038 | 0.1139 | 0.9464 |
| **SABC-S** | 37.877 | 0.1205 | 0.9450 | 42.904 | 0.0033 | 0.9835 | 17.418 | 0.1277 | 0.9984 |

## 4.4 Intraparticle diffusion Model for SABC

The Weber and Morris intraparticle diffusion model was utilized to investigate the adsorption mechanism. The SABC-S has been chosen to be the reference for the experiment, because it had a distinct granulometry and compared to the others it was not affected by the presence of dust. In Figure 4.17 the results from the batch test with 0.5 g of SABC-S in 50 mg/L IBP solution are showed. The adsorption capacities ($q_t$) vs. $t^{1/2}$ are presented in this plot, producing a multi-linear graph with three phases. The first step represents instantaneous adsorption or external surface adsorption; the second stage is a more gradual adsorption, which is characteristic of adsorbate transport within the inner adsorbent surface; and the third step is equilibrium adsorption, which is representative of adsorbate movement from macro and mesopores to micropores. In the first step, the plot passes through the origin, which is indicative of the absence of a boundary layer, so the rate of adsorption is controlled by the intraparticle diffusion only. The regression is also linear in the second and third stage but does not pass through the origin, indicating that intraparticle diffusion is not the main limiting factor in the adsorption process. The intraparticle diffusion slows down even more in the third step, because of the low IBP concentrations in the solutions. The $Kp_i$ values which represent the rate parameter of *i* stage were found to be decreasing ($Kp_1$ = 8.35, $Kp_2$ =4.22, $Kp_3$ =2.12), indicating that the adsorption rate is initially faster and then slows down over time. In Figure 4.18 the intraparticle diffusion of 0.5 g of SABC-C is plotted. The same consideration of the previous modeling can be made on the general trend. The most notable difference is the duration of the second step, which was of 26 h for SABC-S and 63 h for the SABC-C, probably due to the averagely bigger size of the particle in the second one. In addition, the two diffusion rates $Kp_1$ and $Kp_2$ of the two batches are similar, possibly pointing to be characteristics of the material. Whereas the difference in $Kp_3$ can be explained by a lower equilibrium concentration in the solution, so intraparticle diffusion in the third phase of SABC-C was more negatively affected compared to SABC-S. The regression equations of the three-step model are summarized in Table 4.6. In addition, a comment about the SABC-P modeling can be made. The rate obtained as $Kp_1$ is very close to the $Kp_2$ of the previous modeling. This could suggest that the real first step of SABC-P intraparticle diffusion was happening in the initial hour, before the first sample.

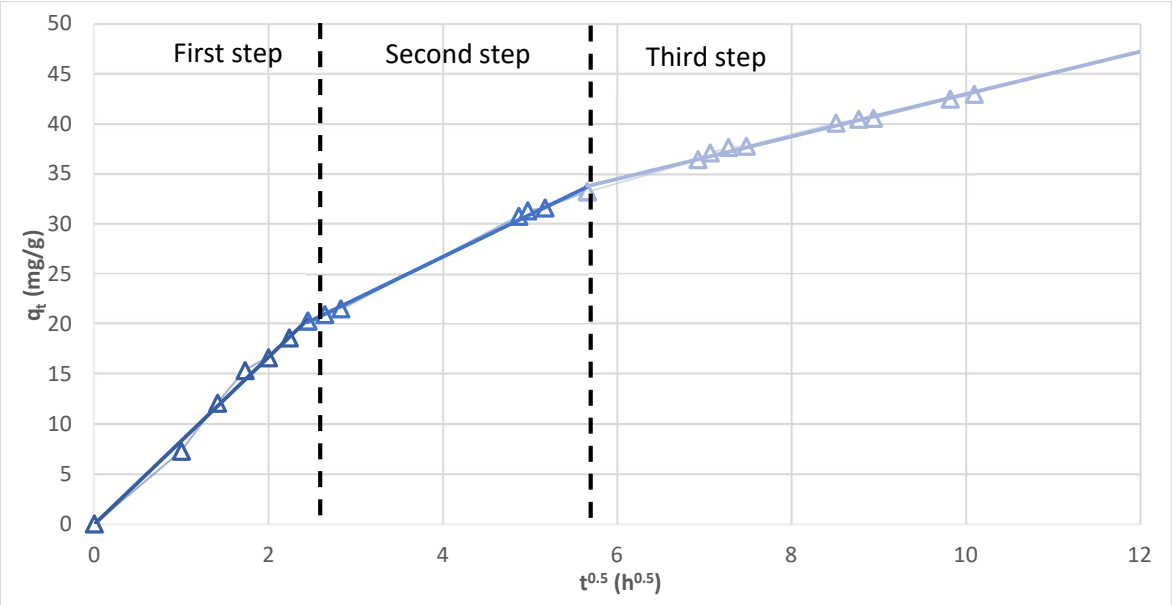


**Figure 4.17** Plot of the intraparticle diffusion of SABC-S according to Weber and Morris model.

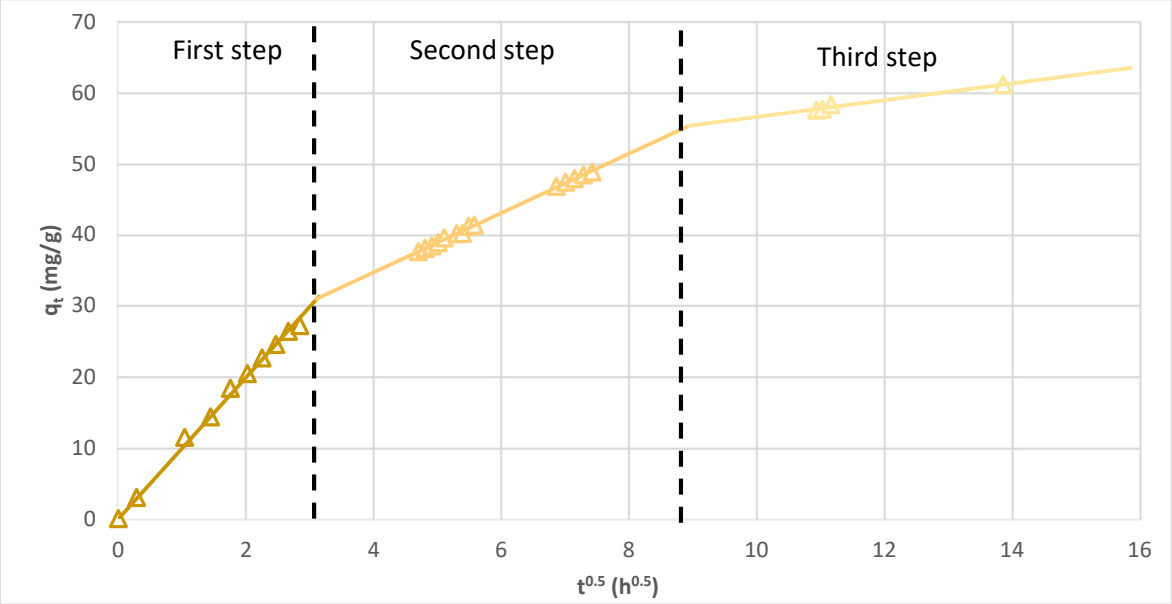


**Figure 4.18** Plot of the intraparticle diffusion of SABC-C according to Weber and Morris model.

**Table 4.6** Regression equations of the intraparticle diffusion model.

| | First Step | Second Step | Third Step |
|---|---|---|---|
| **SABC-P** | $q_t = 4.3748\ t^{1/2}$ | $q_t = 2.1595\ t^{1/2} + 14.872$ | $q_t = 0.7318\ t^{1/2} + 30.61$ |
| | $R^2 = 0.9962$ | $R^2 = 0.9973$ | $R^2 = 0.9866$ |
| **SABC-C** | $q_t = 9.9672\ t^{1/2}$ | $q_t = 4.1834\ t^{1/2} + 17.99$ | $q_t = 1.1801\ t^{1/2} + 44.804$ |
| | $R^2 = 0.9958$ | $R^2 = 0.9987$ | $R^2 = 0.9823$ |
| **SABC-S** | $q_t = 8.3496\ t^{1/2}$ | $q_t = 4.2233\ t^{1/2} + 9.8264$ | $q_t = 2.1165\ t^{1/2} + 21.805$ |
| | $R^2 = 0.9934$ | $R^2 = 0.9966$ | $R^2 = 0.9902$ |

## 4.5 Isotherms results

The study of isotherms was conducted mainly to deduce a maximum adsorption capacity and to understand if they were suitable for the adsorption process in the fixed bed experiment. In Figure 4.19 is the isotherm for the BC. The isotherm can be classified as an S-shape. The S-shape curve displays a small slope in the beginning followed by a sharp rise (Kalam et al., 2021). None of the considered models were able to fit this curve. However, the removal capacity was established to be too low for BC to be considered in the following experiments.

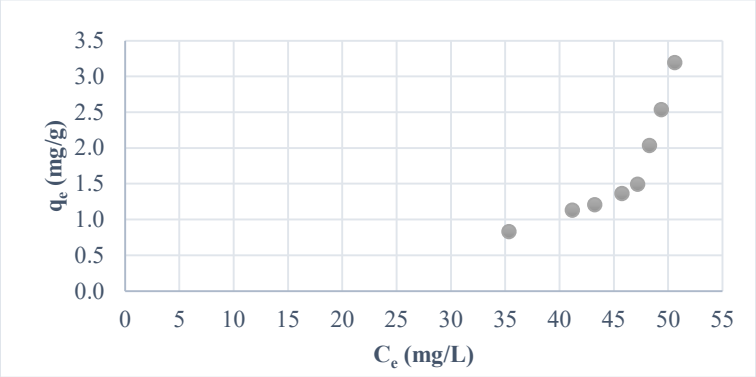


**Figure 4.19** Isotherm for BC.

In Figures 4.20 and 4.21 the experimental data for the SABC-C and SABC-S isotherms are showed. In blue the data at 24 h are plotted and in orange the 120 h ones. From them it can be seen that, for the 24 h the $q_{max}$ was for both around 40 mg/g. For the 120 h a bigger increase in the $q_e$s was achieved in the SABC-C probably due to a milling like action produced by the mixing, exposing new active sites.

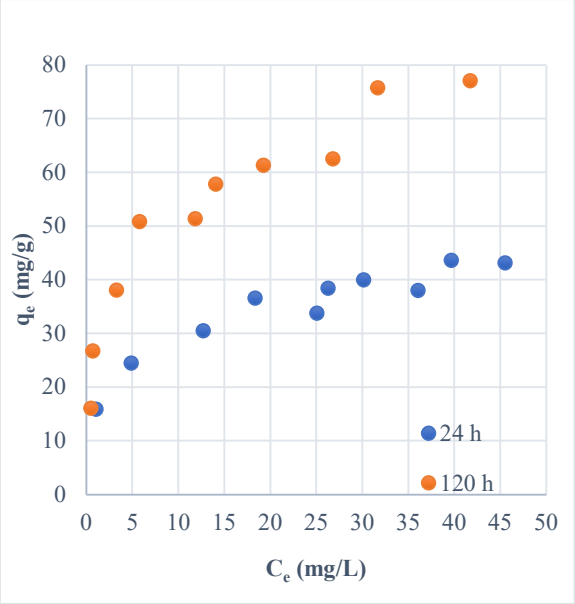


**Figure 4.20** Experimental isotherms SABC-C.

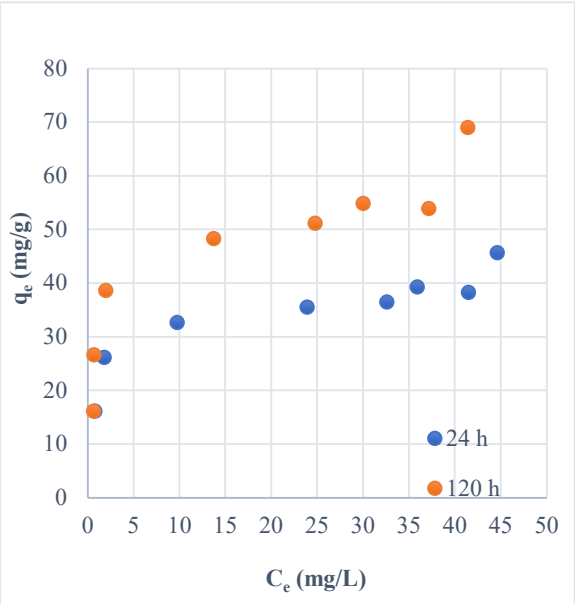


**Figure 4.21** Experimental isotherms SABC-S.

### 4.5.1 Isotherms modeling for SABC

In this section the isotherms modeling of SABC are presented. In Table 4.7, at the end of the section, a summary of all models and parameters used are shown. The Temkin model was fitting well the data. However, in literature it is stated that this isotherm model is not appropriate to present complex adsorption systems as aqueous-phase adsorption isotherms(Al-Ghouti and Da'ana, 2020). The first graph, in Figure 4.22, shows the isotherms for the SABC-C at 24 h. The model of best fit has been the Sips (Freundlich Langmuir) model with an $R^2$ of 0.9574. The $q_{max}$ obtained with the modeling was about 260 mg/g. The Freundlich model was the second best fitting model ($R^2$=0.9566). From it, it can be deduced that the material presents an energetically heterogeneous surface. So active sites do not have the same energy or are available at different times. This can be the result of the different particle dimensions present in this batch, ranging from big particles to dust. Furthermore, the Freundlich isotherm can be used to determine if the adsorption is favorable. The $1/n_F$ was found to be 0.2589, so the isotherm was favorable for the adsorption process.

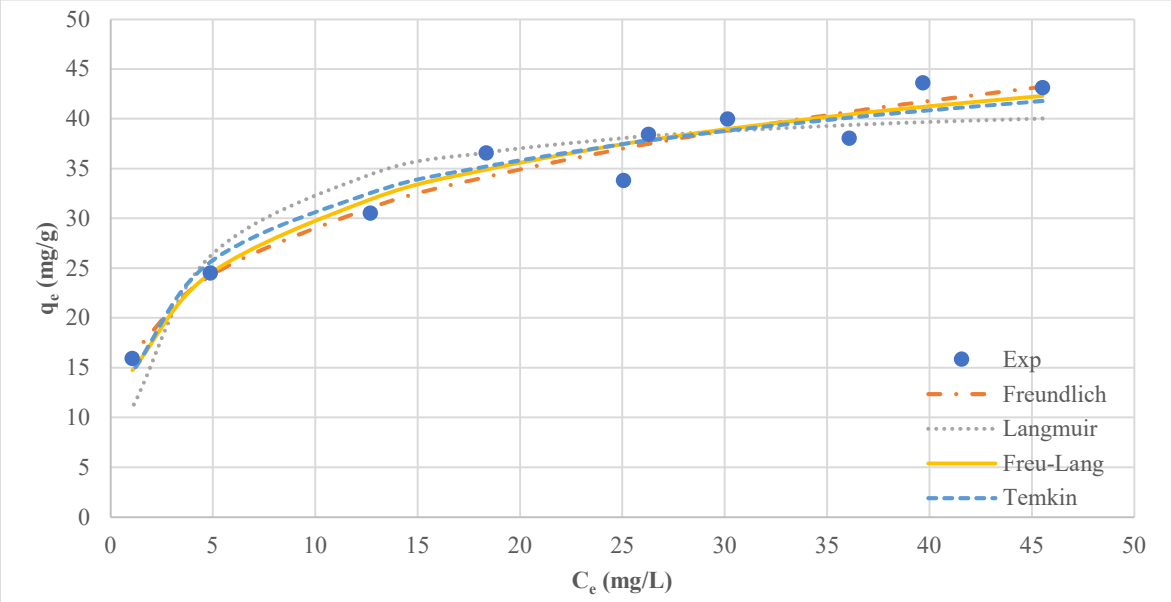


**Figure 4.22** Isotherms of SABC-C at 24 h.

In Figure 4.23 the isotherm of SABC-C at 120 h is presented. Like the previous isotherm, the model that has the highest $R^2$ (0.9607) is the Sips model closely followed by the Freundlich model (0.9561). The same conclusion of the SABC at 24 h about the heterogeneity of the surface can been made. Also, The Langmuir model can be used to assess that with the increase in the contact time the $q_{max}$ has increased from 42.7 to 72.1 mg/g at 24 and 120 h respectively. The Freundlich isotherm was found to be favorable whit a $1/n_F$ of 0.2815.

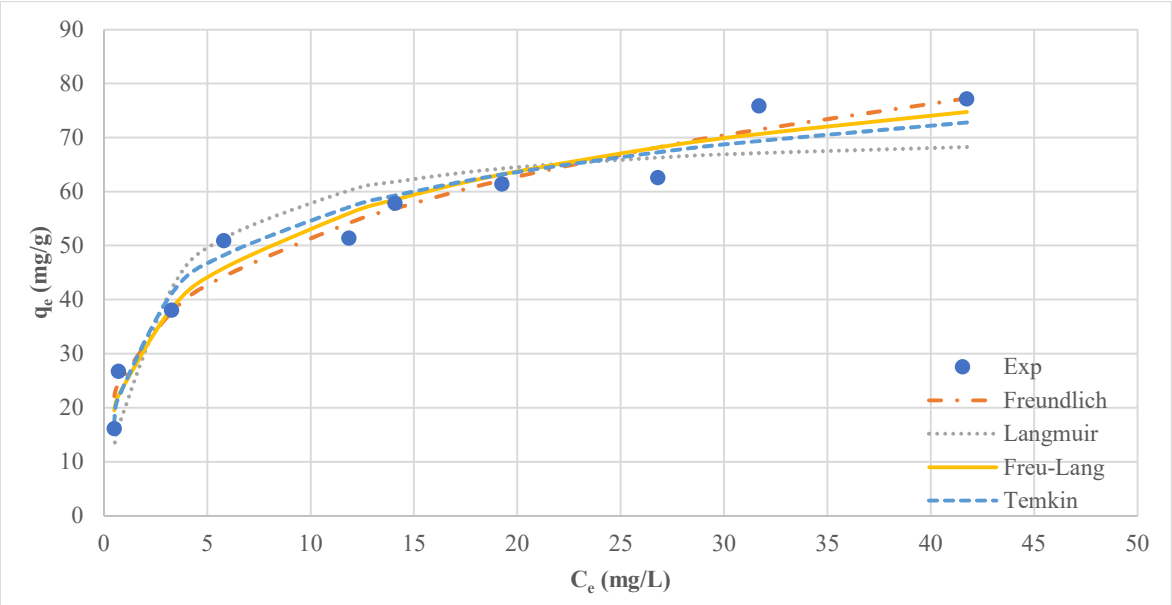


**Figure 4.23** Isotherms of SABC-C at 120 h.

The isotherms for the SABC-S at 24h are plotted in Figure 4.24. The isotherms that best fitted the experimental data were the ones obtained with the Sips end Langmuir models. The respectives $R^2$ are 0.9675 and 0.9664. The $q_{max}$ obtained are around 39.1 and 38.2 mg/g respectively, resulting close to the SABC-C at 24h. From the fitting of Langmuir isotherm, it can be deduced that the surface of the material is energetically homogeneous, this is due to the sieving that has narrowed down the particle size distribution thus the overall heterogeneity of the active site availability. This isotherm can be also used to obtain information about the adsorption nature using the separation factor $R_L$. In this case $R_L$ was found to be between 0 and 1, so the adsorption was favorable, but close to 0 so most likely irreversible.

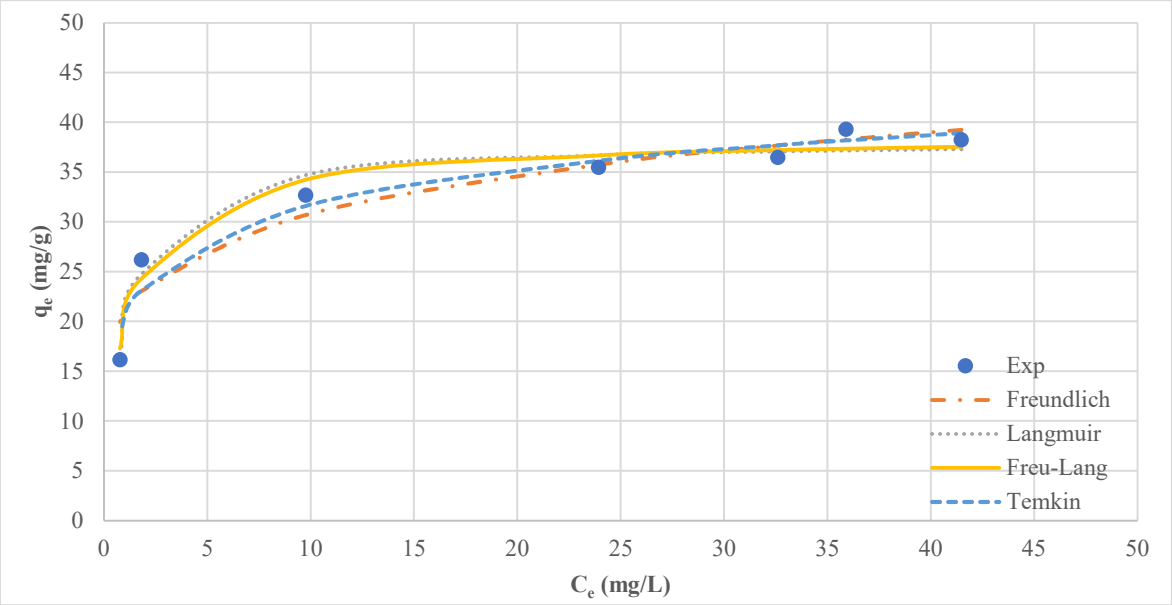


**Figure 4.24** Isotherms of SABC-S at 24 h.

In Figure 4.25 the resulting isotherms form the modeling of the SABC-S at 120 h data are plotted. Like the previous isotherms the most fitting model were the Sips and Langmuir, with an $R^2$ of 0.9543 and 0.9521, respectively. The $q_{max}$ was found to increase with the contact time, reaching the values of 53.2 and 54.5 mg/g at 120 h. The same conclusion of 24 h isotherms can be made about surface homogeneity and the adsorption nature at 120 h.

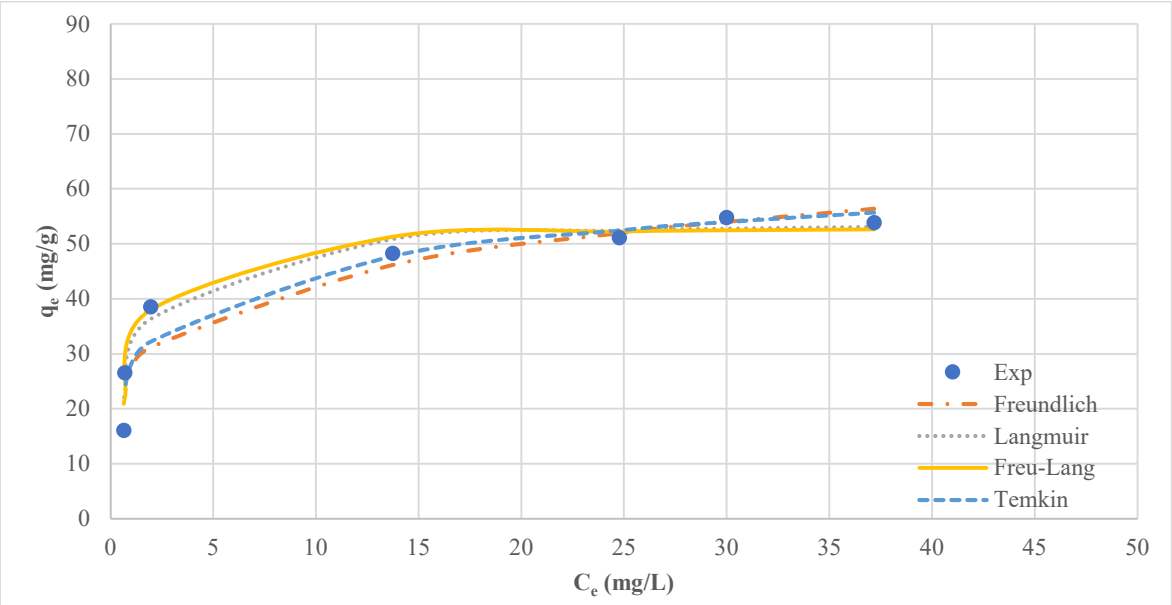


**Figure 4.25** Isotherms of SABC-S at 120 h.

**Table 4.7** Parameters of SABC isotherm models.

| **Model** | | **SABC-C 24h** | **SABC-C 120h** | **SABC-S 24h** | **SABC-S 120h** |
|---|---|---|---|---|---|
| **Freundlich** | $K_F$ | 16.0918 | 27.0238 | 20.8493 | 27.2586 |
| | $n_F$ | 3.8632 | 3.552 | 5.8877 | 4.9726 |
| | $R^2$ | 0.9566 | 0.9591 | 0.9228 | 0.8915 |
| **Langmuir** | $q_{max}$ | 42,7433 | 72.0811 | 38.1963 | 54.5161 |
| | b | 0.326 | 0.4285 | 1.0183 | 1.0214 |
| | $R^2$ | 0.8822 | 0.8984 | 0.9664 | 0.9521 |
| **Sips** | $q_{max}$ | 260.8549 | 215.4386 | 39.0797 | 53.2231 |
| | b | $8.69985 \cdot 10^{-05}$ | 0.004536 | 0.9853 | 1.0826 |
| | n | 3.4123 | 2.7381 | 1.1589 | 0.8217 |
| | $R^2$ | 0.9574 | 0.9607 | 0.9675 | 0.9543 |
| **Temkin** (R= 8.314) | T | 293 | 293 | 293 | 293 |
| | A | 7.043 | 8.363 | 53.914 | 28.97 |
| | b | 336.206 | 195.919 | 482.763 | 305.309 |
| | $R^2$ | 0.944 | 0.954 | 0.9479 | 0.9212 |

## 4.6 Column adsorption results

The experimental data from the fixed bed adsorption column have been plotted in Figure 4.26. The resulting data trends are the experimental breakthrough curve. The green dots are coming from the first sampling point (outlet 1). The curve is strongly asymmetrical, with a slowing rate reaching saturation. This has been attributed mainly to a not fully developed flow, being the bed length 5 cm shorter than the recommended one. Usually, it is suggested that the minimum length should be 10 times the diameter to have a fully developed flow. The breakthrough curves for the outlet 2 it is more symmetrical but also in this case the saturation point was slow to reach. The best of the three curves was found to be the outlet 3. The volumes of solution treated at $t_b$ for the outlets 1, 2 and 3 were about 0.6, 2.5 and 6.4 L.

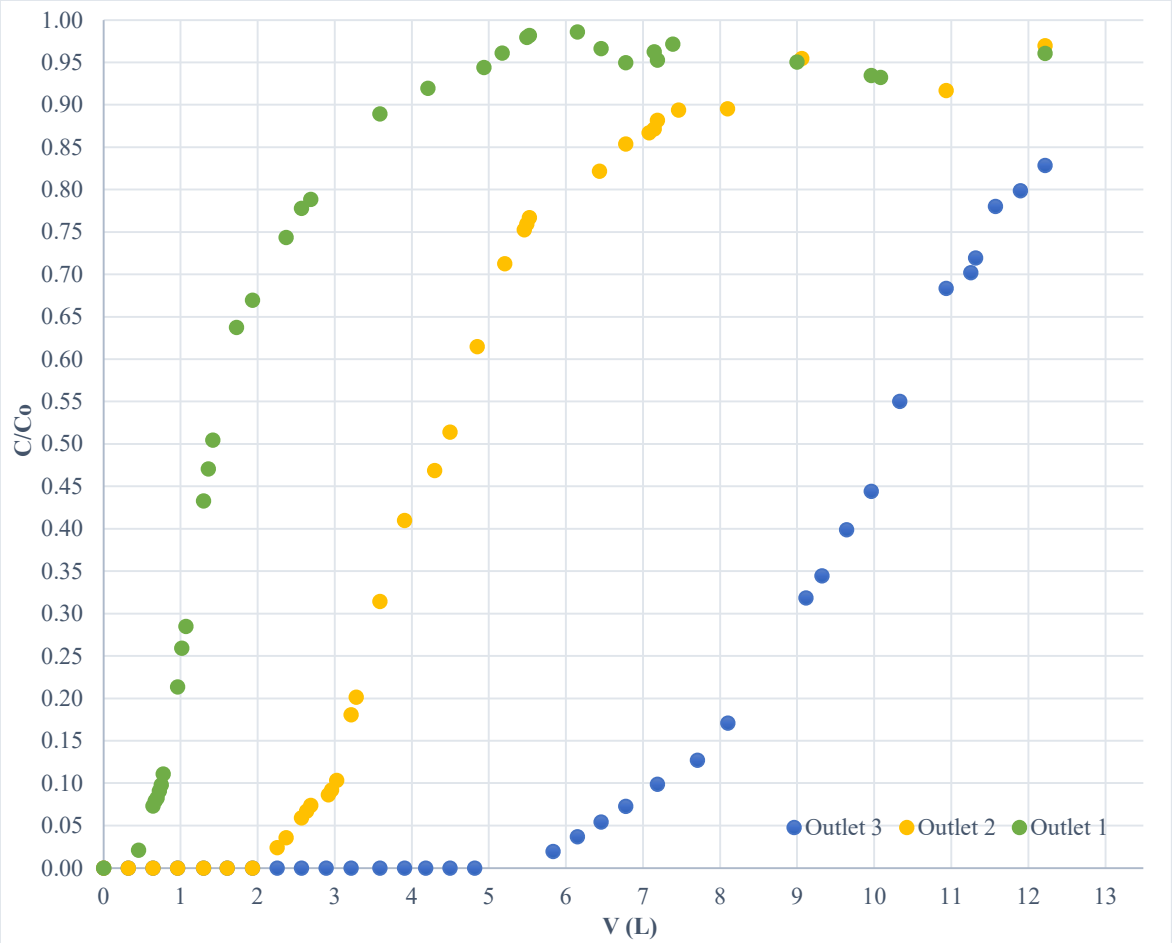


**Figure 4.26** Breakthrough curves for the three length.

In Table 4.8 all the parameter calculated from the experimental data are given. The removal capacity was shown to improve with the length and time, reaching the highest value of 39.8 mg/g at saturation from the outlet 3. The Y from $t_0$ to $t_s$ was estimated for all the three outlets, the highest value is 74.4 % for the outlet 3. Important parameters for upscaling the process are UB and MTZ, the first was found to increase with the length as expected, the second was

found to increase too, this can also be explained by the not fully developed flow. Seen the shape of the curve and the $A_s/t^*$ (0.9899) from the outlet 3, stable condition can be considered reached, so the MTZ of 11 cm can be taken as the proper length of the unused bed.

**Table 4.8** Parameters calculated from the experimental data

| Outlet | $q_b$ | $t_b$ | $q_s$ | $A_s$ | $t_s$ | Y | UB | MTZ | L | t* |
|---|---|---|---|---|---|---|---|---|---|---|
| **1** | 6.68 | 41.7 | 22.09 | 139.0 | 374.8 | 37.08 | 30.22 | 7.0 | 10 | 105.4 |
| **2** | 14.78 | 186.0 | 28.27 | 355.7 | 671.0 | 53.01 | 52.30 | 9.5 | 20 | 331.3 |
| **3** | 25.28 | 476.7 | 39.81 | 751.2 | *1010.0 | 74.38 | 63.50 | 11.0 | 30 | 758.9 |

*$t_s$ for the outlet 3 was estimated using the last two sampling points.

### 4.6.1 Modelling

Here are shown the model results of the breakthrough curves. In Figure 4.27 the experimental data with the Yoon-Nelson and Clark models are plotted, the continuous line has been used to indicate the best fitting model. The Yoon-Nelson was found to be the best to predicts the adsorption for all the bed lengths, reaching an $R^2$ of 0.9979 for the outlet 3.

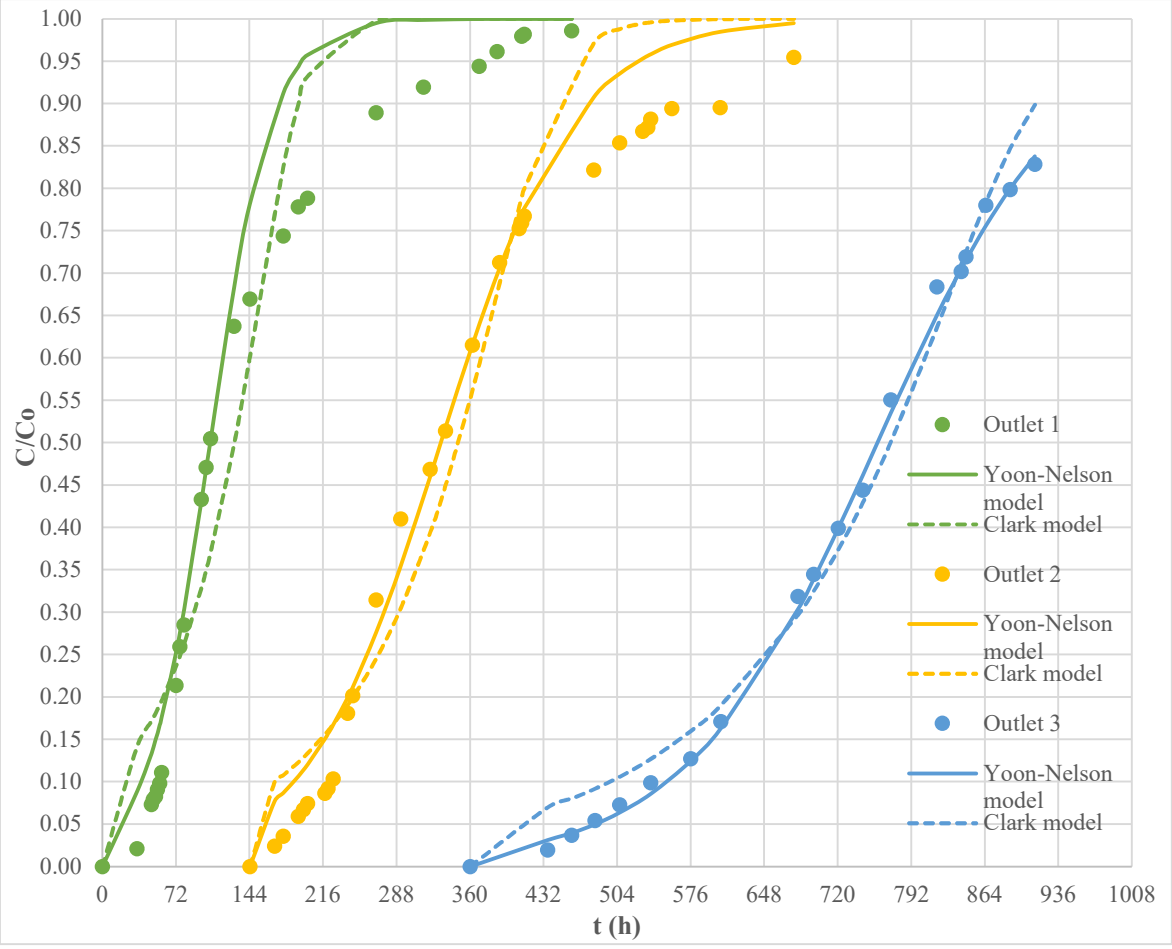


**Figure 4.27** Breakthrogh models.

All the parameters obtained are summarized in the following Table 4.9. The $n_F$ used to fit the Clark model is the one at equilibrium (120h).

**Table 4.9** Parameters of breakthrough curves models.

| | **Yoon-Nelson model** | | | **Clark model** | | | |
|---|---|---|---|---|---|---|---|
| **Outlet** | t* | $K_{YN}$ | $R^2$ | $n_F$ | r | A | $R^2$ |
| **1** | 105.4 | 0.0326 | 0.9508 | 4.9726 | 0.0532 | 14186.5547 | 0.9355 |
| **2** | 331.3 | 0.0153 | 0.9749 | 4.9726 | 0.0360 | 4114920.3584 | 0.9444 |
| **3** | 758.9 | 0.0107 | 0.9979 | 4.9726 | 0.0235 | 1108261264.0675 | 0.9849 |

# Conclusions and Prospectives

This study investigated the possibility of valorizing textiles insulation panels at end-of-life to produce adsorbents for the removal of ibuprofen from wastewaters. Adsorbents were obtained by means of a pyrolysis process, with or without steam activation.

The biochar obtained after pyrolysis was found to have the fastest kinetics but the lowest adsorption capacity, with a maximum of 4 mg/g.

After activation, the surface area has increased and mesopores were developed (24 %). The steam activated biochar has been studied in 3 forms: full pellets, crushed pellets (of various diameters) and sieved granules ($0.5<\Phi<0.8$). The full pellets had the slowest kinetics probably due to the intraparticle diffusion; the model of best fit was the pseudo second order kinetic with a $q_e$ of 45.7 mg/g for 1 g of adsorbent. The crushed pellets had the best adsorption capacity and it is best fitted by a pseudo second order kinetic; the isotherm of this material after 120 h had an experimental $q_{max}$ of around 80 mg/g and fits with Freundlich and Sips as the material is heterogeneous (different size of granules ranging from powder to big size particles). The sieved one had the higher kinetic rate and is best fitted using the Elovich model, the isotherm is best fitted with Sips, but also well fitted with Langmuir as the sieved steam activated biochar presented a more homogeneous surface.

From the dynamic experiment, the fixed bed adsorption column was able to treat 6.4 L of synthetic wastewater at breakthrough and more than 12 L of water at saturation. The adsorption capacity was established to be around 25 and 40 mg/g, respectively. The column needs to be changed after 20 days (breakthrough time) at a flowrate of 0.22 mL/min. The best fitting model has been the Yoon-Nelson.

Analysis of the functional groups present in the surface could be conducted in future studies, to better understand the adsorption mechanisms taking place. Fourier-transform infrared spectroscopy (FTIR) is a suggested technique. This can also help to understand if other molecules can be targeted. Adsorption of other pharmaceuticals such as Tetracycline can be suggested.

On the other hand, to improve the knowledge about ibuprofen adsorption, a desorption test should be conducted, to establish if the reaction is reversible and if a degree of reusability of the adsorbent is present. Also, tests in tap water and real wastewater are desirable, if a study in real conditions is required, in that case, High-performance liquid chromatography (HPLC) is strongly suggested to avoid the problem encountered in this study with the baseline

shifting in the UV-visible spectrophotometer. Additionally, parameters like pH and temperature can be variated to search the optimal conditions for the removal of the target pollutant.

# References


Abbas, Z., Ali, S., Rizwan, M., Zaheer, I.E., Malik, A., Riaz, M.A., Shahid, M.R., Rehman, M.Z. ur, Al-Wabel, M.I., 2018. A critical review of mechanisms involved in the adsorption of organic and inorganic contaminants through biochar. Arab J Geosci 11, 448. https://doi.org/10.1007/s12517-018-3790-1

Acosta, R., Fierro, V., Martinez de Yuso, A., Nabarlatz, D., Celzard, A., 2016. Tetracycline adsorption onto activated carbons produced by KOH activation of tyre pyrolysis char. Chemosphere 149, 168–176. https://doi.org/10.1016/j.chemosphere.2016.01.093

Adhikari, B., De, D., Maiti, S., 2000. Reclamation and recycling of waste rubber. Progress in Polymer Science 25, 909–948. https://doi.org/10.1016/S0079-6700(00)00020-4

Aguilar-Romero, I., Romero, E., Wittich, R.-M., van Dillewijn, P., 2020. Bacterial ecotoxicity and shifts in bacterial communities associated with the removal of ibuprofen, diclofenac and triclosan in biopurification systems. Science of The Total Environment 741, 140461. https://doi.org/10.1016/j.scitotenv.2020.140461

Ahmed, M.B.M., Rajapaksha, A.U., Lim, J.E., Vu, N.T., Kim, I.S., Kang, H.M., Lee, S.S., Ok, Y.S., 2015. Distribution and Accumulative Pattern of Tetracyclines and Sulfonamides in Edible Vegetables of Cucumber, Tomato, and Lettuce. J. Agric. Food Chem. 63, 398–405. https://doi.org/10.1021/jf5034637

Alalwan, H.A., Kadhom, M.A., Alminshid, A.H., 2020. Removal of heavy metals from wastewater using agricultural byproducts. Journal of Water Supply: Research and Technology-Aqua 69, 99–112. https://doi.org/10.2166/aqua.2020.133

Alexandre-Franco, M., Fernández-González, C., Alfaro-Domínguez, M., Gómez-Serrano, V., 2011. Adsorption of cadmium on carbonaceous adsorbents developed from used tire rubber. Journal of Environmental Management 92, 2193–2200. https://doi.org/10.1016/j.jenvman.2011.04.001

Al-Ghouti, M.A., Da'ana, D.A., 2020. Guidelines for the use and interpretation of adsorption isotherm models: A review. Journal of Hazardous Materials 393, 122383. https://doi.org/10.1016/j.jhazmat.2020.122383

Álvarez-Torrellas, S., Rodríguez, A., Ovejero, G., García, J., 2016. Comparative adsorption performance of ibuprofen and tetracycline from aqueous solution by carbonaceous materials. Chemical Engineering Journal 283, 936–947. https://doi.org/10.1016/j.cej.2015.08.023

Al-Wabel, M.I., Al-Omran, A., El-Naggar, A.H., Nadeem, M., Usman, A.R.A., 2013. Pyrolysis temperature induced changes in characteristics and chemical composition of biochar produced from conocarpus wastes. Bioresource Technology 131, 374–379. https://doi.org/10.1016/j.biortech.2012.12.165

Antoniou, N., Stavropoulos, G., Zabaniotou, A., 2014. Activation of end of life tyres pyrolytic char for enhancing viability of pyrolysis – Critical review, analysis and recommendations for a hybrid dual system. Renewable and Sustainable Energy Reviews 39, 1053–1073. https://doi.org/10.1016/j.rser.2014.07.143

Aranda, A., Murillo, R., García, T., Callén, M.S., Mastral, A.M., 2007. Steam activation of tyre pyrolytic carbon black: Kinetic study in a thermobalance. Chemical Engineering Journal 126, 79–85. https://doi.org/10.1016/j.cej.2006.08.031

Azargohar, R., Dalai, A.K., 2008. Steam and KOH activation of biochar: Experimental and modeling studies. Microporous and Mesoporous Materials 110, 413–421. https://doi.org/10.1016/j.micromeso.2007.06.047

Balakrishna, K., Rath, A., Praveenkumarreddy, Y., Guruge, K.S., Subedi, B., 2017. A review of the occurrence of pharmaceuticals and personal care products in Indian water bodies. Ecotoxicology and Environmental Safety 137, 113–120. https://doi.org/10.1016/j.ecoenv.2016.11.014

Barco-Bonilla, N., Romero-González, R., Plaza-Bolaños, P., Martínez Vidal, J.L., Garrido Frenich, A., 2013. Systematic study of the contamination of wastewater treatment plant effluents by organic priority compounds in Almeria province (SE Spain). Science of The Total Environment 447, 381–389. https://doi.org/10.1016/j.scitotenv.2013.01.027

Ben, Y., Fu, C., Hu, M., Liu, L., Wong, M.H., Zheng, C., 2019. Human health risk assessment of antibiotic resistance associated with antibiotic residues in the environment: A review. Environmental Research 169, 483–493. https://doi.org/10.1016/j.envres.2018.11.040

Benjamin, S.E., Sajjid, M.A., 2017. Factors Affecting the Adsorption of Trivalent Chromium Ions by Activated Carbon Prepared from Waste Rubber Tyres. Adv. sci. technol. eng. syst. j. 2, 1660–1664. https://doi.org/10.25046/aj0203206

Bian, R., Chen, D., Liu, X., Cui, L., Li, L., Pan, G., Xie, D., Zheng, Jinwei, Zhang, X., Zheng, Jufeng, Chang, A., 2013. Biochar soil amendment as a solution to prevent Cd-tainted rice from China: Results from a cross-site field experiment. Ecological Engineering 58, 378–383. https://doi.org/10.1016/j.ecoleng.2013.07.031

Bian, R., Li, Lu, Shi, W., Ma, B., Joseph, S., Li, Lianqing, Liu, X., Zheng, J., Zhang, X., Cheng, K., Pan, G., 2018. Pyrolysis of contaminated wheat straw to stabilize toxic metals in biochar but recycle the extract for agricultural use. Biomass and Bioenergy 118, 32–39. https://doi.org/10.1016/j.biombioe.2018.08.003

Boleda, M.R., Alechaga, É., Moyano, E., Galceran, M.T., Ventura, F., 2014. Survey of the occurrence of pharmaceuticals in Spanish finished drinking waters. Environ Sci Pollut Res 21, 10917–10939. https://doi.org/10.1007/s11356-014-2885-9

Boudrahem, N., Delpeux-Ouldriane, S., Khenniche, L., Boudrahem, F., Aissani-Benissad, F., Gineys, M., 2017. Single and mixture adsorption of clofibric acid, tetracycline and paracetamol onto Activated carbon developed from cotton cloth residue. Process Safety and Environmental Protection 111, 544–559. https://doi.org/10.1016/j.psep.2017.08.025

Caicedo, D.F., dos Reis, G.S., Lima, E.C., De Brum, I.A.S., Thue, P.S., Cazacliu, B.G., Lima, D.R., dos Santos, A.H., Dotto, G.L., 2020. Efficient adsorbent based on construction and demolition wastes functionalized with 3-aminopropyltriethoxysilane (APTES) for the removal ciprofloxacin from hospital synthetic effluents. Journal of Environmental Chemical Engineering 8, 103875. https://doi.org/10.1016/j.jece.2020.103875

Carpenter, D., Westover, T.L., Czernik, S., Jablonski, W., 2014. Biomass feedstocks for renewable fuel production: a review of the impacts of feedstock and pretreatment on the yield and product distribution of fast pyrolysis bio-oils and vapors. Green Chem. 16, 384–406. https://doi.org/10.1039/C3GC41631C

Chai, Y., Currie, R.J., Davis, J.W., Wilken, M., Martin, G.D., Fishman, V.N., Ghosh, U., 2012. Effectiveness of Activated Carbon and Biochar in Reducing the Availability of Polychlorinated Dibenzo-p-dioxins/Dibenzofurans in Soils. Environ. Sci. Technol. 46, 1035–1043. https://doi.org/10.1021/es2029697

Chakraborty, P., Banerjee, S., Kumar, S., Sadhukhan, S., Halder, G., 2018. Elucidation of ibuprofen uptake capability of raw and steam activated biochar of Aegle marmelos shell: Isotherm, kinetics, thermodynamics and cost estimation. Process Safety and Environmental Protection 118, 10–23. https://doi.org/10.1016/j.psep.2018.06.015

Chein, S., Clayton, W., 1980. Application of Elovich equation to the kinetics of phosphate release and sorption in soil. J Am Soil Sci Soc 44, 265–8.

Chen, B., Chen, Z., Lv, S., 2011. A novel magnetic biochar efficiently sorbs organic pollutants and phosphate. Bioresource Technology 102, 716–723. https://doi.org/10.1016/j.biortech.2010.08.067

Chen, W.-H., Lu, K.-M., Tsai, C.-M., 2012. An experimental analysis on property and structure variations of agricultural wastes undergoing torrefaction. Applied Energy, Clean Energy for Future Generations 100, 318–325. https://doi.org/10.1016/j.apenergy.2012.05.056

Chiesa, L.M., Nobile, M., Malandra, R., Panseri, S., Arioli, F., 2018. Occurrence of antibiotics in mussels and clams from various FAO areas. Food Chemistry 240, 16–23. https://doi.org/10.1016/j.foodchem.2017.07.072

Cho, D.-W., Kwon, G., Yoon, K., Tsang, Y.F., Ok, Y.S., Kwon, E.E., Song, H., 2017. Simultaneous production of syngas and magnetic biochar via pyrolysis of paper mill sludge using CO2 as reaction medium. Energy Conversion and Management 145, 1–9. https://doi.org/10.1016/j.enconman.2017.04.095

Clark, R.M., 1987. Evaluating the cost and performance of field-scale granular activated carbon systems. Environ. Sci. Technol. 21, 573–580. https://doi.org/10.1021/es00160a008

Cleuvers, M., 2003. Aquatic ecotoxicity of pharmaceuticals including the assessment of combination effects. Toxicology Letters, Hot Spot Pollutants: Pharmaceuticals in the Environment 142, 185–194. https://doi.org/10.1016/S0378-4274(03)00068-7

Collier, R., 2012. Swallowing the pharmaceutical waters. CMAJ 184, 163–164. https://doi.org/10.1503/cmaj.109-4086

Creamer, A.E., Gao, B., Zimmerman, A., Harris, W., 2018. Biomass-facilitated production of activated magnesium oxide nanoparticles with extraordinary CO2 capture capacity. Chemical Engineering Journal 334, 81–88. https://doi.org/10.1016/j.cej.2017.10.035

Cunliffe, A.M., Williams, P.T., 1999. Influence of Process Conditions on the Rate of Activation of Chars Derived from Pyrolysis of Used Tires. Energy Fuels 13, 166–175. https://doi.org/10.1021/ef9801524

Dai, J., Meng, X., Zhang, Y., Huang, Y., 2020. Effects of modification and magnetization of rice straw derived biochar on adsorption of tetracycline from water. Bioresource Technology 311, 123455. https://doi.org/10.1016/j.biortech.2020.123455

Davarnejad, R., Soofi, B., Farghadani, F., Behfar, R., 2018. Ibuprofen removal from a medicinal effluent: A review on the various techniques for medicinal effluents treatment. Environmental Technology & Innovation 11, 308–320. https://doi.org/10.1016/j.eti.2018.06.011

De García, S.A., Pinto Pinto, G., García-Encina, P.A., Irusta-Mata, R., 2014. Ecotoxicity and environmental risk assessment of pharmaceuticals and personal care products in aquatic environments and wastewater treatment plants. Ecotoxicology 23, 1517–1533. https://doi.org/10.1007/s10646-014-1293-8

de Oliveira, M., Atalla, A.A., Frihling, B.E.F., Cavalheri, P.S., Migliolo, L., Filho, F.J.C.M., 2019. Ibuprofen and caffeine removal in vertical flow and free-floating macrophyte constructed wetlands with Heliconia rostrata and Eichornia crassipes. Chemical Engineering Journal 373, 458–467. https://doi.org/10.1016/j.cej.2019.05.064

Doja, S., Pillari, L.K., Bichler, L., 2022. Processing and activation of tire-derived char: A review. Renewable and Sustainable Energy Reviews 155, 111860. https://doi.org/10.1016/j.rser.2021.111860

Dordio, A.V., Duarte, C., Barreiros, M., Carvalho, A.J.P., Pinto, A.P., da Costa, C.T., 2009. Toxicity and removal efficiency of pharmaceutical metabolite clofibric acid by Typha spp. – Potential use for phytoremediation? Bioresource Technology 100, 1156–1161. https://doi.org/10.1016/j.biortech.2008.08.034

Ericson, H., Thorsén, G., Kumblad, L., 2010. Physiological effects of diclofenac, ibuprofen and propranolol on Baltic Sea blue mussels. Aquatic Toxicology 99, 223–231. https://doi.org/10.1016/j.aquatox.2010.04.017

Evgenidou, E.N., Konstantinou, I.K., Lambropoulou, D.A., 2015. Occurrence and removal ibuprofen on Ti/Pt/PbO 2 and Si/BDD electrodes. Electrochim. Acta 54, 1464–1472.

Fang, J., Zhan, L., Ok, Y.S., Gao, B., 2018. Minireview of potential applications of hydrochar derived from hydrothermal carbonization of biomass. Journal of Industrial and Engineering Chemistry 57, 15–21. https://doi.org/10.1016/j.jiec.2017.08.026

Fent, K., Weston, A.A., Caminada, D., 2006. Ecotoxicology of human pharmaceuticals. Aquatic Toxicology 76, 122–159. https://doi.org/10.1016/j.aquatox.2005.09.009

Freundlich, H., 1907. Über die Adsorption in Lösungen. Zeitschrift für Physikalische Chemie 57U, 385–470. https://doi.org/10.1515/zpch-1907-5723

Gelband, H., Miller, P.M., Pant, S., Gandra, S., Levinson, J., Barter, D., White, A., Laxminarayan, R., 2015. The state of the world's antibiotics 2015. Wound Healing Southern Africa 8, 30–34. https://doi.org/10.10520/EJC180082

Godwin, P.M., Pan, Y., Xiao, H., Afzal, M.T., 2019. Progress in Preparation and Application of Modified Biochar for Improving Heavy Metal Ion Removal From Wastewater. Journal of Bioresources and Bioproducts 4, 31–42. https://doi.org/10.21967/jbb.v4i1.180

Gogotsi, Y., Portet, C., Osswald, S., Simmons, J.M., Yildirim, T., Laudisio, G., Fischer, J.E., 2009. Importance of pore size in high-pressure hydrogen storage by porous carbons. International Journal of Hydrogen Energy 34, 6314–6319. https://doi.org/10.1016/j.ijhydene.2009.05.073

González-González, R.B., González, L.T., Iglesias-González, S., González-González, E., Martinez-Chapa, S.O., Madou, M., Alvarez, M.M., Mendoza, A., 2020. Characterization of chemically activated pyrolytic carbon black derived from waste tires as a candidate for nanomaterial precursor. Nanomaterials 10, 1–22. https://doi.org/10.3390/nano10112213

Gupta, V.K., Gupta, B., Rastogi, A., Agarwal, S., Nayak, A., 2011. Pesticides removal from waste water by activated carbon prepared from waste rubber tire. Water Research 45, 4047–4055. https://doi.org/10.1016/j.watres.2011.05.016

Han, S., Choi, Kyungho, Kim, J., Ji, K., Kim, S., Ahn, B., Yun, J., Choi, Kyunghee, Khim, J.S., Zhang, X., Giesy, J.P., 2010. Endocrine disruption and consequences of chronic exposure to ibuprofen in Japanese medaka (Oryzias latipes) and freshwater cladocerans Daphnia magna and Moina macrocopa. Aquatic Toxicology 98, 256–264. https://doi.org/10.1016/j.aquatox.2010.02.013

Han, T.U., Kim, J., Kim, K., 2020. Freezing-accelerated removal of chromate by biochar synthesized from waste rice husk. Separation and Purification Technology 250, 117233. https://doi.org/10.1016/j.seppur.2020.117233

Han, Y., Yang, L., Chen, Xueming, Cai, Y., Zhang, X., Qian, M., Chen, Xingkui, Zhao, H., Sheng, M., Cao, G., Shen, G., 2020. Removal of veterinary antibiotics from swine wastewater using anaerobic and aerobic biodegradation. Science of The Total Environment 709, 136094. https://doi.org/10.1016/j.scitotenv.2019.136094

He, C., Giannis, A., Wang, J.-Y., 2013. Conversion of sewage sludge to clean solid fuel using hydrothermal carbonization: Hydrochar fuel characteristics and combustion behavior. Applied Energy 111, 257–266. https://doi.org/10.1016/j.apenergy.2013.04.084

He, X., Deng, M., Wang, Q., Yang, Yongtao, Yang, Yufeng, Nie, X., 2016. Residues and health risk assessment of quinolones and sulfonamides in cultured fish from Pearl River Delta, China. Aquaculture 458, 38–46. https://doi.org/10.1016/j.aquaculture.2016.02.006

Hirst, E.A., Taylor, A., Mokaya, R., 2018. A simple flash carbonization route for conversion of biomass to porous carbons with high CO2 storage capacity. J. Mater. Chem. A 6, 12393–12403. https://doi.org/10.1039/C8TA04409K

Ho, S.-H., Chen, Y., Yang, Z., Nagarajan, D., Chang, J.-S., Ren, N., 2017. High-efficiency removal of lead from wastewater by biochar derived from anaerobic digestion sludge. Bioresource Technology, Special Issue on Biochar: Production, Characterization and Applications – Beyond Soil Applications 246, 142–149. https://doi.org/10.1016/j.biortech.2017.08.025

Ho, Y.S., McKay, G., 1999. Pseudo-second order model for sorption processes. Process Biochemistry 34, 451–465. https://doi.org/10.1016/S0032-9592(98)00112-5

Hofman, M., Pietrzak, R., 2011. Adsorbents obtained from waste tires for NO2 removal under dry conditions at room temperature. Chemical Engineering Journal 170, 202–208. https://doi.org/10.1016/j.cej.2011.03.054

Holm, J.V., Ruegge, Kirsten., Bjerg, P.L., Christensen, T.H., 1995. Occurrence and Distribution of Pharmaceutical Organic Compounds in the Groundwater Downgradient of a Landfill (Grindsted, Denmark). Environ. Sci. Technol. 29, 1415–1420. https://doi.org/10.1021/es00005a039

Horne, P.A., Williams, P.T., 1996. Influence of temperature on the products from the flash pyrolysis of biomass. Fuel 75, 1051–1059. https://doi.org/10.1016/0016-2361(96)00081-6

Hsieh, C.-T., Teng, H., 2000. Influence of mesopore volume and adsorbate size on adsorption capacities of activated carbons in aqueous solutions. Carbon 38, 863–869. https://doi.org/10.1016/S0008-6223(99)00180-3

Ighalo, J.O., Adeniyi, A.G., Marques, G., 2021a. Internet of Things for Water Quality Monitoring and Assessment: A Comprehensive Review, in: Hassanien, A.E., Bhatnagar, R., Darwish, A. (Eds.), Artificial Intelligence for Sustainable Development: Theory, Practice and Future Applications, Studies in Computational Intelligence. Springer International Publishing, Cham, pp. 245–259. https://doi.org/10.1007/978-3-030-51920-9_13

Ighalo, J.O., Ajala, O.J., Adeniyi, A.G., Babatunde, E.O., Ajala, M.A., 2021b. Ecotoxicology of glyphosate and recent advances in its mitigation by adsorption. Environ Sci Pollut Res 28, 2655–2668. https://doi.org/10.1007/s11356-020-11521-5

International Biochar Initiative [WWW Document], 2022. . biochar-international. URL https://biochar-international.org/ (accessed 1.20.22).

Jeyasubramanian, K., Thangagiri, B., Sakthivel, A., Dhaveethu Raja, J., Seenivasan, S., Vallinayagam, P., Madhavan, D., Malathi Devi, S., Rathika, B., 2021. A complete review on biochar: Production, property, multifaceted applications, interaction mechanism and computational approach. Fuel 292, 120243. https://doi.org/10.1016/j.fuel.2021.120243

Jiang, M., Yang, W., Zhang, Z., Yang, Z., Wang, Y., 2015. Adsorption of three pharmaceuticals on two magnetic ion-exchange resins. Journal of Environmental Sciences 31, 226–234. https://doi.org/10.1016/j.jes.2014.09.035

Jiang, T.-Y., Jiang, J., Xu, R.-K., Li, Z., 2012. Adsorption of Pb(II) on variable charge soils amended with rice-straw derived biochar. Chemosphere 89, 249–256. https://doi.org/10.1016/j.chemosphere.2012.04.028

Kalam, S., Abu-Khamsin, S.A., Kamal, M.S., Patil, S., 2021. Surfactant Adsorption Isotherms: A Review. ACS Omega 6, 32342–32348. https://doi.org/10.1021/acsomega.1c04661

Kalderis, D., Akay, S., 2017. Adsorption of 2,4-dichlorophenol on paper sludge/wheat husk biochar: Process optimization and comparison with biochars prepared from wood chips, sewage sludge and hog fuel/demolition waste.

Kan, T., Strezov, V., Evans, T.J., 2016. Lignocellulosic biomass pyrolysis: A review of product properties and effects of pyrolysis parameters. Renewable and Sustainable Energy Reviews 57, 1126–1140. https://doi.org/10.1016/j.rser.2015.12.185

Khitous, M., Salem, Z., Halliche, D., 2016. Effect of interlayer anions on chromium removal using Mg–Al layered double hydroxides: Kinetic, equilibrium and thermodynamic studies. Chinese Journal of Chemical Engineering 24, 433–445. https://doi.org/10.1016/j.cjche.2015.11.018

Khorram, M.S., Zhang, Q., Lin, D., Zheng, Y., Fang, H., Yu, Y., 2016. Biochar: a review of its impact on pesticide behavior in soil environments and its potential applications. J. Environ. Sci. 44, 269–279.

Kim, K.H., Kim, J.-Y., Cho, T.-S., Choi, J.W., 2012. Influence of pyrolysis temperature on physicochemical properties of biochar obtained from the fast pyrolysis of pitch pine (Pinus rigida). Bioresource Technology 118, 158–162. https://doi.org/10.1016/j.biortech.2012.04.094

Krasucka, P., Pan, B., Sik Ok, Y., Mohan, D., Sarkar, B., Oleszczuk, P., 2021. Engineered biochar – A sustainable solution for the removal of antibiotics from water. Chemical Engineering Journal 405, 126926. https://doi.org/10.1016/j.cej.2020.126926

Kumar, M., Dutta, S., You, S., Luo, G., Zhang, S., Show, P.L., Sawarkar, A.D., Singh, L., Tsang, D.C.W., 2021. A critical review on biochar for enhancing biogas production from anaerobic digestion of food waste and sludge. Journal of Cleaner Production 305, 127143. https://doi.org/10.1016/j.jclepro.2021.127143

Lagergren, S., 1898. Zur theorie der sogenannten adsorption geloster stoffe. Kungliga svenska vetenskapsakademiens. Handlingar 24, 1–39.

Lahijani, P., Mohammadi, M., Mohamed, A.R., 2018. Metal incorporated biochar as a potential adsorbent for high capacity CO2 capture at ambient condition. Journal of CO2 Utilization 26, 281–293. https://doi.org/10.1016/j.jcou.2018.05.018

Langmuir, I., 1916. The constitution and fundamental properties of solids and liquids. Part I. Solids. J. Am. Chem. Soc. 38, 2221–2295. https://doi.org/10.1021/ja02268a002

Lapworth, D.J., Baran, N., Stuart, M.E., Ward, R.S., 2012. Emerging organic contaminants in groundwater: A review of sources, fate and occurrence. Environmental Pollution 163, 287–303. https://doi.org/10.1016/j.envpol.2011.12.034

Lei, Z., Li, Q., Song, X., Wang, W., Zhang, Z., Peng, C., Tian, L., 2018. Biochar mitigates dissolved organic carbon loss but does not affect dissolved organic nitrogen leaching loss caused by nitrogen deposition in Moso bamboo plantations. Global Ecology and Conservation 16, e00494. https://doi.org/10.1016/j.gecco.2018.e00494

Letsinger, S., Kay, P., Rodríguez-Mozaz, S., Villagrassa, M., Barceló, D., Rotchell, J.M., 2019. Spatial and temporal occurrence of pharmaceuticals in UK estuaries. Science of The Total Environment 678, 74–84. https://doi.org/10.1016/j.scitotenv.2019.04.182

Li, C., Zhu, X., He, H., Fang, Y., Dong, H., Lü, J., Li, J., Li, Y., 2019. Adsorption of two antibiotics on biochar prepared in air-containing atmosphere: Influence of biochar porosity and molecular size of antibiotics. Journal of Molecular Liquids 274, 353–361. https://doi.org/10.1016/j.molliq.2018.10.142

Li, D.-C., Jiang, H., 2017. The thermochemical conversion of non-lignocellulosic biomass to form biochar: A review on characterizations and mechanism elucidation. Bioresource Technology, Special Issue on Biochar: Production, Characterization and Applications – Beyond Soil Applications 246, 57–68. https://doi.org/10.1016/j.biortech.2017.07.029

Li, H., Dong, X., da Silva, E.B., de Oliveira, L.M., Chen, Y., Ma, L.Q., 2017. Mechanisms of metal sorption by biochars: Biochar characteristics and modifications. Chemosphere 178, 466–478. https://doi.org/10.1016/j.chemosphere.2017.03.072

Li, X.-W., Xie, Y.-F., Li, C.-L., Zhao, H.-N., Zhao, H., Wang, N., Wang, J.-F., 2014. Investigation of residual fluoroquinolones in a soil–vegetable system in an intensive vegetable cultivation area in Northern China. Science of The Total Environment 468–469, 258–264. https://doi.org/10.1016/j.scitotenv.2013.08.057

Li, Y., Xing, B., Ding, Y., Han, X., Wang, S., 2020. A critical review of the production and advanced utilization of biochar via selective pyrolysis of lignocellulosic biomass. Bioresource Technology 312, 123614. https://doi.org/10.1016/j.biortech.2020.123614

Lima, I.M., Boateng, A.A., Klasson, K.T., 2010. Physicochemical and adsorptive properties of fast-pyrolysis bio-chars and their steam activated counterparts. Journal of Chemical Technology & Biotechnology 85, 1515–1521. https://doi.org/10.1002/jctb.2461

Liu, C., Zhang, H., Xiao, R., Wu, S., 2017. Value-added organonitrogen chemicals evolution from the pyrolysis of chitin and chitosan. Carbohydrate Polymers 156, 118–124. https://doi.org/10.1016/j.carbpol.2016.09.024

Liu, N., Charrua, A.B., Weng, C.-H., Yuan, X., Ding, F., 2015. Characterization of biochars derived from agriculture wastes and their adsorptive removal of atrazine from aqueous solution: A comparative study. Bioresource Technology 198, 55–62. https://doi.org/10.1016/j.biortech.2015.08.129

Liu, W.-J., Jiang, H., Yu, H.-Q., 2015. Development of Biochar-Based Functional Materials: Toward a Sustainable Platform Carbon Material. Chem. Rev. 115, 12251–12285. https://doi.org/10.1021/acs.chemrev.5b00195

Manchón-Vizuete, E., Macías-García, A., Nadal Gisbert, A., Fernández-González, C., Gómez-Serrano, V., 2005. Adsorption of mercury by carbonaceous adsorbents prepared from rubber of tyre wastes. Journal of Hazardous Materials 119, 231–238. https://doi.org/10.1016/j.jhazmat.2004.12.028

Maya, M., Gwenzi, W., Chaukura, N., 2020. A BIOCHAR-BASED POINT-OF-USE WATER TREATMENT SYSTEM FOR THE REMOVAL OF FLUORIDE, CHROMIUM AND BRILLIANT BLUE DYE IN TERNARY SYSTEMS. Environmental Engineering & Management Journal (EEMJ) 19.

Méndez, A., Gómez, A., Paz-Ferreiro, J., Gascó, G., 2012. Effects of sewage sludge biochar on plant metal availability after application to a Mediterranean soil. Chemosphere 89, 1354–1359. https://doi.org/10.1016/j.chemosphere.2012.05.092

Molina-Sabio, M., Gonzalez, M.T., Rodriguez-Reinoso, F., Sepúlveda-Escribano, A., 1996. Effect of steam and carbon dioxide activation in the micropore size distribution of activated carbon. Carbon 34, 505–509. https://doi.org/10.1016/0008-6223(96)00006-1

Mompelat, S., Le Bot, B., Thomas, O., 2009. Occurrence and fate of pharmaceutical products and by-products, from resource to drinking water. Environment International, Pharmaceutical products in the environment: trends toward lowering presence and impact 35, 803–814. https://doi.org/10.1016/j.envint.2008.10.008

Mondal, S., Bobde, K., Aikat, K., Halder, G., 2016. Biosorptive uptake of ibuprofen by steam activated biochar derived from mung bean husk: Equilibrium, kinetics, thermodynamics, modeling and eco-toxicological studies. Journal of Environmental Management 182, 581–594. https://doi.org/10.1016/j.jenvman.2016.08.018

Monga, D., Shetti, N.P., Basu, S., Raghava Reddy, K., Badawi, M., Bonilla-Petriciolet, A., Aminabhavi, T.M., 2022. Engineered biochar: A way forward to environmental remediation. Fuel 311, 122510. https://doi.org/10.1016/j.fuel.2021.122510

Moon, D.H., Hwang, I., Chang, Y.-Y., Koutsospyros, A., Cheong, K.H., Ji, W.H., Park, J.-H., 2017. Quality improvement of acidic soils by biochar derived from renewable materials. Environ Sci Pollut Res 24, 4194–4199. https://doi.org/10.1007/s11356-016-8142-7

Murillo, R., Navarro, M.V., López, J.M., Aylón, E., Callén, M.S., García, T., Mastral, A.M., 2004. Kinetic Model Comparison for Waste Tire Char Reaction with CO2. Ind. Eng. Chem. Res. 43, 7768–7773. https://doi.org/10.1021/ie040026p

Nag, S.K., Kookana, R., Smith, L., Krull, E., Macdonald, L.M., Gill, G., 2011. Poor efficacy of herbicides in biochar-amended soils as affected by their chemistry and mode of action. Chemosphere 84, 1572–1577. https://doi.org/10.1016/j.chemosphere.2011.05.052

Nawab, Q.H.J., Shah, S.K.M.T., Gul, N., Ali, A., Khan, K., 2015. Heavy metal ioaccumulation in native plants in chromite impacted sites: a search for effective remediating plant species. Clean Soil Air Water 43, 1–10.

Oaks, J.L., Gilbert, M., Virani, M.Z., Watson, R.T., Meteyer, C.U., Rideout, B.A., Shivaprasad, H.L., Ahmed, S., Chaudhry, M.J.I., Arshad, M., Mahmood, S., Ali, A., Khan, A.A., 2004. Diclofenac residues as the cause of vulture population decline in Pakistan. Nature 427, 630–633. https://doi.org/10.1038/nature02317

Oba, S.N., Ighalo, J.O., Aniagor, C.O., Igwegbe, C.A., 2021. Removal of ibuprofen from aqueous media by adsorption: A comprehensive review. Science of The Total Environment 780, 146608. https://doi.org/10.1016/j.scitotenv.2021.146608

Osayi, J.I., Iyuke, S., Ogbeide, S.E., 2014. Biocrude Production through Pyrolysis of Used Tyres. Journal of Catalysts 2014, e386371. https://doi.org/10.1155/2014/386371

Parolini, M., Binelli, A., Cogni, D., Riva, C., Provini, A., 2009. An in vitro biomarker approach for the evaluation of the ecotoxicity of non-steroidal anti-inflammatory drugs (NSAIDs). Toxicology in Vitro 23, 935–942. https://doi.org/10.1016/j.tiv.2009.04.014

Parolini, M., Binelli, A., Provini, A., 2011. Chronic effects induced by ibuprofen on the freshwater bivalve Dreissena polymorpha. Ecotoxicology and Environmental Safety 74, 1586–1594. https://doi.org/10.1016/j.ecoenv.2011.04.025

Pomati, F., Netting, A.G., Calamari, D., Neilan, B.A., 2004. Effects of erythromycin, tetracycline and ibuprofen on the growth of Synechocystis sp. and Lemna minor. Aquatic Toxicology 67, 387–396. https://doi.org/10.1016/j.aquatox.2004.02.001

Pomati, F., Orlandi, C., Clerici, M., Luciani, F., Zuccato, E., 2008. Effects and Interactions in an Environmentally Relevant Mixture of Pharmaceuticals. Toxicological Sciences 102, 129–137. https://doi.org/10.1093/toxsci/kfm291

Pounds, N., Maclean, S., Webley, M., Pascoe, D., Hutchinson, T., 2008. Acute and chronic effects of ibuprofen in the mollusc Planorbis carinatus (Gastropoda: Planorbidae). Ecotoxicology and Environmental Safety 70, 47–52. https://doi.org/10.1016/j.ecoenv.2007.07.003

Prabakar, D., Manimudi, V.T., Suvetha K, S., Sampath, S., Mahapatra, D.M., Rajendran, K., Pugazhendhi, A., 2018. Advanced biohydrogen production using pretreated industrial waste: Outlook and prospects. Renewable and Sustainable Energy Reviews 96, 306–324. https://doi.org/10.1016/j.rser.2018.08.006

Prauchner, M.J., Rodríguez-Reinoso, F., 2012. Chemical versus physical activation of coconut shell: A comparative study. Microporous and Mesoporous Materials 152, 163–171. https://doi.org/10.1016/j.micromeso.2011.11.040

PubChem, 2021. Ibuprofen [WWW Document]. URL https://pubchem.ncbi.nlm.nih.gov/compound/3672 (accessed 11.25.21).

Puga, A.P., Abreu, C.A., Melo, L.C.A., Beesley, L., 2015. Biochar application to a contaminated soil reduces the availability and plant uptake of zinc, lead and cadmium. Journal of Environmental Management 159, 86–93. https://doi.org/10.1016/j.jenvman.2015.05.036

Putra, A.E.E., AMALIYAH, N., SYAM, M., RAHIM, I., 2019. Effect of residence time and chemical activation on pyrolysis product from tires waste. Journal of the Japan Institute of Energy 98, 279–284.

Rambau, K.M., Musyoka, N.M., Manyala, N., Ren, J., Langmi, H.W., 2018. Mechanochemical approach in the synthesis of activated carbons from waste tyres and its hydrogen storage applications. Materials Today: Proceedings, 1st Africa Energy Materials Conference, 28-31 March 2017 5, 10505–10513. https://doi.org/10.1016/j.matpr.2017.12.382

Rhodes, A.H., Carlin, A., Semple, K.T., 2008. Impact of Black Carbon in the Extraction and Mineralization of Phenanthrene in Soil. Environ. Sci. Technol. 42, 740–745. https://doi.org/10.1021/es071451n

Roberts, D.A., de Nys, R., 2016. The effects of feedstock pre-treatment and pyrolysis temperature on the production of biochar from the green seaweed Ulva. Journal of Environmental Management 169, 253–260. https://doi.org/10.1016/j.jenvman.2015.12.023

Rodríguez-Reinoso, F., Molina-Sabio, M., González, M.T., 1995. The use of steam and CO2 as activating agents in the preparation of activated carbons. Carbon 33, 15–23. https://doi.org/10.1016/0008-6223(94)00100-E

Ryu, S.K., Jin, H., Gondy, D., Pusset, N., Ehrburger, P., 1993. Activation of carbon fibres by steam and carbon dioxide. Carbon 31, 841–842. https://doi.org/10.1016/0008-6223(93)90025-6

Saifullah, Dahlawi, S., Naeem, A., Rengel, Z., Naidu, R., 2018. Biochar application for the remediation of salt-affected soils: Challenges and opportunities. Science of The Total Environment 625, 320–335. https://doi.org/10.1016/j.scitotenv.2017.12.257

Sakhiya, A.K., Anand, A., Kaushal, P., 2020. Production, activation, and applications of biochar in recent times. Biochar 2, 253–285. https://doi.org/10.1007/s42773-020-00047-1

Saleh, T.A., Danmaliki, G.I., 2016. Influence of acidic and basic treatments of activated carbon derived from waste rubber tires on adsorptive desulfurization of thiophenes. Journal of the Taiwan Institute of Chemical Engineers 60, 460–468. https://doi.org/10.1016/j.jtice.2015.11.008

Saravanan, M., Hur, J.-H., Arul, N., Ramesh, M., 2014. Toxicological effects of clofibric acid and diclofenac on plasma thyroid hormones of an Indian major carp, Cirrhinus mrigala during short and long-term exposures. Environmental Toxicology and Pharmacology 38, 948–958. https://doi.org/10.1016/j.etap.2014.10.013

Shilpa, Kumar, R., Sharma, A., 2018. Morphologically tailored activated carbon derived from waste tires as high-performance anode for Li-ion battery. J Appl Electrochem 48, 1–13. https://doi.org/10.1007/s10800-017-1129-3

Shin, J., Gunten, U., Reckhow, D., Allard, S., Lee, Y., 2018. Reactions of Ferrate(VI) with Iodide and Hypoiodous Acid: Kinetics, Pathways, and Implications for the Fate of Iodine during Water Treatment. Environmental Science & Technology 52. https://doi.org/10.1021/acs.est.8b01565

Silva, M., Feijão, E., da Cruz de Carvalho, R., Duarte, I.A., Matos, A.R., Cabrita, M.T., Barreiro, A., Lemos, M.F.L., Novais, S.C., Marques, J.C., Caçador, I., Reis-Santos, P., Fonseca, V.F., Duarte, B., 2020. Comfortably numb: Ecotoxicity of the non-steroidal anti-inflammatory drug ibuprofen on Phaeodactylum tricornutum. Marine Environmental Research 161, 105109. https://doi.org/10.1016/j.marenvres.2020.105109

Simonic, M., Goricanec, D., Urbancl, D., 2020. Impact of torrefaction on biomass properties depending on temperature and operation time. Science of The Total Environment 740, 140086. https://doi.org/10.1016/j.scitotenv.2020.140086

Sips, R., 1948. On the Structure of a Catalyst Surface. J. Chem. Phys. 16, 490–495. https://doi.org/10.1063/1.1746922

Sirimuangjinda, A., Atong, D., Pechyen, Asst.Prof.Dr.C., 2012a. Comparison on Pore Development of Activated Carbon Produced from Scrap Tire by Hydrochloric Acid and Sulfuric Acid. Advanced Materials Research 626, 706–710. https://doi.org/10.4028/www.scientific.net/AMR.626.706

Sirimuangjinda, A., Hemra, K., Atong, D., Pechyen, C., 2012b. Production and Characterization of Activated Carbon from Waste Tire by H3PO4 Treatment for Ethylene Adsorbent Used in Active Packaging. Advanced Materials Research 506, 214–217. https://doi.org/10.4028/www.scientific.net/AMR.506.214

Smisek, M., Cerny, S., 1970. New books - Active carbon: Manufacture, properties, and applications. Anal. Chem. 42, 81A-81A. https://doi.org/10.1021/ac50160a026

Son, E.-B., Poo, K.-M., Chang, J.-S., Chae, K.-J., 2018. Heavy metal removal from aqueous solutions using engineered magnetic biochars derived from waste marine macro-algal biomass. Science of The Total Environment 615, 161–168. https://doi.org/10.1016/j.scitotenv.2017.09.171

Sopeña, F., Semple, K., Sohi, S., Bending, G., 2012. Assessing the chemical and biological accessibility of the herbicide isoproturon in soil amended with biochar. Chemosphere 88, 77–83. https://doi.org/10.1016/j.chemosphere.2012.02.066

Strategic Approach to Pharmaceuticals in the Environment - Environment - European Commission [WWW Document], 2019. URL https://ec.europa.eu/environment/water/water-dangersub/pharmaceuticals.htm (accessed 1.5.22).

Ströbel, R., Garche, J., Moseley, P.T., Jörissen, L., Wolf, G., 2006. Hydrogen storage by carbon materials. Journal of Power Sources 159, 781–801. https://doi.org/10.1016/j.jpowsour.2006.03.047

Tan, G., Mao, Y., Wang, H., Xu, N., 2020. A comparative study of arsenic(V), tetracycline and nitrate ions adsorption onto magnetic biochars and activated carbon. Chemical Engineering Research and Design 159, 582–591. https://doi.org/10.1016/j.cherd.2020.05.011

Tan, X., Liu, Y., Zeng, G., Wang, X., Hu, X., Gu, Y., Yang, Z., 2015. Application of biochar for the removal of pollutants from aqueous solutions. Chemosphere 125, 70–85. https://doi.org/10.1016/j.chemosphere.2014.12.058

Tao, Y., Yu, G., Chen, D., Pan, Y., Liu, Z., Wei, H., Peng, D., Huang, L., Wang, Y., Yuan, Z., 2012. Determination of 17 macrolide antibiotics and avermectins residues in meat with accelerated solvent extraction by liquid chromatography–tandem mass spectrometry. Journal of Chromatography B 897, 64–71. https://doi.org/10.1016/j.jchromb.2012.04.011

Temkin, M., Pyzhev, V., 1940. Recent modifications to Langmuir isotherms.

Ternes, T.A., Hirsch, R., Mueller, J., Haberer, K., 1998. Methods for the determination of neutral drugs as well as betablockers and β2-sympathomimetics in aqueous matrices using GC/MS and LC/MS/MS. Fresenius J Anal Chem 362, 329–340. https://doi.org/10.1007/s002160051083

Ternes, T.A., Meisenheimer, M., McDowell, D., Sacher, F., Brauch, H.-J., Haist-Gulde, B., Preuss, G., Wilme, U., Zulei-Seibert, N., 2002. Removal of pharmaceuticals during drinking water treatment. Environmental Science and Technology 36, 3855–3863. https://doi.org/10.1021/es015757k

Usevičiūtė, L., Baltrėnaitė-Gedienė, E., 2021. Dependence of pyrolysis temperature and lignocellulosic physical-chemical properties of biochar on its wettability. Biomass Conversion and Biorefinery 11, 2775–2793.

Venegas, A., Rigol, A., Vidal, M., 2016. Changes in heavy metal extractability from contaminated soils remediated with organic waste or biochar. Geoderma 279, 132–140. https://doi.org/10.1016/j.geoderma.2016.06.010

Wan Mahari, W.A., Nam, W.L., Sonne, C., Peng, W., Phang, X.Y., Liew, R.K., Yek, P.N.Y., Lee, X.Y., Wen, O.W., Show, P.L., Chen, W.-H., Chang, J.-S., Lam, S.S., 2020. Applying microwave vacuum pyrolysis to design moisture retention and pH neutralizing palm kernel shell biochar for mushroom production. Bioresource Technology 312, 123572. https://doi.org/10.1016/j.biortech.2020.123572

Wan, X., Li, C., Parikh, S.J., 2020. Simultaneous removal of arsenic, cadmium, and lead from soil by iron-modified magnetic biochar. Environmental Pollution 261, 114157. https://doi.org/10.1016/j.envpol.2020.114157

Wang, B., Gao, B., Fang, J., 2017. Recent advances in engineered biochar productions and applications. Critical Reviews in Environmental Science and Technology 47, 2158–2207. https://doi.org/10.1080/10643389.2017.1418580

Wang, G., Fan, B., Chen, H., Li, Y., 2020. Understanding the pyrolysis behavior of agriculture, forest and aquatic biomass: Products distribution and characterization. Journal of the Energy Institute 93, 1892–1900. https://doi.org/10.1016/j.joei.2020.04.004

Wang, H., Ren, L., Yu, X., Hu, J., Chen, Y., He, G., Jiang, Q., 2017. Antibiotic residues in meat, milk and aquatic products in Shanghai and human exposure assessment. Food Control 80, 217–225. https://doi.org/10.1016/j.foodcont.2017.04.034

Wang, T., Li, G., Yang, K., Zhang, X., Wang, K., Cai, J., Zheng, J., 2021. Enhanced ammonium removal on biochar from a new forestry waste by ultrasonic activation: Characteristics, mechanisms and evaluation. Science of The Total Environment 778, 146295. https://doi.org/10.1016/j.scitotenv.2021.146295

Wang, T., Zhai, Y., Zhu, Y., Li, C., Zeng, G., 2018. A review of the hydrothermal carbonization of biomass waste for hydrochar formation: Process conditions, fundamentals, and physicochemical properties. Renewable and Sustainable Energy Reviews 90, 223–247. https://doi.org/10.1016/j.rser.2018.03.071

Wang, Y., Yin, R., Liu, R., 2014. Characterization of biochar from fast pyrolysis and its effect on chemical properties of the tea garden soil. Journal of Analytical and Applied Pyrolysis 110, 375–381. https://doi.org/10.1016/j.jaap.2014.10.006

Wang, Y., Zeng, Z., Tian, X., Dai, L., Jiang, L., Zhang, S., Wu, Q., Wen, P., Fu, G., Liu, Y., Ruan, R., 2018. Production of bio-oil from agricultural waste by using a continuous fast microwave pyrolysis system. Bioresource Technology 269, 162–168. https://doi.org/10.1016/j.biortech.2018.08.067

Weber, K., Quicker, P., 2018. Properties of biochar. Fuel 217, 240–261. https://doi.org/10.1016/j.fuel.2017.12.054

Weber, W.J., Morris, J.C., 1963. Kinetics of Adsorption on Carbon from Solution. Journal of the Sanitary Engineering Division 89, 31–59. https://doi.org/10.1061/JSEDAI.0000430

Wei, J., Tu, C., Yuan, G., Liu, Y., Bi, D., Xiao, L., Lu, J., Theng, B.K.G., Wang, H., Zhang, L., Zhang, X., 2019. Assessing the effect of pyrolysis temperature on the molecular properties and copper sorption capacity of a halophyte biochar. Environmental Pollution 251, 56–65. https://doi.org/10.1016/j.envpol.2019.04.128

Wiegel, S., Aulinger, A., Brockmeyer, R., Harms, H., Löffler, J., Reincke, H., Schmidt, R., Stachel, B., von Tümpling, W., Wanke, A., 2004. Pharmaceuticals in the river Elbe and its tributaries. Chemosphere 57, 107–126. https://doi.org/10.1016/j.chemosphere.2004.05.017

Wigmans, T., 1989. Industrial aspects of production and use of activated carbons. Carbon 27, 13–22. https://doi.org/10.1016/0008-6223(89)90152-8

Wu, L., Liu, Y., 2018. Application status of biochar as adsorbent in water treatment. Modern Food. 10, 46–47.

Xiang, W., Zhang, X., Chen, J., Zou, W., He, F., Hu, X., Tsang, D.C.W., Ok, Y.S., Gao, B., 2020. Biochar technology in wastewater treatment: A critical review. Chemosphere 252, 126539. https://doi.org/10.1016/j.chemosphere.2020.126539

Xiong, W., Zeng, Z., Li, X., Zeng, G., Xiao, R., Yang, Z., Xu, H., Chen, H., Cao, J., Zhou, C., Qin, L., 2019. Ni-doped MIL-53(Fe) nanoparticles for optimized doxycycline removal by using response surface methodology from aqueous solution. Chemosphere 232, 186–194. https://doi.org/10.1016/j.chemosphere.2019.05.184

Yaashikaa, P.R., Kumar, P.S., Varjani, S., Saravanan, A., 2020. A critical review on the biochar production techniques, characterization, stability and applications for circular bioeconomy. Biotechnology Reports 28, e00570. https://doi.org/10.1016/j.btre.2020.e00570

Yamaguchi, T., Okihashi, M., Harada, K., Konishi, Y., Uchida, K., Do, M., Bui, L., Nguyen, T., Phan, H., Bui, T., Nguyen, P., Kajimura, K., Kumeda, Y., Dang Van, C., Hirata, K., Yamamoto, Y., 2017. Detection of antibiotics in chicken eggs obtained from supermarkets in Ho Chi Minh City, Vietnam. Journal of Environmental Science and Health, Part B 52, 1–4. https://doi.org/10.1080/03601234.2017.1293457

Yang, Q., Wang, X., Luo, W., Sun, J., Xu, Q., Chen, F., Zhao, J., Wang, S., Yao, F., Wang, D., Li, X., Zeng, G., 2018. Effectiveness and mechanisms of phosphate adsorption on iron-modified biochars derived from waste activated sludge. Bioresource Technology 247, 537–544. https://doi.org/10.1016/j.biortech.2017.09.136

Yang, Y., Meehan, B., Shah, K., Surapaneni, A., Hughes, J., Fouché, L., Paz-Ferreiro, J., 2018. Physicochemical Properties of Biochars Produced from Biosolids in Victoria, Australia. International Journal of Environmental Research and Public Health 15, 1459. https://doi.org/10.3390/ijerph15071459

Yoon, Y.H., Nelson, J.H., 1984. Application of gas adsorption kinetics. I. A theoretical model for respirator cartridge service life. Am Ind Hyg Assoc J 45, 509–516. https://doi.org/10.1080/15298668491400197

Yu, X.-Y., Ying, G.-G., Kookana, R.S., 2009. Reduced plant uptake of pesticides with biochar additions to soil. Chemosphere 76, 665–671. https://doi.org/10.1016/j.chemosphere.2009.04.001

Zhang, D., Gersberg, R.M., Ng, W.J., Tan, S.K., 2014. Removal of pharmaceuticals and personal care products in aquatic plant-based systems: A review. Environmental Pollution 184, 620–639. https://doi.org/10.1016/j.envpol.2013.09.009

Zhang, L., Lim, E.Y., Loh, K.-C., Ok, Y.S., Lee, J.T.E., Shen, Y., Wang, C.-H., Dai, Y., Tong, Y.W., 2020. Biochar enhanced thermophilic anaerobic digestion of food waste: Focusing on biochar particle size, microbial community analysis and pilot-scale application. Energy Conversion and Management 209, 112654. https://doi.org/10.1016/j.enconman.2020.112654

Zhang, M., Gao, B., Varnoosfaderani, S., Hebard, A., Yao, Y., Inyang, M., 2013. Preparation and characterization of a novel magnetic biochar for arsenic removal. Bioresource Technology 130, 457–462. https://doi.org/10.1016/j.biortech.2012.11.132

Zhang, Q., Li, Q., Zhang, L., Yu, Z., Jing, X., Wang, Z., Fang, Y., Huang, W., 2017. Experimental study on co-pyrolysis and gasification of biomass with deoiled asphalt. Energy 134, 301–310. https://doi.org/10.1016/j.energy.2017.05.157

Zhao, C., Wang, B., Theng, B.K.G., Wu, P., Liu, F., Wang, S., Lee, X., Chen, M., Li, L., Zhang, X., 2021. Formation and mechanisms of nano-metal oxide-biochar composites for pollutants removal: A review. Science of The Total Environment 767, 145305. https://doi.org/10.1016/j.scitotenv.2021.145305

Zhao, T., Yao, Y., Li, D., Wu, F., Zhang, C., Gao, B., 2018. Facile low-temperature one-step synthesis of pomelo peel biochar under air atmosphere and its adsorption behaviors for Ag(I) and Pb(II). Science of The Total Environment 640–641, 73–79. https://doi.org/10.1016/j.scitotenv.2018.05.251

Zheng, N., Wang, J., Han, R., Xu, X., Zhen, Y., Qu, X., Sun, P., Li, S., Yu, Z., 2013. Occurrence of several main antibiotic residues in raw milk in 10 provinces of China. Food Additives & Contaminants: Part B 6, 84–89. https://doi.org/10.1080/19393210.2012.727189

Zheng, W., Guo, M., Chow, T., Bennett, D.N., Rajagopalan, N., 2010. Sorption properties of greenwaste biochar for two triazine pesticides. Journal of Hazardous Materials 181, 121–126. https://doi.org/10.1016/j.jhazmat.2010.04.103

Zhou, L., Boot, M.D., Johansson, B.H., Reijnders, J.J.E., 2014. Performance of lignin derived aromatic oxygenates in a heavy-duty diesel engine. Fuel 115, 469–478. https://doi.org/10.1016/j.fuel.2013.07.047

Zhou, N., Chen, H., Xi, J., Yao, D., Zhou, Z., Tian, Y., Lu, X., 2017. Biochars with excellent Pb(II) adsorption property produced from fresh and dehydrated banana peels via hydrothermal carbonization. Bioresource Technology 232, 204–210. https://doi.org/10.1016/j.biortech.2017.01.074

Zhou, N., Wang, Y., Yao, D., Li, S., Tang, J., Shen, D., Zhu, X., Huang, L., Zhong, M., Zhou, Z., 2019. Novel wet pyrolysis providing simultaneous conversion and activation to produce surface-functionalized biochars for cadmium remediation. Journal of Cleaner Production 221, 63–72. https://doi.org/10.1016/j.jclepro.2019.02.176

Zhou, X., Moghaddam, T.B., Chen, M., Wu, S., Adhikari, S., 2020. Biochar removes volatile organic compounds generated from asphalt. Science of The Total Environment 745, 141096. https://doi.org/10.1016/j.scitotenv.2020.141096

Zhu, D., Chen, Y., Yang, H., Wang, S., Wang, X., Zhang, S., Chen, H., 2020. Synthesis and characterization of magnesium oxide nanoparticle-containing biochar composites for efficient phosphorus removal from aqueous solution. Chemosphere 247, 125847. https://doi.org/10.1016/j.chemosphere.2020.125847

Zhu, X., Li, C., Li, J., Xie, B., Lü, J., Li, Y., 2018. Thermal treatment of biochar in the air/nitrogen atmosphere for developed mesoporosity and enhanced adsorption to tetracycline. Bioresource Technology 263, 475–482. https://doi.org/10.1016/j.biortech.2018.05.041

Zornoza, R., Moreno-Barriga, F., Acosta, J.A., Muñoz, M.A., Faz, A., 2016. Stability, nutrient availability and hydrophobicity of biochars derived from manure, crop residues, and municipal solid waste for their use as soil amendments. Chemosphere 144, 122–130. https://doi.org/10.1016/j.chemosphere.2015.08.046

Zuriaga, E., Lomba, L., German, B., Lanuza, P.M., Aldea, L., Ribate, M.P., García, C.B., Giner, B., 2019. Ecotoxicity in Aliivibrio fischeri of Ibuprofen, Omeprazole and their Mixtures. Chemistry and Ecology 35, 102–114. https://doi.org/10.1080/02757540.2018.1540608